Spring 2014

Computational and experimental biomechanics of total hip wear increase due to femoral head damage

Karen Marie Kruger
University of Iowa

Recommended Citation

Kruger, Karen Marie. "Computational and experimental biomechanics of total hip wear increase due to femoral head damage." PhD (Doctor of Philosophy) thesis, University of Iowa, 2014.
https://doi.org/10.17077/etd.j4b41sbi

Follow this and additional works at: https://ir.uiowa.edu/etd
Part of the Biomedical Engineering and Bioengineering Commons

COMPUTATIONAL AND EXPERIMENTAL BIOMECHANICS OF TOTAL HIP WEAR INCREASE DUE TO FEMORAL HEAD DAMAGE

by

Karen Marie Kruger

A thesis submitted in partial fulfillment
of the requirements for the Doctor of
Philosophy degree in Biomedical Engineering
in the Graduate College of
The University of Iowa

May 2014

Thesis Supervisor: Professor Thomas D. Brown

Graduate College
The University of Iowa
Iowa City, Iowa

CERTIFICATE OF APPROVAL

PH.D. THESIS

This is to certify that the Ph.D. thesis of

Karen Marie Kruger

has been approved by the Examining Committee
for the thesis requirement for the Doctor of Philosophy
degree in Biomedical Engineering at the May 2014 graduation.

Thesis Committee: ______________________________
Thomas D. Brown, Thesis Supervisor

____
John J. Callaghan

____
Nicole M. Grosland

____
Jia Lu

____
Joseph M. Reinhardt

ACKNOWLEDGMENTS

First, I would like to thank my advisor, Dr. Thomas Brown. It has been an honor to be your final graduate student. I also greatly appreciate Drs. Callaghan, Grosland, Lu, and Reinhardt for serving on my committee. This work would not have been possible without the contributions of many members of the Orthopaedic Biomechanics Laboratory. I would like to thank Dr. Anneliese Heiner for her work in coordinating the retrieval collection and photography setup development. Tom Baer’s experimental designs were also essential to the completion of this work. I would also like to thank the former and current graduate students for their help and friendship along the way. Andrew Kern provided significant assistance in the image analysis development. It was also nice to spend four years sitting two feet away from a good friend.

Additionally, the contributions from Dr. John Lannutti’s laboratory at Ohio State University allowed the retrieval analysis to progress to this point. Dr. Nishant Tikekar spent countless hours to compete the required OP scanning for this work. I would also like to acknowledge the NIH (AR057780) for funding this work.

Finally, I would like to thank my family who have been there to support me through every pursuit of my life. I would also like to thank Ryan and Nezzie for their continuous love and support.

ABSTRACT

Aseptic loosening due to wear-induced osteolysis remains a leading cause of failure in total hip arthroplasty (THA), particularly in revisions required beyond the second decade of use. Historically, there have been large amounts of variability of wear within individual THA patient cohorts. Evidence indicates that femoral head damage can be a cause of this variability. While femoral head damage as a result of third body particles and subluxation and dislocation events has been well documented, direct quantifiable linkage between such femoral head damage and wear acceleration remains to be established. Due to large ranges of observed retrieval damage, wear testing protocols for simulating third body and other damage effects have been widely variant, making it difficult to know where the clinical reality lies.

To study the effect of retrieval femoral head damage on total hip implant wear, a damage-feature-based finite element (FE) formulation was developed, which allowed for wear prediction due to individual scratch, scrape, and transfer deposit features. A multi-scale imaging procedure was also developed to globally map and quantify micron-level damage features appearing on retrieval femoral heads. This allowed for wear simulations of damage patterns observed on specific retrieval femoral heads. Retrieval damage was shown to be highly variable among patients, and capable of producing up to order-of-magnitude wear increases when compared to undamaged heads. Damage following dislocation and subsequent closed reduction maneuvers was found to be particularly detrimental, with average wear rate increases in the range of half an order of magnitude. These data were used to develop wear testing protocols for simulating clinically-occurring third body and other damage effects.

TABLE OF CONTENTS

LIST OF TABLES

LIST OF FIGURES

CHAPTER 1: BACKGROUND AND SIGNIFICANCE

Total hip arthroplasty (THA) is the treatment of choice to relieve pain and restore function to the end-stage arthritic hip joint. Modern total hip replacement was one of the most successful surgical innovations of the last century [121]. Since Charnley's breakthrough with low friction designs in the late 1950s [37], advances in joint replacement implants and improved surgical techniques have led to excellent success rates for this procedure. Long term follow-ups have reported good implant survivorship at 20-year follow-up (>80%) [34], and 35-year follow-up (78%) [30]. Despite continual changes in surgical technique and implant design, however, the burden of revision total hip arthroplasty in the United States has not decreased over time [18, 152]. Long term survivorship is affected by wear properties of the bearing couple, by component positioning, and by many patient-related factors.

Currently, over 250,000 primary and 40,000 revision THA surgeries are performed annually in the United States [114]. These numbers have been increasing steadily and are projected to increase by an additional 174% by the year 2030 [114]. The economic burden of revision THA is high. A recent analysis found hospital resource utilization to be $45,000 per revision procedure versus $35,000 per primary case [1]. Medicare is the primary payer for more than 60% of the hip arthroplasty procedures that are performed in the United States. Major arthroplasty procedures of the lower extremity represent the single largest procedural cost in the Medicare budget [145].

THA was originally conceived as a procedure for elderly patients with low activity levels [36]. Over time, however, the indications have expanded to include both younger and more active patients. The proportion of patients younger than 65 years of age is projected to increase to 50% of all arthroplasties by 2030 [112]. Increased patient activity levels [36] and the need for longer implant life continues to constitute a design challenge for the THA construct. While the long-term survival rates for modern THA designs have been excellent, results for younger patients have been less acceptable than for the THA population as a whole. Recent reports have documented failure rates of 44% for patients below age 56 [70] and 47% for patients under 35 [117] at follow-ups beyond 20 years.

Polyethylene wear is considered to be a major limiting factor in improving the longevity of implants. Aseptic loosening resulting from osteolysis is the leading cause late revision in metal-on-polyethylene implants [39]. Historically, there have been large amounts of variability of wear within individual THA patient cohorts. Evidence indicates that femoral head damage can be a cause of this variability. While femoral head damage as a result of third body particles and subluxation and dislocation events has been well documented, direct quantifiable linkage between such femoral head damage and wear acceleration remains to be established. Therefore, the objective of this body of work has been to study the effect of retrieval femoral head damage on total hip implant wear. This thesis presents a damage-feature-based finite element (FE) formulation, which allows for wear prediction due to individual scratch, scrape, and transfer deposit features. A multi-scale imaging procedure was also developed to globally map and quantify micron-level damage features appearing on retrieval femoral heads. This allows for wear simulations of damage patterns observed on specific retrieval femoral heads.

Osteolysis and wear

Osteolysis, or loss of periprosthetic bone, is acknowledged as the major limiting factor for THA longevity past the second decade [88]. It occurs due to an inflammatory response to wear debris shed during implant use. In metal-on-polyethylene implants, submicron-sized polyethylene particles (0.1 to 1.0 μm in size) are recognized as the primary form of osteolytic debris [89]. Once released into the joint fluid, the large numbers of these submicron-sized polyethylene particles initiate a cascade of biological events resulting in osteolysis. Osteolysis can progress to eventual implant loosening, resulting in pain for the patient and the need for revision surgery. Wear-related factors have been responsible for a significant percentage of THA revisions. Loosening, bearing surface wear, and periprosthetic osteolysis were responsible for 20%, 5%, and 7% of revision surgeries, respectively [21]. Wear-related revision rates are significantly higher for younger patients. Aseptic loosening was responsible for 86% of revisions in patients below age 56 [70] and 100% in patients below age 35 [117] in follow-ups beyond 20 years.

The progression of osteolysis and polyethylene (PE) wear can be monitored *in vivo* through radiographic images taken at clinical follow-ups of THA patients. While linear wear (i.e., site specific dimension change at the bearing surface) is the most commonly calculated measure *in vivo*, volumetric wear (total change in implant component volume) is a more physiologically pertinent measurement because it provides a more robust estimate of the total amount of polyethylene release into the joint. Volumetric wear has also been measured *ex vivo* through gravimetric measurements of retrieval implants obtained at revision surgery and well-functioning implants obtained at autopsy [96, 181]. Coordinate measuring machines (CMMs) have also been used to evaluate the (linear) wear distribution over the worn surface of acetabular liners [169]. In this approach, 3-D coordinates of large numbers of points on the wear surface are sampled, to produce surface wear maps. When CMMs are used on polyethelene liners, creep must be accounted for to properly assess wear [62].

A 10-year follow-up study by Dowd et al. found that osteolysis was strongly associated with increasing linear wear rate [47]. Osteolysis was present in 0% implants with linear wear rates less than 0.1 mm/year, in 43% of implants with linear wear rates between 0.1 and 0.2 mm/year, in 80% of implants with linear wear rates between 0.2 and 0.3 mm/year, and in 100% of implants wearing >0.3 mm/year. Dumbleton et al. suggested that a linear wear rate of 0.1 mm/year should be considered an "osteolysis threshold" [54] based on a literature review that showed that patients with linear wear rates less than 0.1 mm/year rarely developed osteolysis, while patients with linear wear rates greater than 0.1 mm/year had a substantially greater risk of developing osteolysis. Orishimo et al. reported that for every 0.1 mm/year increase in linear wear rate, patients had a 4-fold increase in risk for developing osteolysis. Similarly, for every 40 mm^3/year volumetric wear rate increase, patients had a 3-fold increase in risk for osteolysis onset. Given that the relationship between wear debris and osteolysis has been well-documented [36, 81, 98], reducing *in vivo* wear rates remains an important clinical goal.

Advances in implant technology have aimed to decrease wear rates and increase implant longevity. Increased usage of ceramic bearings, and especially the development and widespread acceptance of highly cross-linked polyethylenes (HXPEs) [20] have led to increased expected implant lifetimes. These alternatives to "conventional" ultra-high-molecular-weight polyethylene (UHMWPE) bearings have their own problems, however, including stripe wear, squeaking, and fracture risk in ceramics [133, 193], and decreased fracture toughness and ductility in HXPEs [69].

The advent of HXPEs has unquestionably decreased the overall wear rates of metal-on-polyethylene implants [157, 174]. Radiation crosslinking and thermal stabilization technology to produce these HXPEs was introduced clinically in 1995, and most technical aspects of first-generation materials are now covered by international standards [111]. In a 10-year follow-up of first-generation HXPE, Snir et al. reported average total linear wear rates of 0.122 mm/year [176]. These wear rates decreased significantly after an initial bedding-in, with average linear wear rates of 0.05 mm/year over the last 5 years. In a systematic review of clinical wear and osteolysis outcomes for first-generation HXPE by Kurtz et al. [111], HXPE resulted in 69% less wear than conventional UHMWPE and had an 87% lower risk of osteolysis.

Second-generation HXPEs were introduced in 2005. These involve alternative methods to stabilize the polymer [111]. Sequential irradiation and annealing processes were shown to preserve mechanical strength properties and to have the highest survivorship in functional fatigue testing in laboratory tests [53]. The long-term clinical track record has not yet been established, but it is promising. Callary et al. recently published the results of a 5-year follow-up on second-generation HXPE [31], with average linear wear rates of 0.001 mm/year, and no patient recording a wear rate of more than 0.04 mm/year. D' Antonio et al. also reported follow-up results of a second-generation HXPE [43] with average wear rates of 0.024, 0.020, and 0.008 mm/year at 3, 4, and 5 years, respectively.

Despite the dramatic overall decrease in cohort-average wear rates, however, ongoing concern lies with the relatively small number of “outlier” patients for whom excessive wear is a problem. In nearly every patient cohort, there are a few patients (typically 5-10%) whose wear rates fall outside of the normal “bell curve” distribution, and whose wear rates are up to an order of magnitude higher than the cohort mean [158]. The occurrence of outlier wear is an important clinical concern due to the strong correlation between wear debris burden and osteolysis [196]: These are the patients most greatly at risk. Scratching and roughening of the femoral head, as from third body particles or from subluxation or dislocation, is a likely explanation for many of these extreme outlier cases [138]. Such damage effects have been postulated as having the potential to increase the rate of wear by orders of magnitude [138].

In vivo evidence of third body and dislocation damage

Third body particles are, by definition, debris that did not originate from normal articulation in the joint (Figure 1). Such debris can arise from a variety of sources including bone particles produced intra-operatively, metal particles created from surgical instrument impaction of the implant, bone cement, fragmented trochanteric cable/wire [72], or from metallic pieces broken off from porous coatings. The particles can be carried into the bearing space by joint fluid [129] and they can become embedded in the polyethylene cup[83]. Once embedded, they can scratch the originally smooth surface of the femoral head during normal joint movements. These scratches can lead to acceleration of polyethylene wear. Laboratory wear tests have shown that much of HXPE's superb wear reduction can be lost when the material articulates against a scratched or roughened counterface [46].

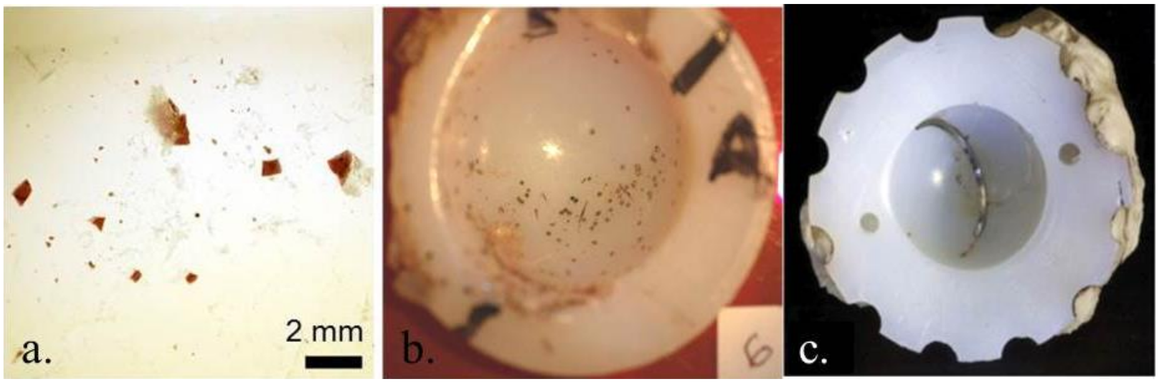

Figure 1: Examples of third body particles found embedded in the polyethelene liner – a. bone cement, b. Porous coating beads [128], and c. trochanteric wire fragments [72].

Third body wear has been remarked upon in the literature for decades [14]. Analyses of components obtained following revision surgery or post-mortem have commonly shown third body particles embedded in PE liners [3, 9]. Large variations in particle sizes are observed. The most commonly observed particles are on the order to 200-700 μm in diameter [98, 103, 188]. Larger ceramic [101] and metallic [128] particles several millimeters in length have been reported, with one reported case of an embedded trochanteric wire spanning nearly the entire acetabular diameter (Figure 1c) [72].

Third body particles have been directly implicated in femoral head roughening and scratching. Jasty et al. reported numerous multidirectional fine scratches caused by third body abrasive wear [97]. Mai et al. [132] reported similar scratches on CoCr heads revised for reasons other than dislocation. It was noted that the material that was "snowplowed" along the sides of the scratches formed tall, sharp edges that could gouge or scratch the polyethylene liner and potentially increase wear. These areas of scratching generally appeared as discrete areas 1-20 mm^2 in size [96] and were usually present on the proximal surface of the implant. These discrete areas of scratching were described as potentially containing tens to hundreds of multidirectional scratches.

The presence of third body particles has been correlated with femoral head roughening/scratching and with increased wear rates *in vivo*. In a study of autopsy retrievals, Sychterz et al. [181] reported higher femoral head roughness for components having embedded particle debris in the polyethylene liner. The corresponding wear rates of these debris-embedded cups were statistically significantly higher than the wear rates for cups without embedded debris. A retrieval study of 159 femoral heads obtained at revision surgery found that polyethylene wear was directly related to femoral head roughness [115] .

Retrieval studies have attributed substantial femoral head damage to dislocation-related events [17, 63, 106]. Closed reduction is the initial treatment for most THA dislocations. In this procedure, the displaced femoral head is maneuvered and repositioned into the acetabular liner with the patient under general anesthesia. Fluoroscopy can be helpful in achieving and confirming reduction [177]. Femoral head damage on dislocation retrievals is presumed to be caused by contact with the acetabular shell during the dislocation event or the attempted closed reduction. This damage consists of areas of scraping, gouging, and metal transfer. Analysis of retrievals has shown many of these damage features to contain titanium, the material of which the acetabular shell is normally composed [35, 184]. In retrieval studies, metal transfer to ceramic femoral heads has been shown to correlate with increased surface roughness of the head and with increased *in vivo* wear rates [102]. Another retrieval study of dislocated Oxinium® (surface-oxidized zirconium) femoral heads [95] documented extensive visual damage, with scratches and scrapes covering more than 20% of the head surface, and with frank gouges with lip height up to 66 μm. Dislocation-induced damage on CoCr femoral heads has historically received less attention than damage on ceramic or Oxinium® heads, probably because the former is relatively inconspicuous visually in the presence of reflections from the metallic surface under normal ambient lighting.

In vitro wear models

While third body and counterface damage effects have been recognized in the literature for decades [138], there is no clear quantifiable link between *in vivo* debris burden, degree of femoral head damage, and wear acceleration. Laboratory simulations are most often used to determine the effects of third body burden, but tend to often under-predict clinical wear rates [48]. The test designs of these simulations involve a wide range of surrogate damage mechanisms, and as intuitively expected, they therefore show large degrees of variability in resulting wear rates.

One source of variability lies in the methodology of damage introduction, which has involved numerous test protocols. Methods to induce damage for laboratory simulations include regionally roughening a part of the bearing surface with SiC grit paper [20, 195], adding particles to joint fluid [91, 162], creating discrete scratches at prescribed locations [8, 122], and working with retrieval implants [57, 94].

Each of these damage generation methods has been subject to additional variability. In the case of experiments that have involved adding particles to the lubricant fluid, differing particle compositions [22], particle size ranges [45], and effective concentrations [194] have been utilized. Another source of variability has involved the timeline of the third body challenge. Situations involving a one-time particle addition [45] versus continuously ongoing challenges either by continuously circulating particulate-containing fluid [22], or adding additional particles to joint fluid [161], would obviously lead to different levels of wear acceleration.

The kinetics and kinematics of joint articulation are another source of variability. Some wear tests have been conducted using simplified unidirectional motions (i.e. pin-on-disc experiments) [50, 144], whereas other tests have utilized full joint simulators, which implement multi-directional motions [20, 60, 122], some of which have attempted to replicate physiologic duty cycles [8]. Overall, full joint simulators have tended to produce higher increases in wear than that which occurs for simple reciprocal-motion simulators under both undamaged and third body-damaged situations [23]. This suggests that the direction of movement of damaged areas can play a role in wear rates. The addition of jogging activity and of episodes of stumbling, when combined with level walking, resulted in increased wear in a hip simulator, especially in the presence of femoral head roughening [20].

Although less common than third body wear tests, laboratory experiments have been used to study the effects of closed reduction and dislocation damage. Metal transfer has been simulated through *in vitro* models. Eberhardt et al. [55] and Chang et al. [35] reported average roughness values of 1.63 µm and 0.98 µm, respectively, in regions of *in vitro* simulated metal transfer, a significant increase over undamaged regions, which are typically on the order of 0.01 µm [8]. These *in- vitro*-simulated roughness values were similar to those measured on retrievals as a part of each study. Eberhardt et al. reported increased polyethylene wear to be associated with this induced metal transfer when wear tests were run of these femoral heads versus undamaged heads.

Empirical laboratory tests have documented metal transfer to the femoral head following contact with a titanium acetabular shell under loads as low as 10 kg [35]. The surface roughness values in such transfer regions significantly increased with increasing test loads. Moreover, as the contact force was increased, increasingly severe scratching of the head surface and metal transfer occurred. In another *in vitro* study, Jaffe et al. [95] created titanium-containing gouges on Oxinium® femoral heads by moving the femoral heads against a titanium shell as would happen following a dislocation and attempted closed reduction. Those gouges were reported to contain peak asperity heights in excess of 16 µm. *In vitro* wear tests of those damaged heads showed a 2- to 50-fold wear increase versus undamaged Oxinium® wear rates.

With so many different test designs to study the wear consequences of femoral head damage, it is difficult to know where the clinical reality lies. Despite the large amount of variability in both the techniques implemented and the degrees of damage induced, however, investigators have virtually always stated that the bearing surface damage was consistent with that which is observed clinically.

Retrieval analysis

Assessments of retrieval implants obtained at revision have been the primary source of information regarding *in vivo* clinical damage resulting from third bodies and/or subluxation/dislocation. Numerous retrieval studies have been published which characterize femoral head damage (both qualitatively and quantitatively) [19, 35, 42, 55, 77, 78, 87, 94, 96, 106, 132, 149, 181, 191, 192], but most have involved only subjective or semi-quantitative assessment. The variability in study design of such retrieval work underscores that assessment of femoral head damage has not been straightforward. There are several challenges. First, bearing surface damage occurring *in vivo* (as assessed from retrievals) obviously varies from implant to implant, and from site to site on any given implant [181]. Second, while all bearing surface damage is obviously deleterious in terms of whole-implant-level wear acceleration, the specific damage features most critical to wear acceleration are unknown. Finally, the many retrieval studies that have relied on protocols with subjective assessments necessarily have had issues regarding observer bias and inter-observer variability. A summary of large-scale metal-on-polyethylene retrieval studies performed on metallic femoral heads is included in Table 1.

Table 1: Large-scale ($n \geq 10$) retrieval studies performed on metal-on-polyethylene implants.

Author	**Retrievals Analyzed**	**Analysis Modalities**
Bauer et al. [11]	45	Dissecting microscopy, 3D stylus profilometry
Bourne et al. [17]	133	2D stylus profilometry
Currier et al. [42]	73	3D optical profilometry
Drabu et al .[51]	18	2D stylus profilometry, SEM, EDS
Eberhardt et al. [55]	16	2D stylus profilometry, SEM, EDS
Elfick et al. [57]	42	3D optical profilometry
Hall et al. [77]	35	2D stylus profilometry, SEM
Haraguchi et al. [80]	22	2D stylus profilometry, SEM
Isaac et al. [92]	78	2D stylus profilometry, SEM
Ito et al. [94]	108	2D optical profilometry
Jasty et al. [96]	54	Dissecting microscopy, SEM
Kusaba et al. [115]	149	2D stylus profilometry, SEM
Mai et al. [132]	10	3D optical profilometry, SEM
McKellop et al. [140]	20	Light microscopy, SEM
McNei et al. [144]	12	2D stylus profilometry
Scott et al. [171]	12	Dissecting microscopy, laser profilometry, SEM
Sychterz et al. [181]	24	Light microscopy, 2D stylus and laser profilometry, SEM
Walker et al. [191]	10	Light microscopy, 2D Stylus Profilometry

Qualitative assessments of femoral head damage have been used to map damage to the entire femoral head and to study different damage types and wear modes. These assessments have often relied on a combination of whole-implant photographs, gross-level inspection, and low-power light microscopy [87, 192]. Viewing and photographing of femoral head damage has often been hindered by the implant's highly reflective metallic surface, making visual assessments of damage difficult.

Scanning electron microscopy (SEM) has been used to provide enhanced information on the morphology of these damage features at higher magnification [78, 87, 96], but again this has been mainly in the form of pictorial information. Scanning electron microscopes are often equipped to preform energy dispersive spectroscopy (EDS), which can be used to investigate material transfer. EDS is an analytical technique that is used for the elemental analysis of a sample. The fundamental principle that guides this analysis is that each element has a unique atomic structure that allows X-rays characteristic of each element's atomic structure to be uniquely identified. EDS has been useful to investigate damage modes on retrieval femoral heads[19, 87]. Evidence of titanium alloy can be used to as evidence to show acetabular liner contact during dislocation or closed reduction. These optical methods hold attraction because they allow specimens to be investigated nondestructively [118], although drawing quantitative conclusions from such data can be difficult.

A number of retrieval studies have been conducted which have mapped regions of damage, based on estimations from these visualization techniques. Unfortunately, such damage mapping has lacked a standardized classification system. The types of damage mapped have varied from study to study, and have been subject to observer bias. For instance, visual appearance under varying levels of magnification has been used to define different damage modes. Najjar et al. [149] used brightness levels as observed under an optical microscope to differentiate damage types. High-brightness areas showed only isolated scratches, areas of intermediate brightness had moderate damage (including a high density of small, randomly orientated scratches), and areas of low brightness contained large, deep scratches. Isometric plots obtained by a three-dimensional contacting profilometer showed pile-up of metallic material on the sides of large scratches in some areas but not in others. Based on appearance, Howie et al. [87] identified wear types through visual assessment, light microscopy, and SEM. The wear types defined consisted of polishing, fine abrasive wear, multi-directional dull abrasive wear, and unidirectional dull abrasive wear, all of which were assessed based on their visual appearance. The percentage of each retrieval specimen covered by these respective wear types was measured. Walker et al. also defined wear types based on their visual appearance under low power microscopy [192]. In that study, the wear types reported upon were (1) initial scratching, (2) scratches that had been smoothed down, and (3) pitting on a (smoothed) scratched surface.

Another approach to damage taxonomy has been by defining how the damage took place [139]. Damage modes used in this paradigm are: (i) normal wear due to articulation as intended by the designer, (ii) one bearing surface rubbing against a non-bearing surface, (iii) third body abrasive wear, and (iv) two non-bearing surfaces rubbing together (Figure 2). Bowsher et al. [19] used this paradigm to map damage to a retrieval femoral head removed after multiple dislocations. While such damage maps can provide information on damage patterns and frequency, they unfortunately provide little quantitative information from which to directly relate femoral head damage to wear acceleration.

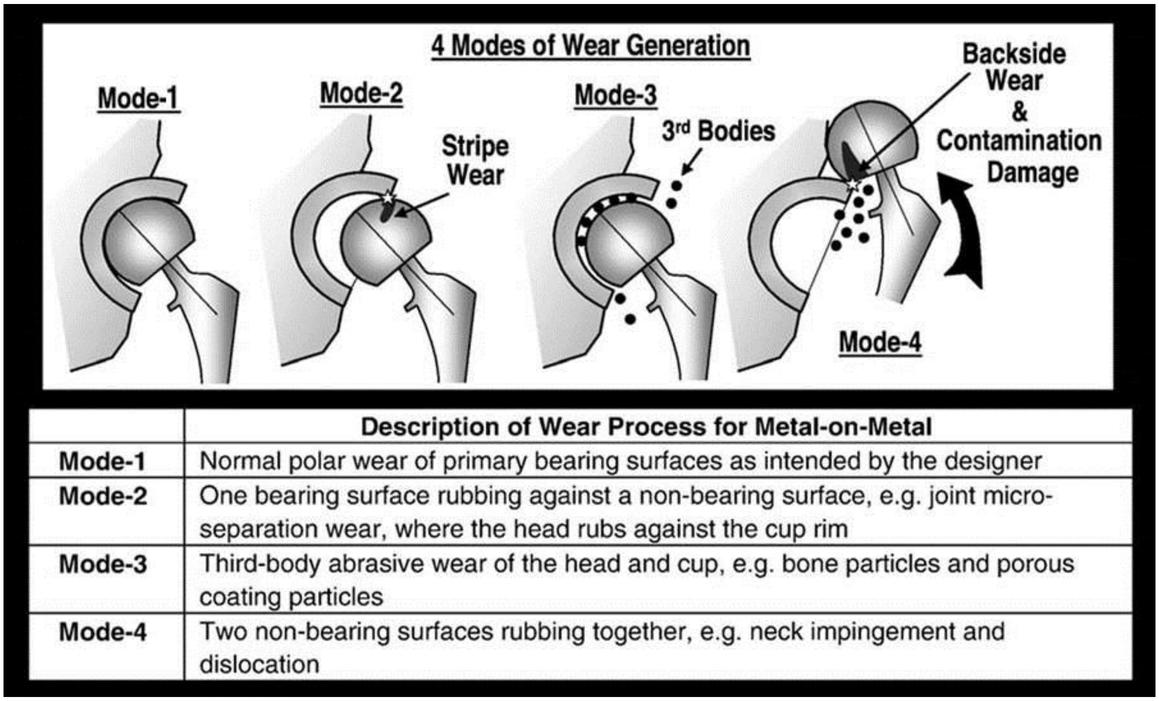

	Description of Wear Process for Metal-on-Metal
Mode-1	Normal polar wear of primary bearing surfaces as intended by the designer
Mode-2	One bearing surface rubbing against a non-bearing surface, e.g. joint micro-separation wear, where the head rubs against the cup rim
Mode-3	Third-body abrasive wear of the head and cup, e.g. bone particles and porous coating particles
Mode-4	Two non-bearing surfaces rubbing together, e.g. neck impingement and dislocation

Figure 2: Possible wear modes in hip arthroplasty [19]. Modes 2 to 4 are due to contact mechanisms not intended by the manufacturer.

Quantitative evaluation of femoral head damage features has primarily been accomplished by means of profilometry [19, 77, 87, 94, 133, 193], which uses either a mechanical stylus or laser to measure surface height variations as a function of position. Profilometry studies typically quantify femoral head damage in terms of conventional tribological parameters (Table 2). While traditional roughness parameters of this class are straightforward to evaluate and interpret, their suitability for quantifying wear-consequential surface damage is less than ideal. Microscopic retrieval examination has shown damage often takes the form of multidirectional scratches with small amount of material built up (snowplowed) along the sides of each scratch furrow/valley[132]. Roughness parameters are unable to provide definitive information on the number, severity, and orientation of scratches. For example, average roughness (R_a) is unable to distinguish between large groups of fine scratches versus small numbers of severe scratches. Similarly, the peak height (R_p) fails to differentiate between a single asperity, versus multiple asperities of similar height. There has yet to be a systematic attempt to catalog implant retrieval surface damage on a scratch-population basis.

Table 2: Standard surface roughness parameters commonly reported during retrieval analyses.

Parameter	Definition
R_a	Arithmetic average of absolute deviation of sampling points from the surface-mean centerline.
R_q	Root mean square average of the deviation of sampling points from the surface-mean centerline.
R_p	Maximum height of profile above the surface-mean centerline.
R_{pm}	Mean distance between the highest peak and the surface-mean centerline in five consecutive sampling lengths.
R_v	Maximum depth of the profile below the surface-mean centerline.
R_t	Distance between highest peak and lowest valley.
R_z	Difference in height between the average of the five highest peaks and the five lowest valleys.
R_{sk}	Third central moment of profile amplitude probability density function, measured over the assessment length. It is used to measure the symmetry of the profile about the surface-mean centerline.

Another limitation of traditional roughness parameters is that they fundamentally misrepresent damage as being homogeneous and isotropic. Including the predominant directionality of microscopic-level damage is an important consideration, however, because physical wear tests have shown that differing angles between scratch orientation and the direction of relative surface motion can produce order-of-magnitude differences in wear rate elevation [73]. Additionally, for scrape damage features, the directionality of the micro-scratches within a given macro-level scrape is not necessarily coincident with the scrape's macro-level directionality. For example, the micro-scratches in scrape damage generated at an edge-loaded femoral head region during a THA dislocation event tend to be substantially askew to the macro-direction of the scrape (Figure 3).

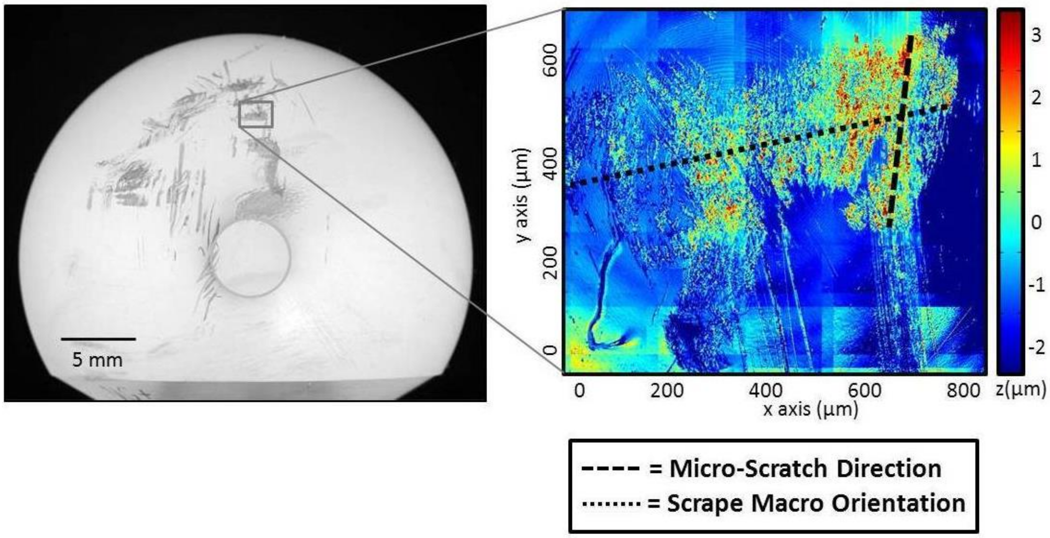

Figure 3: Damage to femoral head following subluxation. The circle at the center of the femoral head is a photographic artifact, the specifics of which are discussed below in Chapter 3.

The majority of quantitative damage assessments done by profilometry has involved mechanical stylus instruments, where variations in the vertical surface height are recorded as the stylus is physically drawn short distances tangentially across the surface of interest [149, 192]. The most appealing aspect of this method is that most of the world's surface finish standards are written for contact profilometers [7]. Stylus profilometry is also advantageous because it is less likely to measure dust and other loose surface contaminants, as compared to non-contact methods [26]. The accuracy of some contact profilometers allows asperities as small as 5 nm to be detected.

However, since stylus profilometry recordings provide height variation data only along individual sampling lines, they have limited utility for quantifying the morphology of entire implant surfaces. Most commonly, therefore, investigators using stylus profilometry have resorted to spot samplings of investigator-defined representative damage regions in order to define whole-head damage. These measurements have been taken in either the area judged to be most damaged, or else at specified locations on the head. For example, Hall et al. [77] quantified damage of retrieval femoral heads on the basis of 20 line profiles (each 1.4 mm in length) per specimen, taken in what was judged to be each specimen's most heavily scratched region. Atkinson et al. [6] used profilometry scans taken in the superior region of the femoral head to assess R_a increases. Besides being limited to surface height samplings along individual traverse lines, the short sweep length of most line profile instruments also has made it difficult to quantify heterogeneous topography within large areas of damage [192].

More recently, surface morphology has increasingly come to be characterized by optical profilometry (OP). This technique captures surface features at sub-nanometer vertical resolution, using light interferometry [57]. (Laser illumination has also been used for interferometry instruments, but the coherence of laser illumination produces surface noise that is approximately twice as high as that for conventional light illumination [151].) In a typical OP setup, light from a white-light interferometer is divided into two paths by a beam splitter. One path directs the light onto the surface being tested while the other path directs the light to a reference mirror. Reflections from the two surfaces are recombined and projected onto an array detector. When the path difference between the recombined beams is on the order of a few wavelengths of light or less, interference occurs. This interference contains information about the surface contours of the test surface. Vertical resolution ranges from 0.5-1.0 nm [199].

OP's high vertical resolution is well suited to quantifying the microscopic damage present on retrieval implant surfaces, and to doing so with relatively high speed and high accuracy [151]. OP has been validated against stylus profilometry [199], and in turn has served as a gold standard for evaluating other imaging techniques [105]. The maximum sampling region size for OP scans is on the order of a few square millimeters. In final results, depth information can be obtained through intensity-coded depth images, with the darkness directly relating to the defect depth [44]. This allows deviations both positive and negative from the surface to be mapped in multiple directions. While most previous applications of OP have still resorted to judgment-based spot samplings [57], the relatively large scan sizes (as compared to standard stylus profiometry) allow for substantial fractions of whole joint surfaces to be scanned.

OP has been used similarly to conventional stylus profilometry in applications where higher resolution is desired [57, 155]. Commercial software is available with many OP setups to mathematically remove features such as low-order curvature of spherical surfaces [189]. Standard surface roughness parameters are also reported from the resulting data, sampled over a 2D area. Line profiles can of course also be obtained from the resulting 3D data, a capability beneficial for detecting the height and width of individual scratches in the scanned area. OP has not been used nearly as extensively in quantifying surface damage as contact-based methods have, although several recent retrieval studies have adopted this method. Elfick et al. [57] used OP to measure area roughness parameters on retrievals, obtaining a higher degree of accuracy than previous contact-based measurements. Patten et al. [155] used OP to determine the volume of areas of raised titanium deposits, a parameter which is directly related both to peak height and to the area raised above the adjacent undamaged surface.

In vitro relationships between damage and wear elevation

While the micro-topography of the hard-surface counterface clearly has a major influence on the rate of polyethylene wear [66], direct quantification of the damage-vs.-wear relationship for whole-joint wear presently lacks formal physical basis. Most work in this area has instead been empirical, and has relied on simplified articulations such as those in pin-on-disc simulations [49, 50, 73]. For uniformly roughened areas, counterface roughness can be related to the pin-on-disc wear factor k by the equation

$$k = 4.0\, x\, 10^{-5} * (R_a)^{1.2}$$

as reported by Dowson et al. [49], where k is in units of $mm^3/N^{-1}m^{-1}$, and R_a is in units of μm. However, when tested to estimate wear for in retrieval cases, this correlation equation alone was found to be a poor predictor for wear performance [56, 79]. Damage on retrieval femoral heads is highly non-uniform, a possible explanation of this discrepancy. SEM images for retrieval femoral heads show that damage tends to be a collection of discrete scratches and transfer deposits, rather than areas of homogeneous isotropic roughening [77].

Further work has investigated the effect of single scratches of metallic counterfaces on the wear rates of ultra-high molecular weight polyethylene (UHMWPE) [50]. Scratches of various sizes were diamond stylus-ruled onto medical grade stainless steel plates. They were measured and modeled as had been previously reported by Buttery and Archard [29], who represented each scratch as a valley of material removed and two peaks of material piled up, as shown in Figure 4.

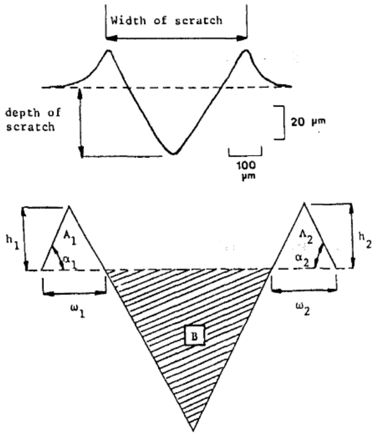

Figure 4: Buttery and Archard’s representation of an ideal scratch [29].

While it was initially hypothesized by Dowson et al. [50] that scratch depth would be the biggest factor contributing to wear elevation, scratch lip height was found to be a better predictor. This relationship was confirmed by lapping the damaged surfaces so that the scratch lip was removed while the valleys remained. When the plates were run through wear tests again, the resulting wear factors showed no statistically significant differences from the undamaged surfaces. These wear tests showed that scratches with lip heights as low as 1 μm could generate detectable increases in wear rates.

Further work with single asperities showed that scratches that were capable of increasing wear by a factor of 70 when compared to a smooth, lapped surface [67] only increased the corresponding to R_a value from 0.007 μm to 0.013 μm. This increased R_a value was still well below the ASTM-required R_a value of 0.05 μm for metallic femoral heads [64]. This lack of a strong correlation shows that one standard parameter alone does not capture all of the asperity features required in order to fully understand wear acceleration as it relates to surface damage. This disconnect is also apparent in attempts to relate retrieval femoral head damage to heads' respective *in vivo* wear rates. In a study of 35 retrieval implants [77], for example, there was only marginal correlation (r = 0.374, p=0.099) between clinical wear factors and R_a, with corresponding R_p values having an even weaker relationship with wear (r=0.211, p=0.225). Similarly, a later study showed the strength of the relationship between area roughness (S_a), as measured from 3D OP scans, and clinical wear factor to be considerably weaker than that achieved in laboratory experiments [56].

The influence of scratch articulation directionality on wear elevations has also been studied. Physical wear tests of scratched plates against UHMWPE showed pronounced wear peaks when the angle between scratch orientation and articulation direction was highly acute [73]. The data from that study suggest that unfavorable scratch directionality can liberate large amounts of polyethylene debris at critical (acute) angles by a slicing/shearing mechanism.

To date, there have been no concerted attempts to catalog retrieval surface damage on a damage-feature basis. A large reason for this knowledge gap lies in the difficulty in performing geometric registration of damage on two very different size scales (microscopic scratch and scrape features, versus the global implant surface). In order to move beyond empirical observations, and to help underpin physics-based models of damage vs. wear, it was felt to be essential to identify other technique(s) to quantify the severity and directionality of individual scratches and scrapes.

Computational models

While physical wear tests are necessary for predicting wear rates, they are expensive and time-consuming. Computational models have therefore come to be used in conjunction with physical tests, in order to reduce the impact of these logistical constraints. In some contexts parametrically, evaluation times can be reduced from months to hours, which allows for a wide variety of design factors to be considered. Maxian et al. [137] developed and validated the first sliding-distance-coupled FE model for THA wear. That model used the Archard/Lancaster [5] relationship for adhesive/abrasive wear to calculate wear rates. This relationship quantifies linear wear at a given location as a function of contact pressure, sliding distance, and a tribologically dependent wear factor. The wear factor depends on surface parameters such as materials, surface finish, and lubrication, and it normally needs to be determined empirically. Linear wear depths integrated over the surface provide a basis to calculate the total volume of material worn away. The specifics of the implementation of the Archard wear equation for THA wear and the specifics of the model developed by Maxian et al. and other computational wear simulations is extensively discussed below in Chapter 2.

Finite element models have also been developed to study wear rate increases due to third body damage. Such models fall into two broad classes. The first class has addressed the micromechanics of scratches and particles. McNie et al. [142] used a 2D FE model to investigate the mechanism by which femoral head scratches result in wear increases. That model showed that the presence of scratches produced high plastic strains, and that the aspect ratios of scratch lips were an important factor. A later variant of that model showed that the size of the UHMWPE regions undergoing plastic strain increased with increasing asperity area [144]. In another FE model of scratch articulation, Paul et al. [156] showed that cumulative compressive total normal strain in the direction of loading, and maximum instantaneous compressive total normal strain transverse to the sliding direction, best correlated with experimental scratch-direction-dependence of wear [73].

A series of FE models has also been developed to address counterface embedment of particles into the (polyethylene) bearing surface. Using a 2D formulation, it had earlier been shown that third body particles of stainless steel [143], cobalt chromium alloy, or zirconium oxide [147] can cause femoral head scratching. Raimondi et al. [165] found that wear-consequential femoral head damage could be induced by a prismatic-shaped particle having free sharp edges 5 μm in length facing the metallic head surface.

A second class of computational damage models has explored global, implant-level wear increases. This series of models allowed for an area of homogeneous isotropic local roughening [28] to be added to the femoral head. The formulation was used to computationally study implant-level effects of third body damage. Applications included determining critical regions of femoral head roughening [130], the influence of nonidentical duty cycles [91], and sensitivity to debris embedment location [22]. While this patch-roughened FE model agreed well with corresponding physical wear tests of grit-blasted surface patches [27], such homogeneous isotropic roughening fails to replicate *in vivo* damage. Retrieval femoral heads instead show damage in the form of multidirectional scratching [96, 192] and scraping [19]. And, as noted above, damage directionality plays a critical role in wear rate [73]. In addition to directional scratches and scrapes, many femoral heads in retrieval collections also show global regions of roughening/darkening, due to bearing-foreign material transfer (typically titanium) [35, 55]. An FE model that allows for damage representation of these various *in vivo* damage types holds the attraction of allowing for estimation of wear rates accompanying damage on an implant-specific basis.

Rationale

Polyethylene wear in total joint replacement remains a leading cause of implant failure, particularly beyond the second decade of use. Historically, there have been large amounts of variability of wear within individual THA patient cohorts. Evidence indicates that femoral head damage can be a cause of this variability.

While femoral head damage as a result of third body particles and subluxation and dislocation events has been well documented, direct quantifiable linkage between femoral head damage and wear acceleration remains to be established. Due to large ranges of observed retrieval damage, wear testing protocols for simulating third body and other damage effects have been subject to a wide range of variability, making it difficult to know where the clinical reality lies.

A damage-feature-based finite element (FE) formulation, described in Chapter 2, allows for wear prediction due to clinically occurring damage features. Retrieval analysis has shown that damage is highly variable among patients, presumably leading to substantially different wear rates. A multi-scale imaging procedure consisting of diffused-light photography and optical profilometry, described in Chapter 3, was developed to globally locate and quantify femoral head damage as measured on retrievals.

These tools were used to build a registry of individual damage features observed on retrievals and to quantify their potential wear acceleration (Chapters 4 and 5). Finally, the development damage templates to be used in wear testing protocols simulating third body and other damage effects using this registry is described in Chapter 6.

CHAPTER 2: DAMAGE-FEATURE-BASED FINITE ELEMENT MODEL

The damage-feature-based finite element model enabling the present work was grounded in the sliding-distance-coupled FE model for THA wear that was originally developed by Maxian et al. [137] (Figure 5). In the Maxian et al. formulation, wear was modeled using the Archard-Lancaster [5] relationship for abrasive/adhesive wear. This relationship calculates the instantaneous linear wear rate as the product of (i) contact pressure (σ), (ii) sliding velocity (v), and (iii) a wear coefficient (k) whose value depends on the tribological properties of the two surfaces in contact. For studying wear in total hips, this relationship is implemented by the equation:

$$W(\theta,\phi) = \int \left(k(\theta,\phi)\sigma(\theta,\phi)v(\theta,\phi)\right) dt,$$

where W is local wear depth per duty cycle, θ and ϕ are angular position coordinates, and the integral is evaluated from beginning to end of the duty cycle. In order to computationally implement the Archard wear relationship, the equation was discretized into the form:

$$Wear\ depth(\theta,\phi) = \sum_{i=1}^{ninst} k(\theta,\phi)\sigma_i(\theta,\phi)d_i(\theta,\phi)$$

The FE model was driven by force components from 16 (=ninst) instants of the stance portion of a level walking gait cycle, which earlier had been measured with an instrumented total hip implant [25]. Contact stress (σ) was calculated by means of the FE model. Sliding distance (d) was calculated from incremental changes in the flexion/extension, abduction/adduction, and internal/external rotation angles, again from the stance portion of the gait cycle. The baseline wear coefficient (k) was taken as

1.0656×10^{-6} mm^{3}N^{-1}m^{-1} , corresponding to an undamaged femoral head with an average roughness value on the order of 0.01 μm[137].

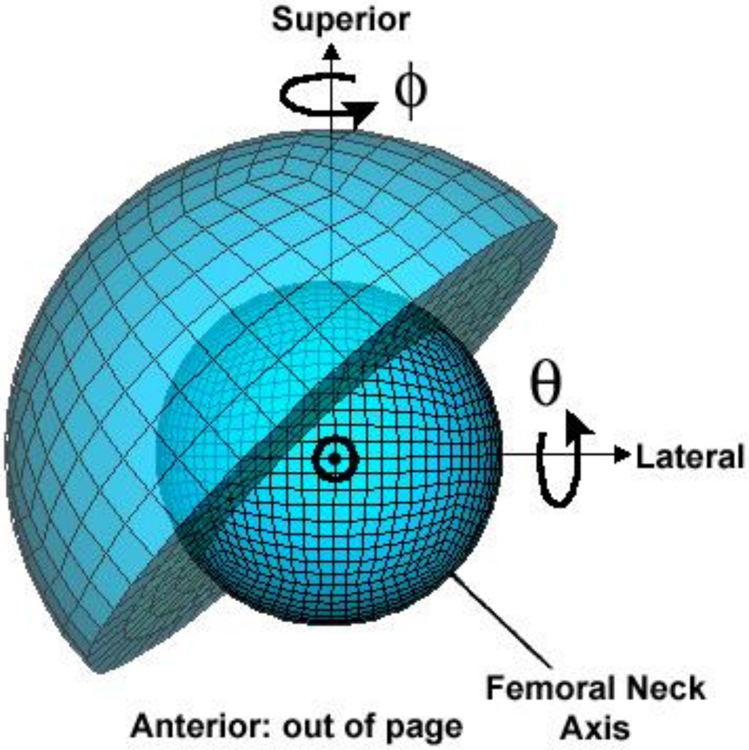

Figure 5: The sliding-distance-coupled contact finite element model [130] is shown. The femoral neck (not involved in articular contact) is omitted. The superior-anterior-lateral coordinate system is centered at the center of the femoral head. θ and ϕ indicate position, where (θ, ϕ) = (0º, 0º) is on the surface of the femoral head along the positive anterior axis. θ is about the negative lateral axis, and ϕ is about the positive superior axis.

This formulation was later extended by Brown et al. [28] to allow a specific area of the femoral head to be designated as isotopically roughened. In the isotropic roughening model, the instantaneous local wear coefficients were elevated for acetabular liner nodes in contact with femoral head surface elements that had been designated as roughened. Custom-written FORTRAN software calculated wear depths at each interval, and adaptively re-meshed the acetabular liner to reflect conformity/contact changes accompanying progressive material removal. Gawk, a pattern matching language, was used to find stresses in ABAQUS output files and to change nodal coordinates for the acetabular surface in the ABAQUS input deck. Unix scripts controlled this procedure, monitoring FE analyses, calling Gawk and FORTRAN programs, and starting new FE analyses. Custom scripts also tracked the coordinates of the roughening patch and elevated the local wear coefficient of acetabular nodes in contact with that patch, for each increment of the duty cycle.

This patch-roughened model was used to determine kinetically critical regions of femoral head roughening [130]. The model showed two such sites, of nominally comparable importance. These critical sites were located quasi-superiorly near the sagittal midline of the head, one slightly anterior and one slightly posterior of the coronal midline. The model also was used to explore the influence of non-identical duty cycles [169]. Without femoral head roughening, combination walk/stair-climb wear simulations did not result in appreciably higher volumetric wear than a walk-only simulation. But when a roughened zone was included, walk/stair-climb volumetric wear increased by approximately 57% above that of a similarly roughened walk-only simulation. This patch-roughened model was physically validated, and showed excellent agreement with experimental simulation of the same damage pattern, which had been produced physically by grit-blasting [27] (Figure 6).

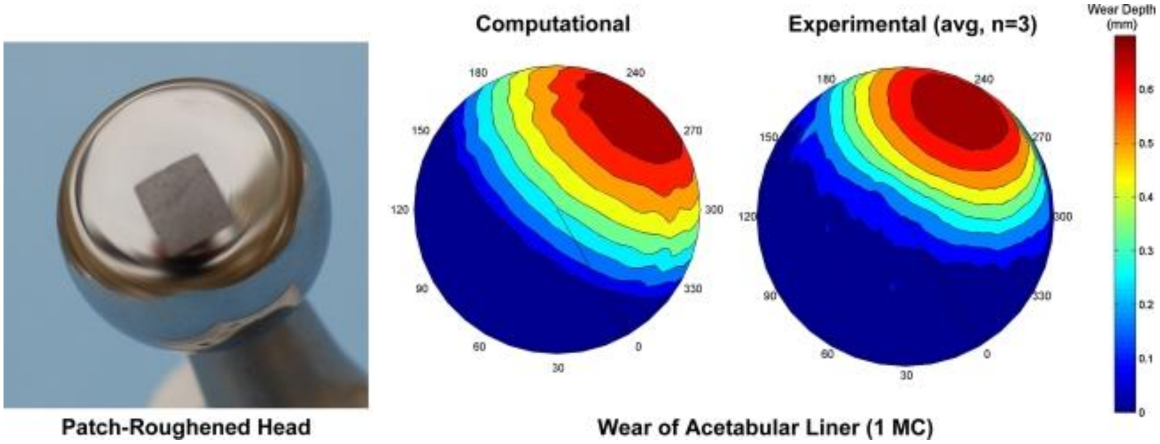

Figure 6: Validation trials for patch-roughening (by grit blasting) of otherwise undamaged femoral component heads showed close agreement with UHMWPE removal in a laboratory wear simulator [27].

Subsequent extensions of the sliding-distance-coupled FEA wear formulation are summarized in Table 3. Variations of this computational approach have been used to address the effects of cross shear [65], material nonlinearities [183], femoral head roughening [28, 130], non-identical duty cycles [52], creep [155], and frictional heating effects [65]. Computational models growing out of the Maxian et al. THA work have been applied in many other orthopaedic applications including total knees (TKRs) [55, 93, 94], total shoulders (TSRs) [79], total spinal disc replacements (TDRs) [23, 41], and hip resurfacing prostheses [125], as well as in non-implant machine bearings [156].

Table 3: Summary of computational wear studies in biomechanics, originally reported through 2009 by Goreham-Voss et al. [74].

Year	Author	Study Design	Wear Factor ($mm^3/(N\text{-}m)$)	Implementation of Contact/Geometry Updates
1996	Maxian et al. [136]	FEA of THR	1.07×10^{-6}	ABAQUS/Custom Script
1996	Maxian et al. [134]	FEA of THR	1.07×10^{-6}	ABAQUS/None
1996	Maxian et al. [135]	FEA of THR	1.07×10^{-6}	ABAQUS /Gawk Script
1997	Maxian et al. [137]	FEA of THR	1.53×10^{-6}	ABAQUS/None
1998	Pietrabissa et al. [160]	Analytical solution of THR with wear dependent on surface roughness (R_a)	$(0.235 \times 10^{-6}) \times (R_a)^{2.03}$	Custom Script/Custom Script
1999	Kurtz et al. [113]	FEA of frontside and backside wear in THR	1.07×10^{-6}	DYNA3D/ANSYS Script
2001	Raminondi et al. [164]	Analytical solution of THR with wear dependent on surface roughness (R_a)	$(8.68 \times 10^{-6}) \times (R_a) + (1.51 \times 10^{-6})$	Custom Script/Custom Script
2002	Teoh et al. [201]	FEA of THR with elastoplastic UHMWPE properties	1.07×10^{-6}	ABAQUS/Not reported
2002	Brown et al .[28]	FEA of THR with localized roughening	1.07×10^{-6}	ABAQUS/Custom Script
2003	Patil et al. [154]	FEA of THR with nonlinear elastic UHWMPE properties	1.07×10^{-6}	Marc/Not reported
2003	Wu et al. [198]	FEA of THR	8×10^{-7}	Fortran/Fortran
2005	Bevill et al. [13]	FEA of THR with creep	1.07×10^{-6}	ABAQUS/Python Scripting
2005	Lundberg et al. [130]	FEA of THR with localized roughening	1.07×10^{-6} where smooth	ABAQUS/Custom Script
2005	Fregly et al. [68]	Multibody dynamic/Elastic foundation simulation of TKR with creep	2.2×10^{-7}	ProMECHANICA Motion/Custom Script
2006	Penmetsa et al. [159]	FEA of THR with creep	1.07×10^{-6} (standard)	ABAQUS/Custom Script
2006	Kang et al. [99]	Simplified elasticity contact model of THR with standard and crosslinked UHWMPE	1.07×10^{-6} (standard) 2.00×10^{-7} (cross-linked)	Custom Script/Custom Script
2007	Lundberg et al. [131]	FEA of THR with localized roughening and outlier duty cycles	1.07×10^{-6} where smooth	ABAQUS/Custom Script
2007	Rawlinson et al. [166]	FEA of TDR with experimental calibration	1.98×10^{-6}	ABAQUS/Custom Matlab

Table 3 - continued

2007	Hopkins et al. [86]	FEA of TSR	1.53 x 10^{-6}	PAMCRASH/None
2007	Fialho et al. [65]	FEA of THR with heat effects	1.07 x 10^{-6}	ANSYS/None
2007	Knight et al. [104]	Rigid body FEA of TKR and experimental verification	2.64 x 10^{-7}	ABAQUS/Python Scripting
2007	Sfantos and Aliabadi [172]	Boundary Element Method (BEM) of THR	1.5 x 10^{-6} to 1.8 x 10^{-6}	Custom Script / Custom Script
2007	Sfantos and Aliabadi [173]	BEM of THR	2.63 x 10^{-10}	Custom Script / Custom Script
2008	Pal et al. [153]	Probabilistic, Explicit FEA of TKR	2.63 x 10^{-6}	ABAQUS / Not reported
2008	Liu et al. [127]	FEM of Metal-on-Metal hip resurfacing prosthesis	1.13 x 10^{-8} (bedding-in phase) 1.20 x 10^{-9} (steady-state phase)	ABAQUS / Custom Script
2008	Zhao et al. [201]	Multibody dynamic/Elastic foundation simulation of TKR with creep	2.59 x 10^{-7}	ProMECHANICA Motion / C++ Script
2009	Kang et al. [100]	Simplified elasticity contact model of THR with cross-shear	Dependent on cross-shear and contact pressure	Custom Script / Custom Script
2009	Willing et al. [197]	FEA of TKR with creep and direction dependence	Dependent on sliding direction and creep	ANSYS/ Matlab Script
2009	Strickland and Taylor [179]	Retrospective rigid body analysis of wear tests in literature	Dependent on cross - shear	MSC.ADAMS/ None
2010	Goreham-Voss et al. [74]	FEA of TDR with cross-shear	Dependent on cross - shear	ABAQUS/UMESHMOTION
2010	Barreto et al. [10]	Influence of pelvic bone on THR wear	1.07 x 10^{-6}	ABAQUS/None
2011	Abdelgaied et al. [2]	FEA of TKR with cross-shear and creep	Dependent on cross - shear	ABAQUS/Matlab script
2011	Liu et al. [126]	FEA of metal-on-metal hip resurfacing prosthesis	Dependent on cross-shear and contact pressure	ABAQUS/Not reported
2011	Li et al. [123]	FEA of articular cartilage	Dependent on experimental results	ProMECHANICA Motion/Custom Script
2011	Ribeiro et al. [167]	FEA of anatomical and reversed shoulder components	1.53 x 10^{-6}	ABAQUS/None
2012	Goreham-Voss et al. [75]	FEA of TDR with cross shear	Dependent on cross - shear	ABAQUS/UMESHMOTION
2014	Kruger et al. [108]	FEA of THR with scratch damage	Dependent on scratch lip height	ABAQUS/UMESHMOTION

Table 3 – continued

2013	Queiroz et al. [163]	Acetabular liner wear according to lateral tilt	1 x 10^{-6}	ANSYS/None
2013	Uddin et al. [187]	FEA of hard-on-hard joint prostheses	Ceramic-on-ceramic 0.2 x 10^{-8}. Metal-on-metal (running in) 0.5 x 10^{-8}. Metal-on-metal (steady state) 0.15 x 10^{-8}	ANSYS/Not reported
2014	O'Brien et al. [150]	Energy dissipation and cross-shear of TKR	Dependent on cross-shear and energy	ABAQUS/Python Script
2014	Elkins et al. [58]	Wear at trunnion interface in THR	1.13 x 10^{-8}	ABAQUS/None
2014	Zhang et al. [200]	Wear at trunnion interface in THR	Based on dissipated energy	ABAQUS/UMESHMOTION

Note: 'None' indicates that wear calculations were based on a single contact analysis, without evolution of surface topography. 'Not reported' indicates that the study included evolving surface topography, but did not specify method of implementation.

While the patch-roughened model showed excellent agreement with a physical simulation of the same damage pattern [27], it required finite-area roughening zones that were discretizable in terms of surface element facets having elevated Archard wear factors. In contrast, retrieval implants typically show damage in the form of (infinitesimal area) multi-directional scratching (Figure 7a), directional scraping (Figure 7b), and/or raised transfer deposits (Figure 7c), which make a damage-feature-based rather than an area-based damage representation a better approximator for actual clinical damage. To pursue this direction, the sliding-distance-coupled FE model was modified to allow for computations of wear acceleration due to these specific damage features.

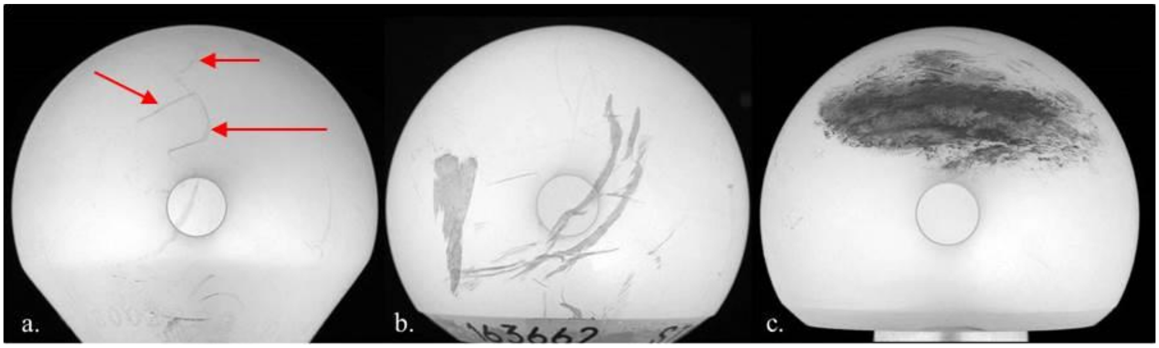

Figure 7: Retrieval femoral heads displaying (a) scratch (indicated by red arrows), (b) scrape, and (c) transfer deposit damage.

Scratch-based finite element model

The damage-feature-specific formulation was first developed to allow computation of wear rate increases due to isolated scratches [108]. The locations of these scratches were registered to the original, undamaged FE model. The scratch-based model utilized the adaptive meshing capabilities of the ABAQUS UMESHMOTION subroutine to account for conformity changes associated with wear of the PE surface [74]. The ABAQUS adaptive meshing capability allowed the user to specify a set of elements for which ABAQUS would automatically adjust interior nodes to maintain element geometric quality. The user could also select exterior regions (surfaces, edges) on which to define mesh constraints, which specify nodal motion independent of stresses and strains. Thus, material removal was able to be simulated by moving surface nodes in a direction normal to the surface, while ABAQUS automatically adjusted interior nodes to preserve admissible element geometry. Such mesh updates were performed at discrete intervals (typically each 41,667 physical duty cycles), corresponding to approximately 15 days of *in vivo* service). The user-defined UMESHMOTION subroutine was custom-written in FORTRAN, so that a full wear test simulation could be completed within a single ABAQUS job.

The ABAQUS subroutine UFIELD allowed outputs specific to wear simulation (such as sliding distance and local wear depth) to be easily calculated and stored as user-defined field variables as the analysis progressed. The volumetric wear of the polyethylene liner was reported by the ABAQUS history variable VOLC, which was reported following each mesh update.

This formulation augment was implemented in ABAQUS v6.9.1. The FE model utilized brick continuum elements for the titanium cup backing and PE liner, and it used rigid quadratic surface elements for the femoral head. The titanium acetabular liner backing and the PE liner were assigned linearly elastic material properties, with a Poisson's ratio of 0.3 and with elastic moduli of 110 GPa and 1400 MPa [183], respectively. The wear coefficient of this model was based on conventional (i.e., non-highly-crosslinked) UHMWPE. Generally, similar relative behavior would be expected for HXPE, although not quite proportionately so, due to the material removal nonlinearity. Femoral head boundary conditions were applied through a rigid body reference node located at the femoral head center.

Additions were made to the standard UMESHMOTION subroutine to allow for areas of polyethylene that were overpassed by specific femoral head damage features to be determined (Figure 8). The wear coefficient of those overpassed areas was then elevated based on the severity (as measured through OP scanning, discussed below) and the relative motion directionality of each individual damage feature.

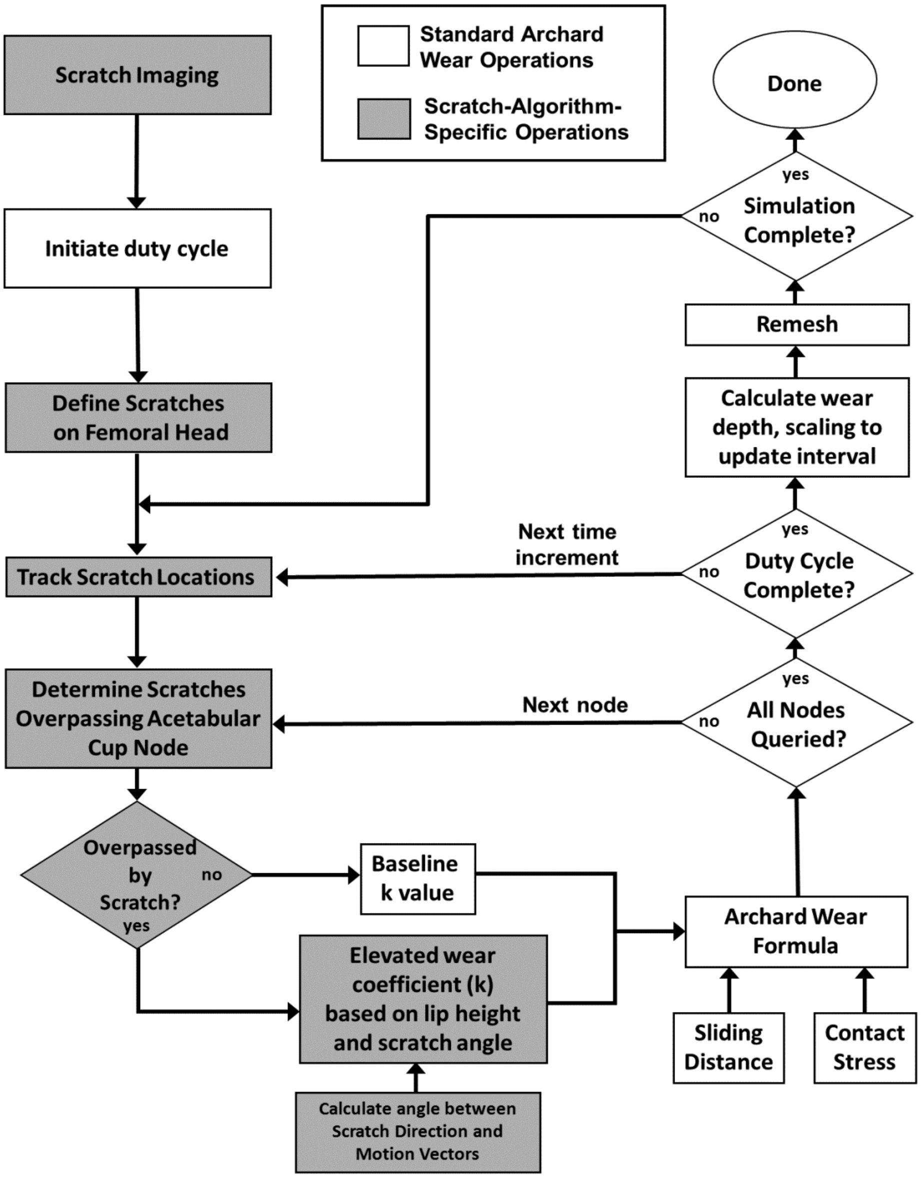

Figure 8: Flowchart of scratch-based FE wear model

Scratches were modeled as concatenations of discrete, straight-line segments. Each such scratch segment was represented by its two endpoints and its average lip height. Scratch endpoints were imported to the FE model as an additional node set, which was prescribed to have the same rotational boundary conditions as the rigid femoral head. This node set had no defined elements, but rather acted simply as a placeholder for the scratch locations during the duty cycle. A lookup table, called by the FORTRAN subroutine UEXTERNALDB, identified each scratch segment's lip height.

The UMESHMOTION subroutine was written so as to also allow the motion of each such scratch segment to be tracked throughout the duty cycle. For each increment of the cycle, the coordinates of the ends of the scratch segment at the beginning and termination of the increment were used to determine the trapezoidal area overpassed by the segment (Figure 9a). The plane of this trapezoid was calculated in three dimensions, and its scalar area was evaluated. For each node on the acetabular cup surface, a position vector from the cup center to that node, along with the intersection point between that position vector and the trapezoid plane, were calculated. For each such vector, the area of four triangles was computed, each triangle being formed by one edge of the trapezoidal area and by the two lines connecting those two edge endpoints to the intersection point. When the surface area of these four triangles was equal to the trapezoidal area (within 1% accuracy, to allow for rounding errors), the node necessarily fell within the area overpassed by the scratch segment, and its wear coefficient was correspondingly elevated. If the node did not meet this equal-area criterion, it was flagged as not falling within the trapezoidal region. For nodes not overpassed by the scratch, the wear coefficient was kept at baseline value. This procedure was executed for each scratch segment.

At each time step, the angle θ between the scratch segment's orientation and its direction-of-motion was also calculated (Figure 9b). The direction-of-motion vector was computed using the midpoint of the scratch segment at the beginning and termination of the increment. As noted above, physical wear tests [73] had shown that when this angle is highly acute, wear increases of up to an order of magnitude are experienced due to a slicing/shearing mechanism. The wear coefficient of scratch-overpassed nodes was correspondingly elevated, based on this relationship between θ and wear elevation. The referenced bench tests had been carried out in 5° increments. Of the various angles tested, only the 15˚ case had shown statistically significant acceleration over the other angles for conventional UHMWPE. In the present formulation, therefore, when the relative angle (θ) was between 13˚ and 17˚, it was designated as being in this critical range.

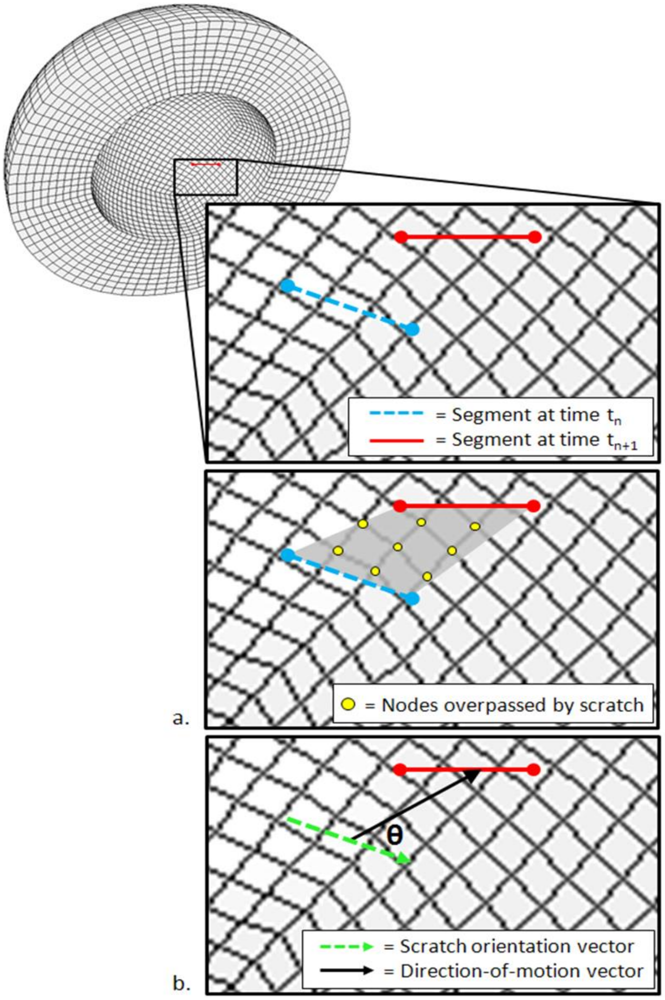

Figure 9: Identification of acetabular cup nodes overpassed by a scratch segment during a given time increment. a. The delimit points of the scratch segment at time t_n and time t_{n-1} were used to define the vertices of the trapezoidal area (shaded) overpassed by the scratch. Each node of the acetabular cup surface was tested to determine if it fell into this overpassed area. b. Scratch segment orientation and direction-of-motion vectors were used to calculate the angle θ between the two vectors. The endpoints of the segment at time t_n were used to define the scratch segment orientation vector. The direction-of-motion vector was calculated using the midpoints of the scratch segment at time t_n and time $t_{n-1.}$

Wear coefficient elevation was scratch-segment-specific, and was dependent on the scratch's lip height. Physical wear results from the literature [50] were used to infer a relationship between scratch severity and wear acceleration. A series of single-scratch bench studies (as reviewed above) had shown that wear elevation is dependent primarily on the amount of metal piled up along the lip of the scratch, rather than on the scratch's depth or width. Using the data from those earlier bench studies, a power law relationship was identified for implementation in the wear model:

$$k_{inc} = 58.0985\text{-}58.0985 \cdot e^{-0.2237*h_L}$$

where k_{inc} is the scratch-dependent incremental wear coefficient scaling factor and h_L is the peak scratch lip height, in microns (Figure 10). The k_{inc} value was then further scaled to incorporate the relative motion directionality, θ. The algorithm allowed for a summation effect if a single acetabular node was overpassed by multiple scratch segments, with the total wear coefficient elevation taken as being equal to the sum of each overpassing segment's elevation factor.

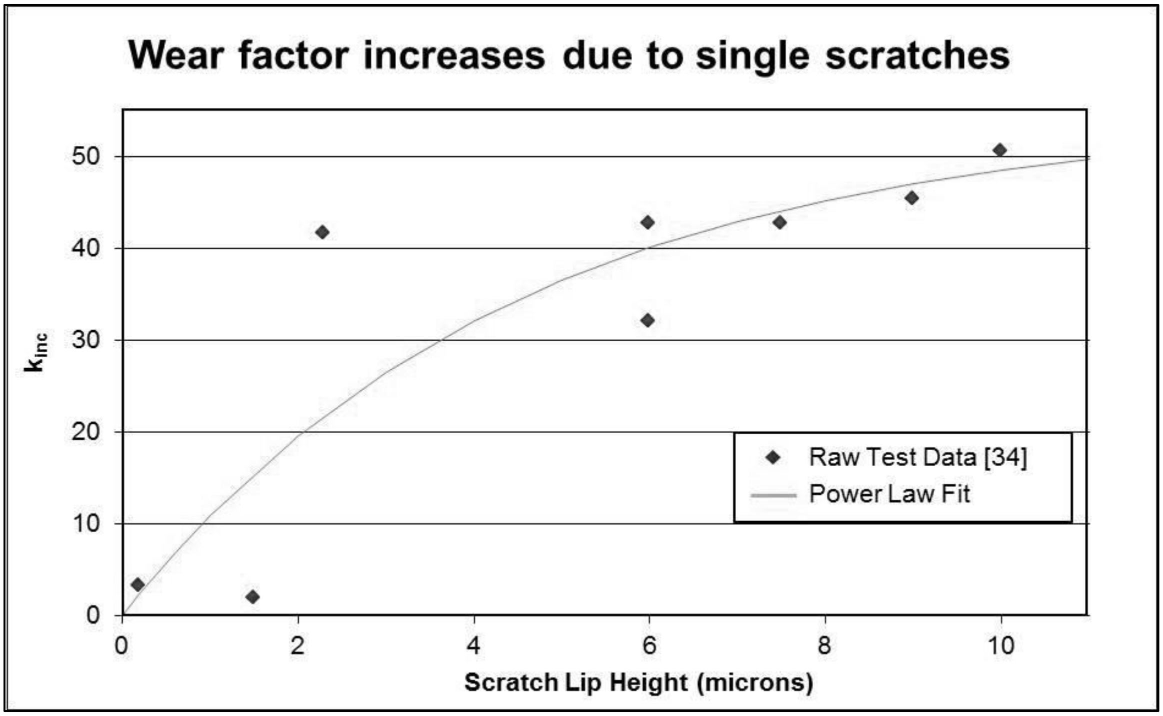

Figure 10: Single-scratch bench study data were used to generate a power law relationship between wear coefficient elevation and scratch lip height (as measured in microns.) Power law fit was performed by the author (KMK).

To pilot test the functionality this scratch-based damage approach, a simple model was created that had five parallel scratches near the pole of the femoral head, each scratch being 5 mm in length and having lip heights of 1.3 μm. This model showed detectable increases in both linear and volumetric wear (Table 4). The UFIELD subroutine allowed for wear depths to be plotted over the entire wear domain to visualize the varying patterns of wear depth (Figure 11). These wear contours displayed the computed wear depth at each node identified in the adaptive mesh domain.

Table 4: Wear increases due to a single scratches.

	Undamaged Head	**Scratched Head**
Linear Wear (*mm*/10^6 *cycles)*	.0843	.0855
Volumetric Wear (*mm*^{3}/10^6 *cycles*)	27.7	30.1

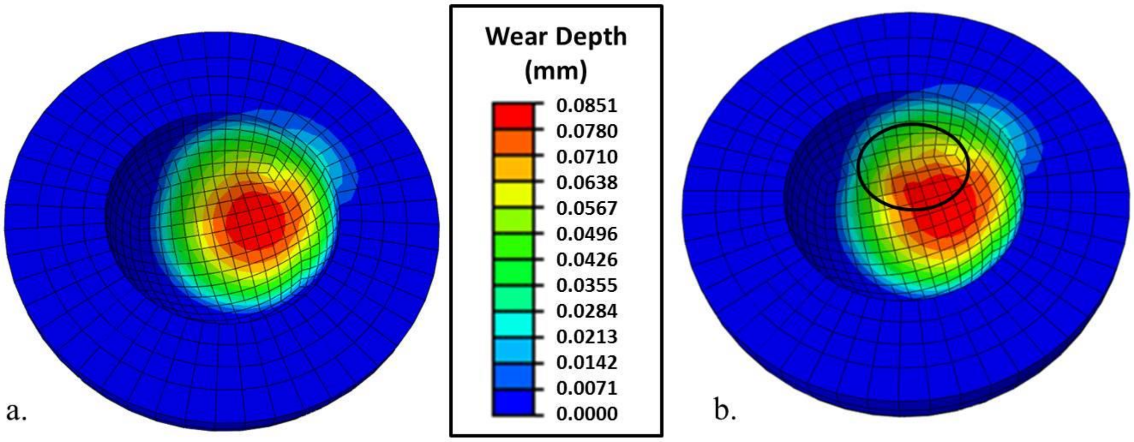

Figure 11: Functionality test for the scratch-based wear simulation algorithm. Wear of an UHMWPE acetabular cup (a) articulating against an undamaged femoral head, and (b) against a scratched femoral head was considered. The area of increased wear depth is indicated on the scratched head wear contour.

Validation

As a next step, the scratch-based wear algorithm was validated through simulation of three previous laboratory wear tests. In the physical wear tests [8, 61], damage had been created by stylus ruling of discrete scratches on an otherwise pristine femoral head. Three equally spaced scratches had been used, with each scratch extending 180˚ from the equator, through the pole, and back to the equator, to form a stellate pattern (Figure 12).

Experiments with scratch lip heights of 0.29 μm and 2.9 μm had been reported by Barbour et al. [8], and experiments with scratch lip heights of 2.0 μm had been reported by Endo et al. [60] (3 replicate specimens for each). Corresponding FE models were built to replicate this stellate pattern. Each scratch was discretized into scratch segments approximately 2 mm in length, for a total of 60 scratch segments. Elevations of wear were computed, relative to a baseline situation of an undamaged femoral head (Figure 13). Wear acceleration was defined as the wear volume of the damage head FE model divided by the wear volume for a simulation of an identical diameter undamaged femoral head. The FE model correctly predicted relative wear acceleration to within approximately 4%, 8%, and 10% for the 0.29 μm, 2.0 μm, and 2.9 μm lip height cases, respectively.

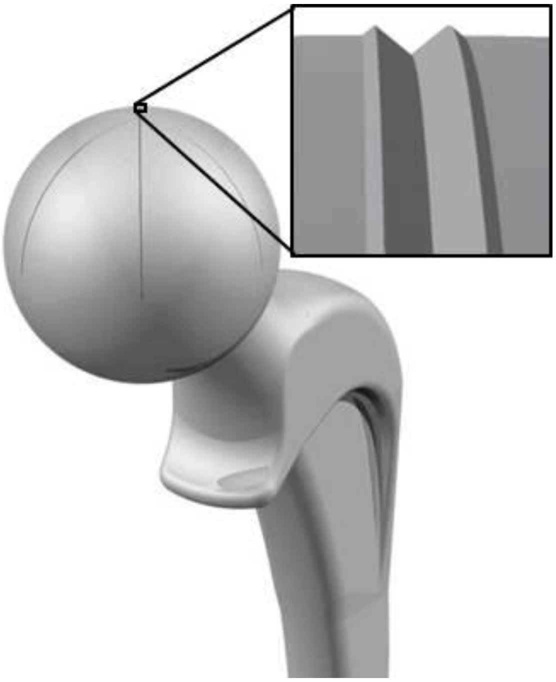

Figure 12: Stellate pattern of scratches to femoral head, for physical validation simulation.

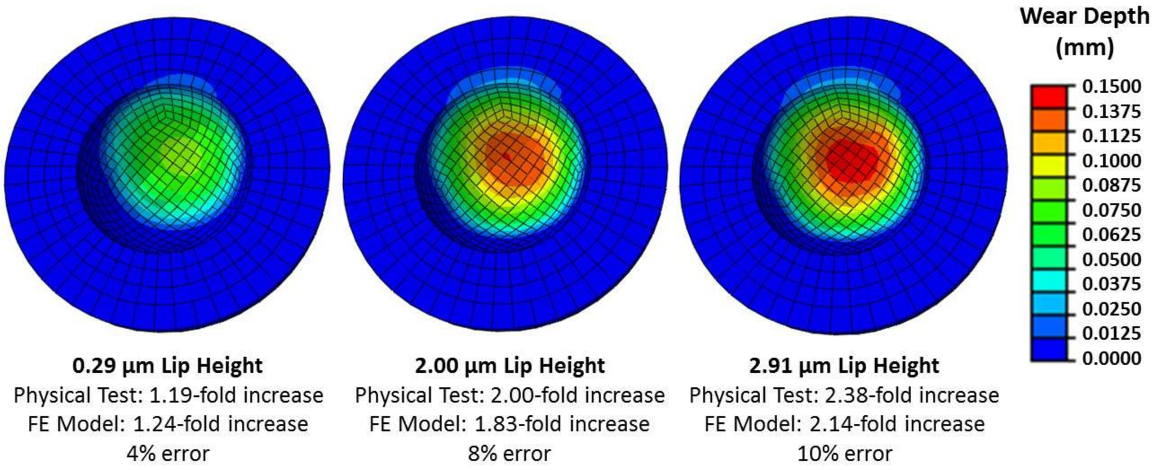

Figure 13: Computed distribution of linear wear and comparison to previously published physical wear tests. Physical wear test results had been reported by Barbour et al. [8] for 0.29 μm and 2.91 μm cases and by Endo et al. [61] for the 2.00 μm case.

Further validation was completed using a much more severe damage simulation, a spirograph pattern ruled onto the femoral head using a diamond indenter. This pattern was chosen to reflect the multidirectional nature of scratches found on retrievals (Figure 14) [122]. The FE model was able to reproduce the extremely elevated wear rate accelerations (4.6-fold) reported in the physical wear tests to within 8.5% (Figure 15). While not replicated in the FE model, physical wear tests of femoral heads with this spirograph pattern had also been run against two commercial HXPE liners. Those results showed lower wear volumes, as expected. However, the relative wear increases compared to simulations using undamaged heads were higher for both cases. Results such as this dataset could be used to replicate various types of polyethylene in the present FE model.

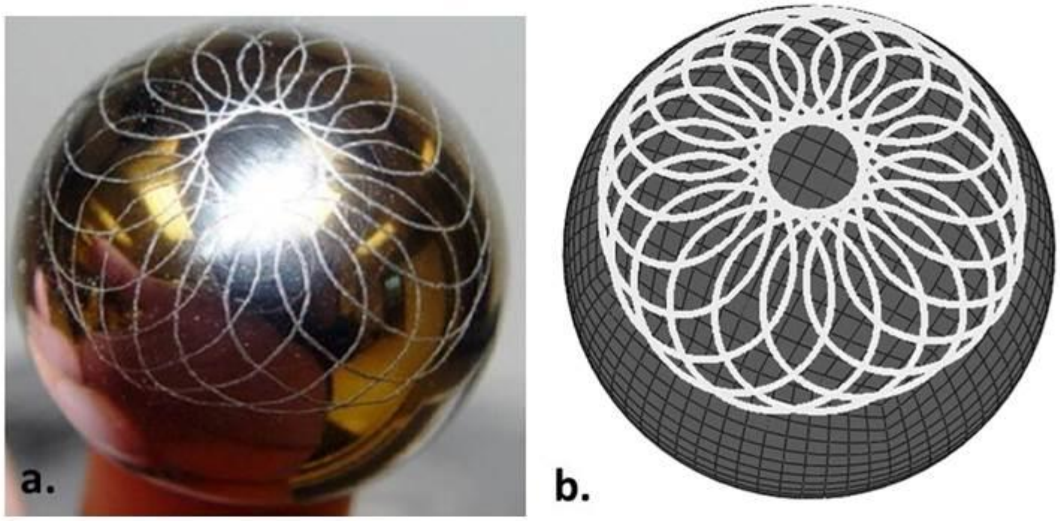

Figure 14: Multi-directional spirograph scratch around the superior point of the femoral head (a) on a physical head and (b) in FE model.

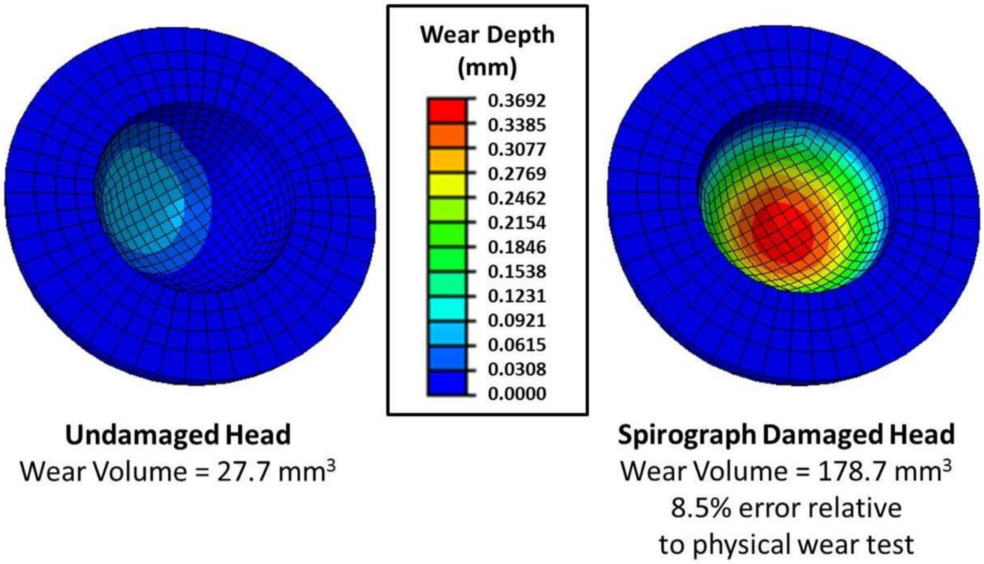

Figure 15: Comparison of wear depths computed for undamaged versus spirograph-damaged femoral heads

Finite element formulation for scrapes and transfer deposits

The sliding-distance-coupled FE model was further augmented to allow for wear simulation of clinically observed damage features for which the scratch-based representation was not appropriate. These "other" damage features were of two types: scrapes and transfer deposits. Both of these other two damage types tend to result from subluxation and dislocation events, and involve regions of net material pile-up above the surrounding surface. They differ however in appearance on OP scans, in that scrapes appear as collections of tightly packed micro-scratches with a preferred orientation (Figure 16), whereas transfer deposits show no preferential orientation (Figure 17). The lack of apparent directionally in the transfer deposits may be the result of multiple subluxation and/or dislocation scraping events (in non-identical directions) over the same areas, resulting in large regions of material built-up, for which directionality is inapparent due to "overwriting".

Scrapes were represented in the FE model as concatenations of triangular- or quadrahedron-shaped sectors. Sector-average roughness (R_a) and directionality were used to characterize the severity of this damage type. Average roughness was used because the tightly packed "micro"-scratches did not lend themselves to being discretized into individual scratches in the same manner as could be done for isolated "macro"-scratches. R_a has been validated as reasonably predictive of wear acceleration for larger damage patches [27], a situation much more similar to scrapes than to very narrow scratches.

The scrape damage assessment differed from the previous patch-roughened model, however, in that it also allowed for damage directionality to be modeled, rather than assuming the damage to be isotropic. The scrape-based wear algorithm also differed from the earlier patch-roughening algorithm in that it computed the total area of polyethylene overpassed by each scrape sector during each time increment, as opposed to only the area of polyethylene in contact at the end of the increment. The step of including area overpassed was applied in the same manner as for the scratch-based wear algorithm, with each scrape edge being treated like a scratch segment, and with the acetabular nodes overpassed by each edge being determined. A previously derived relationship [49] was used to relate wear acceleration to R_a:

$$k_{inc} = 37.538 \cdot (Ra)^{1.2}$$

Each triangular or quadrahedral scrape sector was identified in the FE model by its three or four vertices and by a directionality vector. For each time increment, the angle θ between this directionality vector's orientation and the sector centroid's direction of motion was also calculated. Similar to the scratch algorithm, when an area of polyethylene was overpassed by the scrape sector, its wear coefficient was elevated, based on the scrape sector's R_a value and its relative motion directionality.

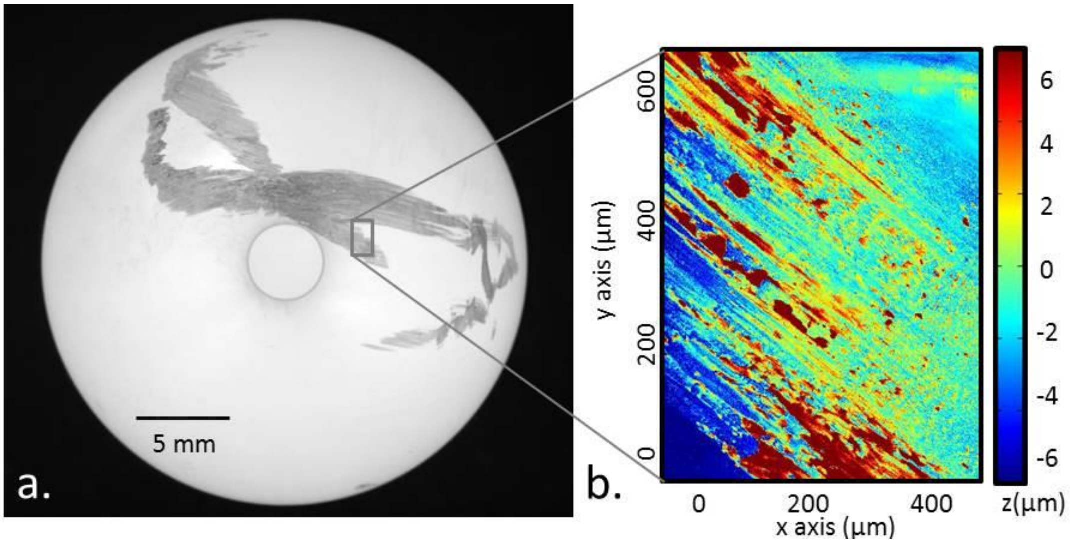

Figure 16: Example of scraped retrieval femoral head. (a) Global photograph. (b) OP scan displaying characteristic “micro”-scratch damage.

Damage due to bearing-foreign material deposition consisted of large, “mesa”-like areas of roughening, raised from the surrounding undamaged surface. Deposition damage differs from scrape damage in that there is no apparent orientation to the deposition, again illustrated by OP scans (Figure 17). With deposition damage, three mechanisms potentially contribute to wear acceleration [110]. First, the presence of the raised deposit changes (global) surface congruency and therefore influences the contact stress distribution (height effect). Second, when an area is overpassed by the edge of a deposit, the wear coefficient is elevated depending on the height and directionality of the deposit edge (gouging effect) [50, 73]. Third, when a given area of the cup is in contact with the deposit, the wear coefficient would be elevated based on the surface roughness of the deposit [50] (roughening effect). The transfer deposit in Figure 17 was shown to be raised approximately 9 μm from the surrounding area, as measured by OP scans. These OP scans also showed the deposit to have R_a values in the range of 0.2 μm to 0.9 μm, values multiple orders of magnitude higher than undamaged regions.

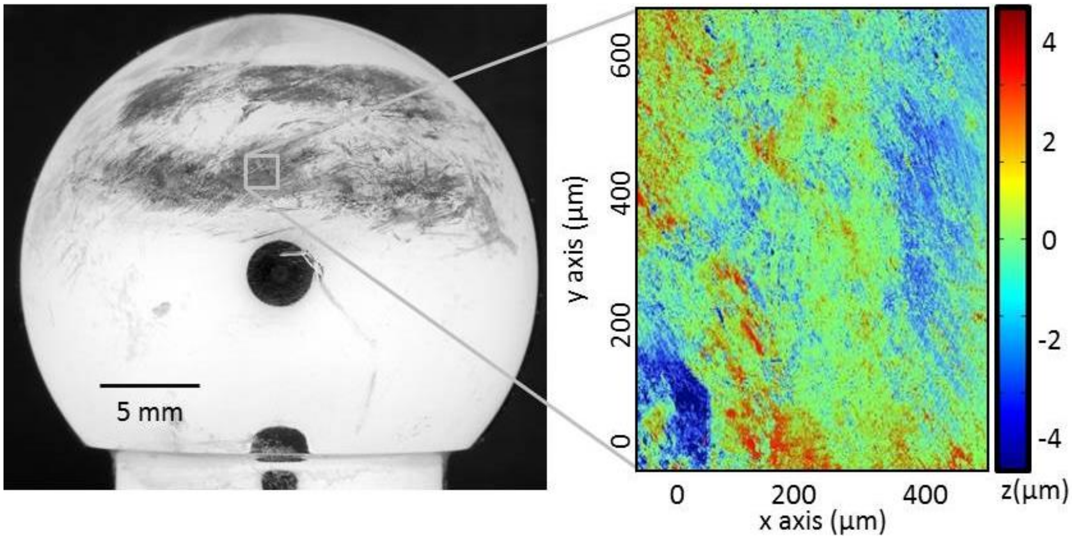

Figure 17: Example of transfer deposit region on retrieval femoral head. (a) Global photograph. (b) Micro-level OP scan displaying characteristic surface morphology.

To represent these three potential wear mechanisms of transfer deposits in the FE model, elements on the femoral head covered by the deposit were first identified. The surface nodes of those elements were extruded from the surrounding surface by a distance equal to the local deposit height. Changes in stress due to this height effect were computed by the FE model. The boundary of the deposit was defined by a collection of straight-line segments. The areas of polyethylene overpassed by these edges were elevated based on the height of the deposit, similar to the logic used to characterize scratch overpassages. Finally, the wear coefficient for areas in contact with the deposit was elevated based on the R_a value of the deposit, similar to the treatment used for scrapes (except that the deposits were modeled as isotropic).

CHAPTER 3: DAMAGE IDENTIFICATION AND QUANTIFICATION

A goal of the damage-feature-based FE algorithm was to predict wear acceleration due to damage observed on actual retrieval femoral heads. To gather the necessary input data for these FE models, a novel multi-stage, multi-scale imaging procedure was developed for identification, localization and quantification of regions of femoral head damage [107]. Identified femoral head damage features were imported to the FE model to predict the wear acceleration as a function of the damage present on specific femoral head retrieval specimens.

Diffused-light photography

Femoral head damage has historically been difficult to visually document, due to room-feature image reflection from the highly polished metallic surface. A novel global-level diffused-light photography technique [82] was introduced to overcome this problem. This technique involved digitally photographing the femoral head while it was positioned inside of a matte-finish, translucent tube snugly fitted around the camera lens (Figure 18)[*]. The tube eliminated extraneous reflections of ambient room objects caused by the highly reflective metallic femoral head surface. This new lighting technique dramatically improved the ability to visually observe the apparent physical damage (Figure 19).

---

[*] Development of this diffused-light photography technique was led by Dr. Anneliese Heiner, with design assistance and digital image combination completed by the author.

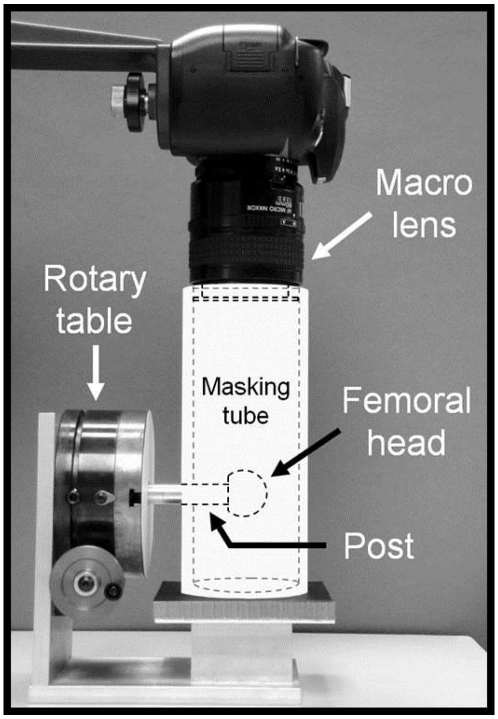

Figure 18: Diffused-light photography set-up. The (indexed) rotary table allows for global navigation on the femoral head, to register with high-magnification local OP scans.

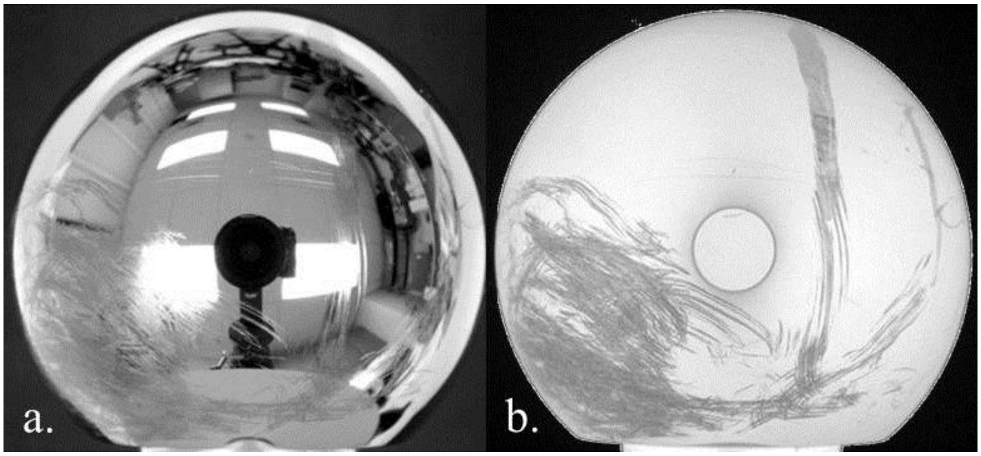

Figure 19: Retrieval femoral head photographed (a) under room lighting, and (b) with masking.

The femoral head was positioned on a rotary table to aid in global navigation on the femoral head. Photographs were taken from the polar direction and from multiple circumferential orientations, such that the entire bearing surface could be captured (Figure 20). On the polar image, the 0˚ location on the rotary table was positioned on the right side of the photograph. Circumferential images were shot in 30˚ increments, with each photograph identified by the rotary table coordinate at the photograph's center. This coordinate system allowed exact damage locations to be identified and used in an automated image alignment program, discussed below.

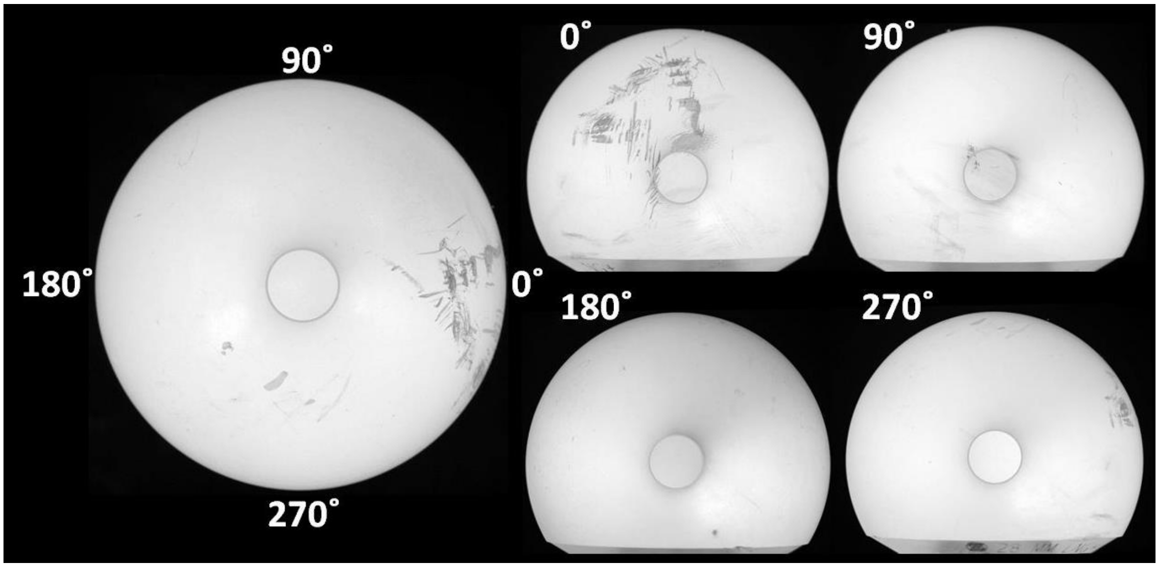

Figure 20: Polar view (left side), and circumferential views (right side) of a single femoral head. The coordinate on each circumferential view indicates the longitude coordinate at the center of the image, which corresponded to rotary table position.

The circle at the center of the femoral head shows the area of data "black-out" due to camera lens reflection (Figure 21a). The area of lens blackout on the original, base photograph was identified on a photograph taken at a different angle (Figure 21b).

Control points were identified from identifiable features near the blackout region on both images. Those control points were used to build an affine transform structure, which was applied to the second image so that the blackout area could be aligned to that area in the original image. The circular blackout area was cut out of that transformed image in Photoshop and overlaid on the blackout area of the original image (Figure 21c).

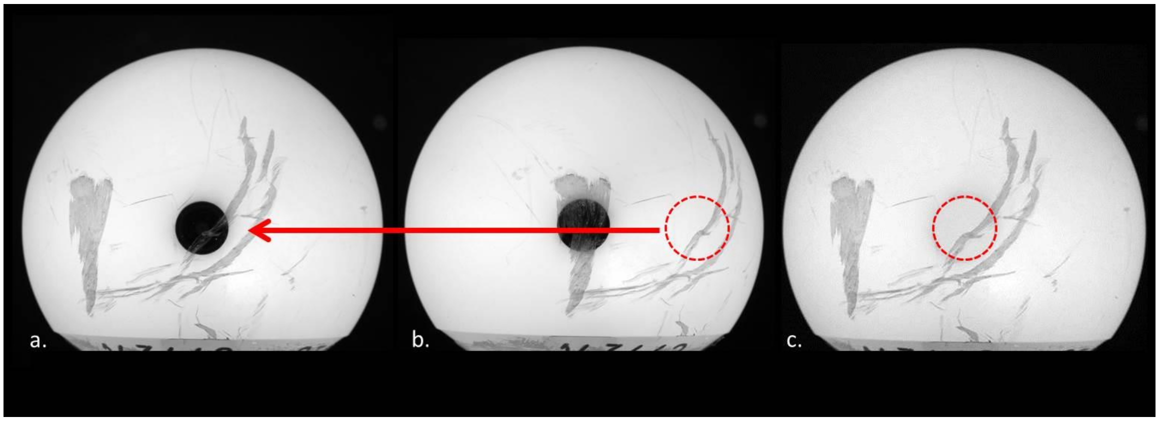

Figure 21: Digital combination of two circumferential images (a&b) taken 30˚ apart. The area of data blackout in (a) was identified in (b), and was transposed onto (i.e. substituted for) the first image's blackout region (c).

Resulting photographs were image analyzed to determine regions of damage. First, Canny edge detection was performed on the photographs to determine visually apparent regions of damage. The Canny filter is a commonly used image processing tool that enables multidirectional edge detection. This filter finds edges by calculating the local maxima of the gradient of the image being analyzed. This gradient is calculated using the derivative of the Gaussian filter [33]. Edges were flagged if their gradients fell above an analyst-set threshold (Figure 22). This threshold was set such that it was sensitive enough to detect the fine-scale micro-scratches, but insensitive enough so as not to be influenced by gray scale modulations due to subtle background brightness variations associated with the necessarily varying distance from and orientation relative to the camera lens.

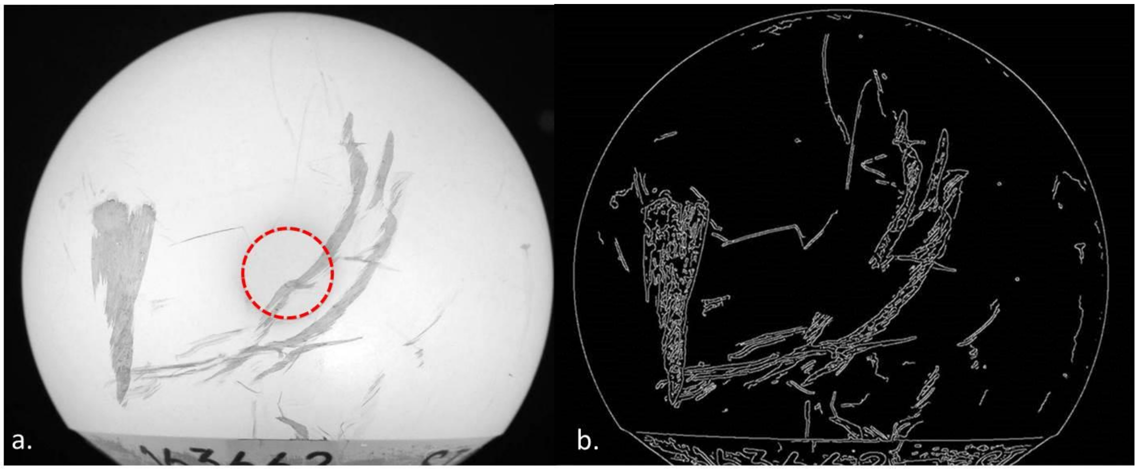

Figure 22: Damage identification. (a) Diffused-light photograph (b) Canny edge detection used to segment regions of damage.

Next, a median filter was applied to the original images. This filter replaced each pixel's intensity with the median of pixel intensities in a surrounding square region of analyst-specified size. This operation had the effect of "blurring away" line-like damage features (i.e. scratches) whose breadths were below a specific threshold. Analyst specification of the median filter size thus provided a basis for objectively distinguishing between scratches versus larger damage features (i.e. scrapes and transfer deposits). Various filter sizes were applied to a representative original image that contained both scratches and scrapes (Figure 23). A 20x20 filter size was judged appropriate for distinguishing between scratches and scrapes for retrievals analyzed. The diffused-light photographs used for this work were 3000 x 2000 pixels in size. The resolution of the photographs was 300 dpi, which was the maximum resolution capability of the DSLR camera used. For future work with this image processing procedure using different equipment, the median filter may need to be resized for new set-ups to properly separate scratch and scrape damage.

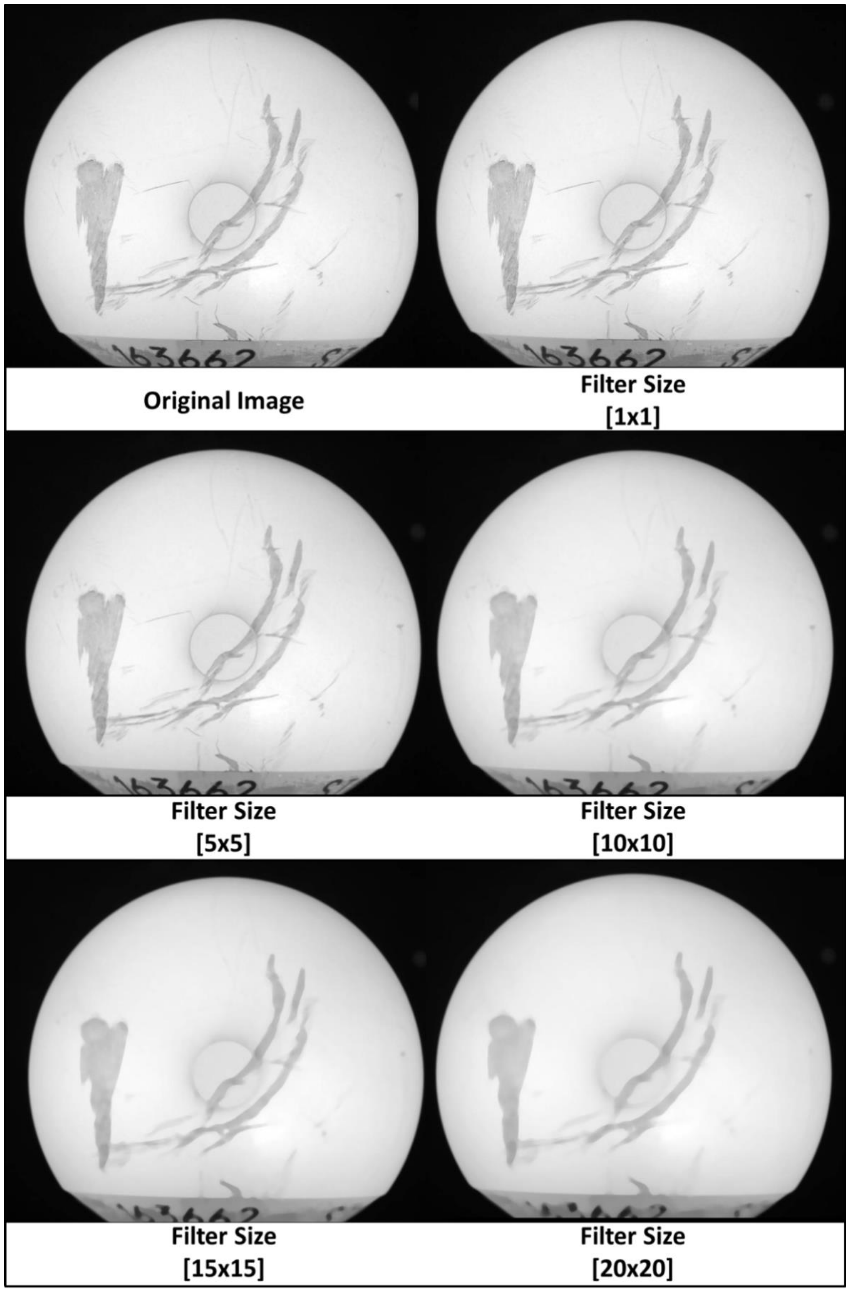
Original Image

Filter Size [1x1]

Filter Size [5x5]

Filter Size [10x10]

Filter Size [15x15]

Filter Size [20x20]

Figure 23: Successively stronger median filters of various sizes applied to an original image of a retrieval femoral head.

Regions remaining after median filter operation were classified as either scrapes or deposits. A preliminary analysis was performed on several retrievals, during which intensity values of common scrape and deposit features were recorded. Based on that analysis, an intensity threshold was determined, on the basis of which the darkened areas falling below that threshold were automatically identified as scrape or deposit regions. The analyst had the option to change this intensity threshold if damage features on a particular retrieval fell above this default threshold. These features were then removed from the pre-median-filtered Canny edge detection results. This left the remaining damage features to be classified as scratches (Figure 24).

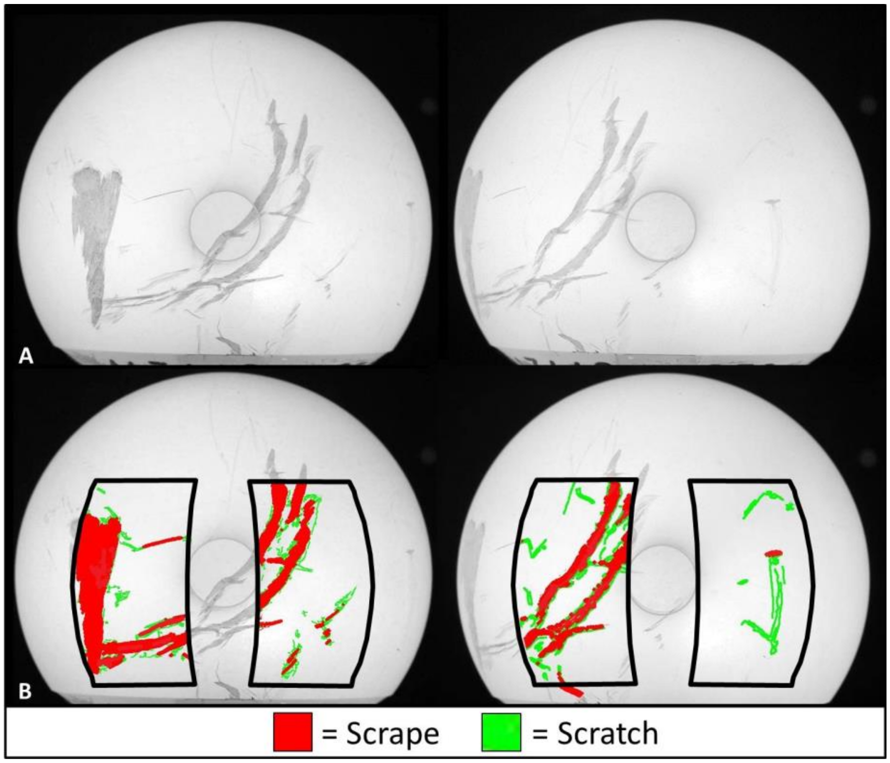

Figure 24: Scratch and scrape identification. (a) Diffused-light images of a femoral head displaying both scratch and scrape damage, captured from two orientation directions 30˚ apart circumferentially. (b) Image processed results characterizing regions of damage. The sectors outlined in black indicate regions of interest analyzed for this particular image. (The top of the femoral head was captured and analyzed in companion polar images.)

A Hough transform [52] was then used to discretize the scratch damage features into straight-line scratch segments (Figure 25). This transform was applied to the Canny edge detection result following the removal of the features identified as scrapes. This analysis technique used the equation of a straight line, defined in polar coordinates, to determine the number of Canny-detected edge points falling along any given candidate straight line. Those candidate lines whose lengths fell above an analyst-set threshold (typically 0.5 mm) were flagged, thus discretizing curvilinear scratches into concatenations of straight-line scratch segments.

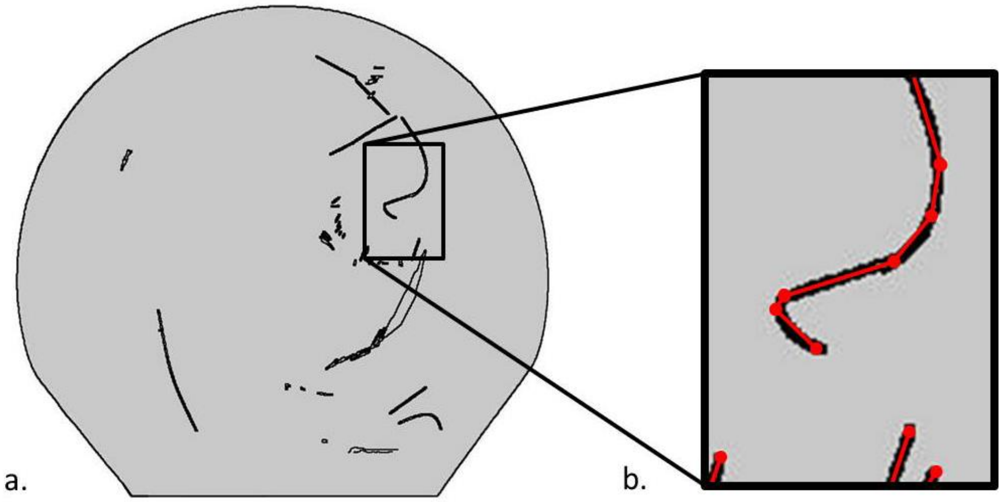

Figure 25: Discretization of scratch segments. a. Canny edge detection. b. Hough transform discretization of this damage into straight line scratch segments (red).

Quantification of damage severity

At the beginning of the author’s research effort, the then-recent development of a three-dimensional laser micrometry (3DLM) instrumentation system (Figure 26) held promise for fully automated local-to-global damage feature mapping [105]. The instrument utilized a laser micrometer (having an accuracy of 0.5 μm) and a specimen rotational stage and motor, whose stepper motor incrementally (0.05 degrees) rotated the specimen about a fixed axis. The laser scanned the surface to generate a 2D line profile for each specimen pose. These individual 2D profiles were reconstructed into a 3D point cloud. The point cloud contained on the order of 1 million data points and required approximately 40 hours of scan time to analyze the entire femoral head.

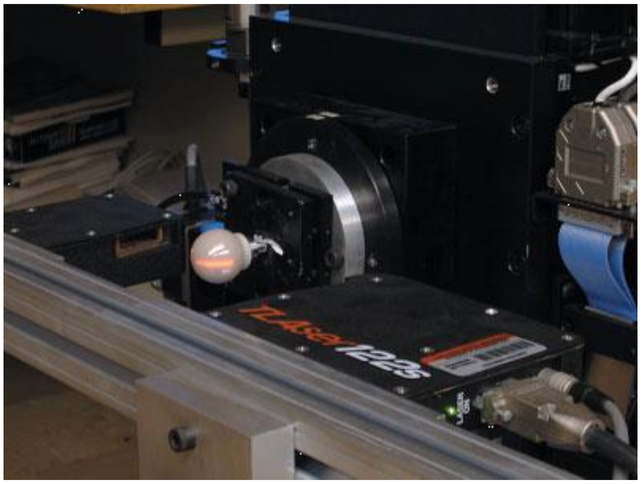

Figure 26: Femoral head in 3DLM system

The 3D point cloud was imported to Geomagic Qualify where it was converted to a triangulated solid surface. Geomagic had the capability to compare this surface to geometric primitives and report location-to-location variations. It was hypothesized that the 3DLM scans of damaged femoral heads could be compared to ideal spheres using this procedure, for which deviations could then be reported as scratches or other damage features. In pilot work, however, analysis of a scratched femoral head showed distortion on a global level, most prominent near the polar region of the head (Figure 27). This was considered to be a critical limitation, because it meant the polar region would not be able to be meaningfully analyzed. Since surface damage in the polar region has been shown to be kinetically critical in terms of wear acceleration [130], inability to quantify polar-region damage proved to be a major limitation for 3DLM in this application.

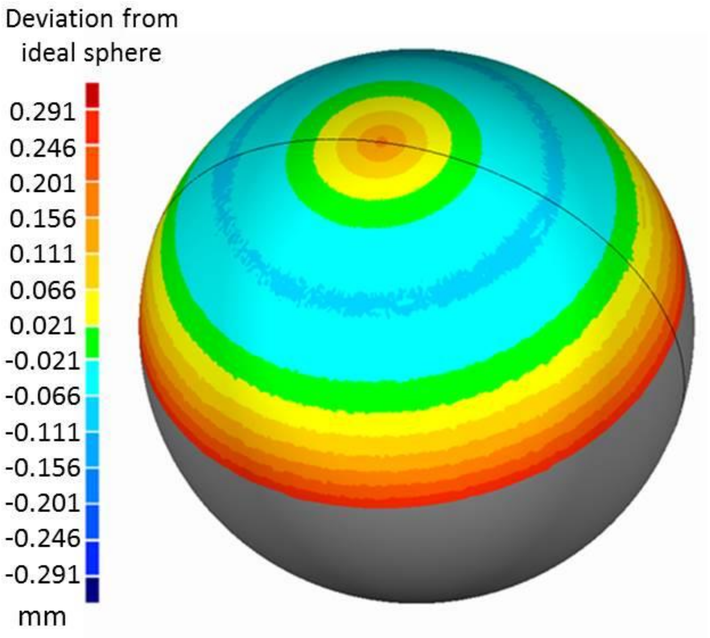

Figure 27: Comparison of 3DLM data to geometric primitive illustrating deviation from sphericity.

Another critical limitation was that the 3DLM scanner was unable to detect micron-sized scratches on the head. A femoral head containing five laboratory-created scratches (Figure 28a) was scanned using this setup. The scratches had peak lip heights on the order of 1 μm. When the resulting surface was compared to an ideal sphere, a significant area of scratching proved undetectable (Figure 28b). Because scratches of this level of severity had been shown to cause substantial increases in wear [50, 67], it was concluded that the 3DLM instrument was not suitable for detecting wear-consequential damage on retrieval femoral heads.

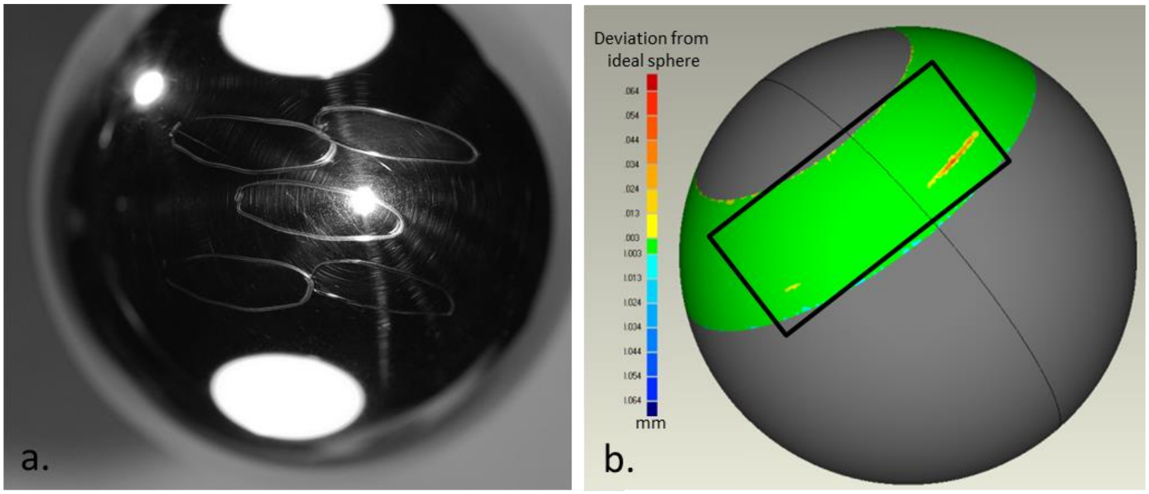

Figure 28: 3DLM limitation. a. Laboratory-created femoral head scratches on a test specimen (room lighting not masked). Peak lip heights were on the order of 1 μm. b. 3DLM scan sector compared to an ideal sphere. The black box indicates the approximate location of the scratches. A majority of these scratches proved undetectable by 3DLM.

Due to these limitations of the 3DLM, a different approach to damage quantification was obviously necessary. An attractive possibility in that regard was optical profilometry. While most previous applications of OP had resorted to judgment-based spot samplings [57], the high speed and 3D capabilities of OP scanning in principle allowed for selected substantial fractions of entire joint surfaces to be analyzed. Since the global photograph image processing program was able to identify specific areas of femoral head damage, there would not be need for the entire femoral head to be OP scanned.

Early in this phase of work, femoral heads with minimal amounts of damage were selected, to provide relatively “easy” cases conducive to development of this analysis. As preliminary work and further experience with the OP set-up showed that progressively larger areas of femoral head damage could be analyzed, femoral heads with progressively more extensive damage were analyzed. Finally, the large number of OP scans required to scan very large damage areas prompted the development of an automated image processing routine for damage encoding, although physical scans still needed to be performed manually. In the future, addition of a stepper motor to the OP positioning stage potentially could provide full automation for measuring head damage features and encoding them into FE wear models.

As noted above, OP captures surface features by means of light interferometry. Veeco non-contact profilers (Wyko NT1100 and Contour GT, Bruker, Tuscon, AZ) were used, which have a maximum in-plane resolution of 0.25 μm^2, and maximum out-of-plane resolution of 0.01 μm. These instruments were capable of directly imaging individual areas of sizes up to ~1 mm x 1 mm, and could autostitch those captured individual images into composite images sized up to ~ 5 mm x 5 mm. Scans were obtained at a scanning speed of 14 μm^2/sec. The “backscan” parameter on the OP software controlled the distance the lens moved up from its starting position, which distance needed to be increased when taller surface features were encountered. Scanning time was typically on the order of 15-30 seconds per 1 mm x 1 mm scan, with more severe damage features requiring the longer scan times due to the necessarily longer vertical lens traverse.

The instruments’ internal software allowed for removal of the global spherical curvature that was present in raw femoral head scans (Figure 29). The parameters of global spherical curvature were estimated using a least-squares-error algorithm to achieve a quadratic fit to the raw surface data. Removal of this spherical form from the raw data therefore enabled determination of local deviations from the native implant surface. The internal software also included capability to report standard surface roughness parameters (R_a, R_p, etc).

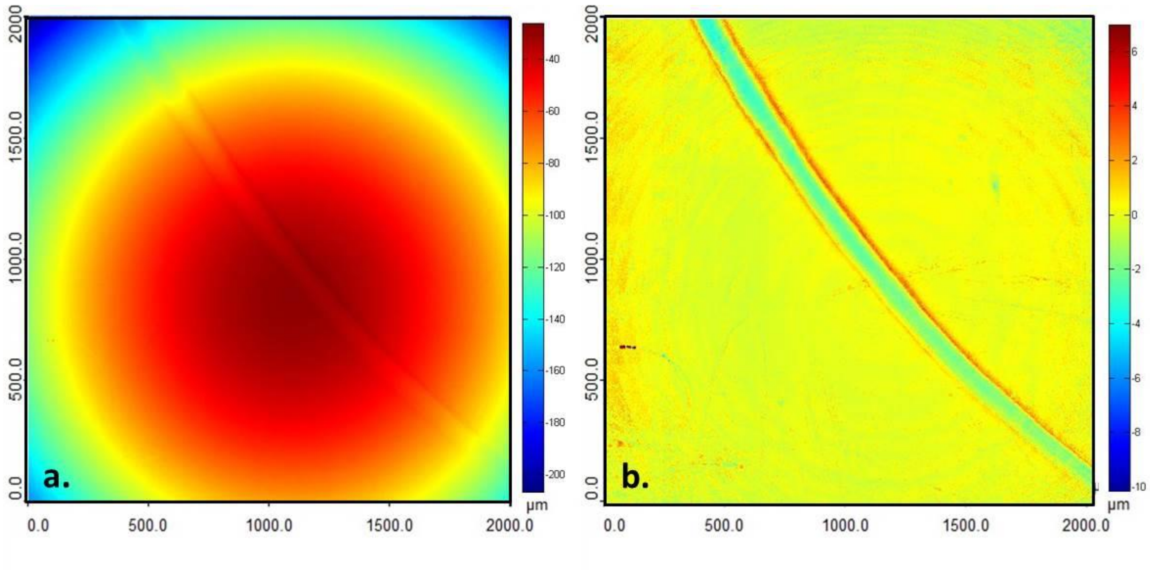

Figure 29: OP scan of a spherical surface. a. Raw OP scan of a single scratch. b. OP scan following completion of (spherical) form removal.

A custom-designed biaxial indexing stage was used to allow for global navigation on the femoral head (Figure 30). The indexing stage featured a pair of concentrically mounted goniometers, which allowed for rotation in two degrees of freedom †. This gave the user the ability to easily position the femoral head to a prescribed location, defined in polar coordinates. This allowed detailed investigation of specific regions of interest of the femoral head as detected from the global image analysis. The OP for a majority of this work was performed at Ohio State University (OSU) under a consortium subcontract. Locations of femoral head damage on the global photographs as detected by the image processing program were provided to the analyst at OSU (a post-doctoral fellow, Dr. Nishant Tikekar) responsible for OP scanning. Following completion of scanning, the scan data were transferred to the University of Iowa and the approximate scan locations were registered on the global photographs.

---

† This biaxial indexing stage was designed and built by our laboratory's designer and machinist, Thomas Baer.

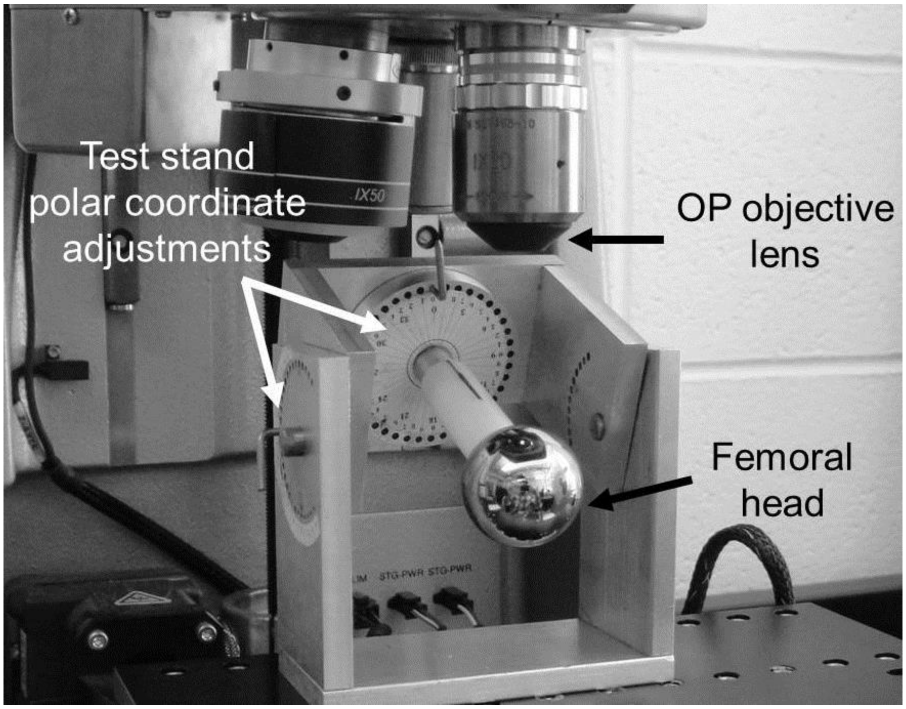

Figure 30: Wyco NT1100 optical profilometry setup with custom-built test specimen positioner, to allow for global femoral head navigation. The OP objective lens has been retracted for clarity.

OP scans were registered to their respective positions in the global-level photographs in order to be sampled for damage severity. For each OP scan, sets of (registration) control points were chosen from damage features that were visually distinguishable on both the global-level photograph and the OP scan (Figure 31). These control points were used to compute a 2D transformation structure, based on second-order polynomials. The polynomial transformation required a minimum of six control point pairs. This transformation type is most useful when objects in an image are curved, which many damage features fortunately are. The global image was then transformed based on this 2D transformation, to associate the detected damage features with their respective locations on the OP scan.

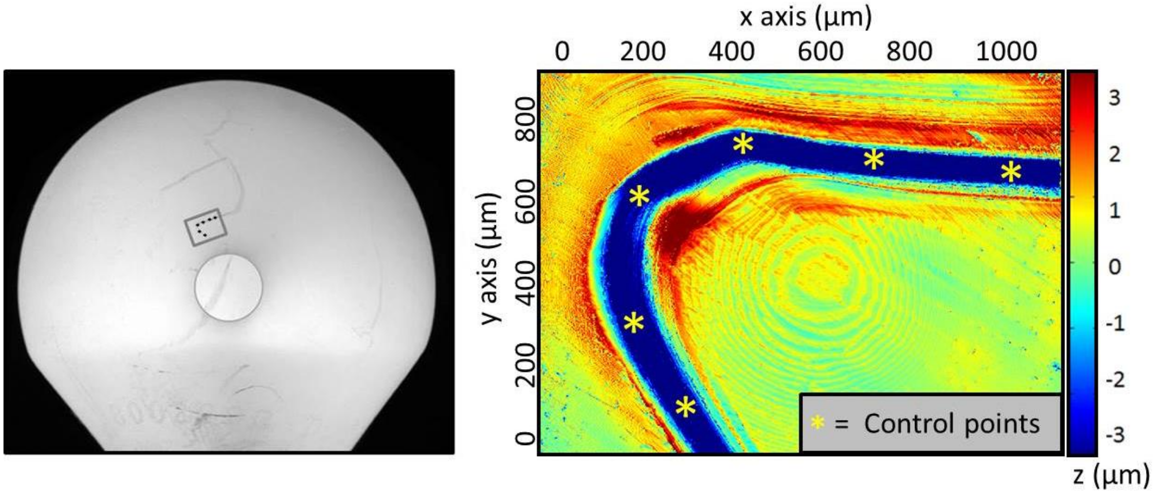

Figure 31: Global photograph and local OP scan of a selected region. The control points used to align the two datasets are indicated.

As discussed above, scratch severity was quantified based on each scratch segment’s average lip height. To make this severity calculation, each designated scratch segment was first superimposed on its corresponding OP image(s). Values of surface vertical height were then queried from the OP dataset(s) along a series of equally-spaced sampling lines perpendicular to the scratch segment (Figure 32). The peak surface height was identified on each such sampling line, and the mean of those peak heights was designated as the scratch lip height for that individual scratch segment.

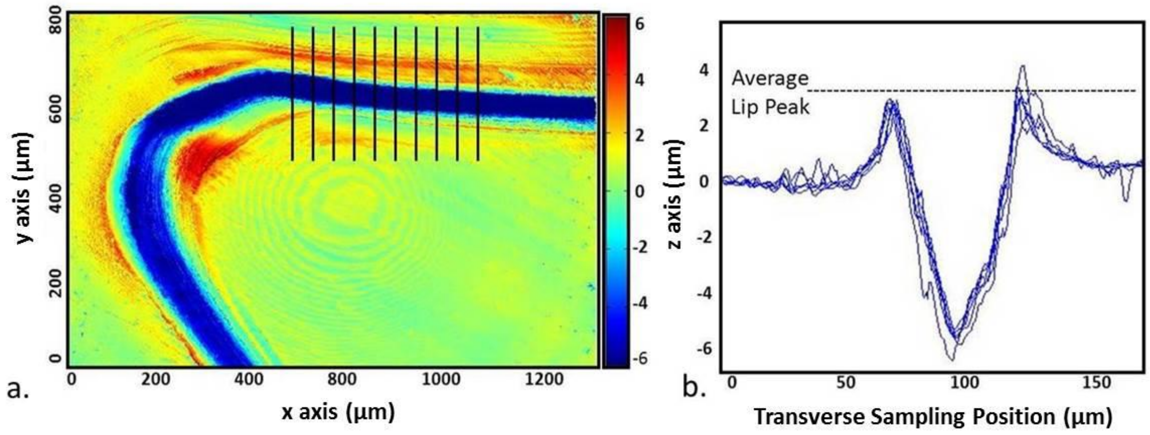

Figure 32: Scratch lip height computation. a. OP scan illustrating characteristic lip-and-valley morphology. b. OP scan profiles used to determine scratch lip height.

A convergence analysis was performed to determine appropriate density of the sampling lines. The results of this convergence study showed the OP scan needed be sampled at least every 10 µm along the scratch length to accurately represent the scratch lip height (Figure 33).

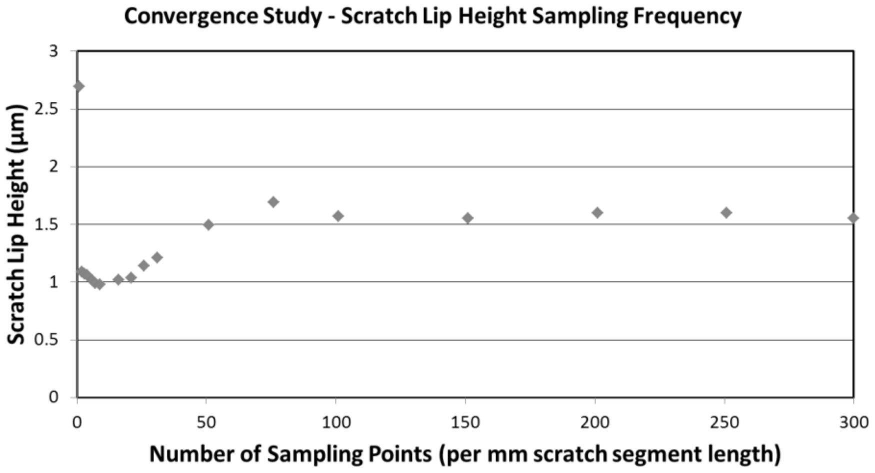

Figure 33: The results of a sampling convergence series, undertaken to determine appropriate sampling frequency.

An important distinction between transfer deposits and scrapes was evident from their differing appearance on OP scans. As noted above, the micron-level damage features on scrapes showed prominent directionality, whereas those on transfer deposits did not. Scrapes appeared on OP scans as collections of tightly packed micro-scratches. The individual micro-scratches did not lend themselves to being easily discretized. Severity of scraping was therefore quantified in terms of the average roughness within the scrape region. Scape regions in OP scans were automatically polygon-delineated. The average roughness (R_a) values were computed within scrape regions by taking the average of the height differences of individual pixels, relative to the mean surface height of all the pixels within the scrape region.

For purposes of polyethylene wear modeling, the directionality of interest was the direction of the micron-level scratching within the scrape, rather than the overall macro-level orientation of the perimeter of the scrape region. While these two orientations were nearly the same in most cases, in some, particularly those scrapes presumably resulting from transverse sliding during egress of edge-loaded femoral heads during subluxation, the two directions were nearly perpendicular (Figure 34). To identify the direction of micro-scratching, a Hough transform was performed on each scrape OP dataset. This detected the micro-scratch lines within the scrape. The directionality of the ten longest micro-scratch lines was determined. The average of these directions was computed and was designated as the micro-scratching direction for that scrape region.

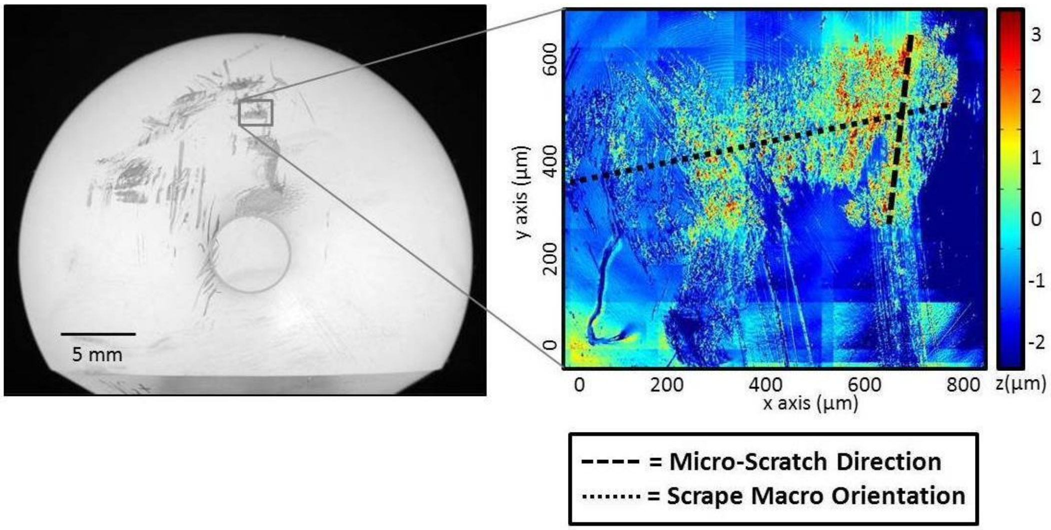

Figure 34: OP scan of a scrape, distinguishing scrape region macro-directionality from the predominant directionality of scraping

Coordinates of the polygon vertices of each designated scrape or deposit region were saved, along with scrape directionality and transfer deposit edge height. These locations were input to the FE model as node sets, to allow the locations of these damage features to be tracked throughout the duty cycle. Due to the typically large sizes of the transfer deposits, OP scanning of entire deposit regions was usually not practical. Rather, 2 mm x 2 mm OP scans were taken at multiple sites (typically ~8) in representative regions. These scans were used to determine the height of the deposit and its average R_a value [184].

Brown et al. had previously reported that variability of the location of femoral head damage is associated with wear acceleration variability (both in magnitude and direction) [28]. While that study determined locations of femoral head damage causing maximum wear acceleration, it did not report if there were any regions of femoral head damage that would not cause wear acceleration. In the interest of streamlining the scanning process, a parametric FE series was therefore conducted to determine if there were specific regions of femoral head damage that would not affect wear. Patches of femoral head damage 1 x 1 mm in size with k_{inc} values of 50 were positioned in 5˚ increments on the femoral head, starting at the equator and extending down toward the base ("south pole") of the head. Each damage patch was rotated in 30˚ increments about the trunnion axis and FE wear simulations were run for each such orientation. The results of that analysis showed that damage located 25˚ or more below the equator would not cause wear acceleration no matter how the head was oriented on the trunnion (Figure 35). Due to the overall project goal of measuring damage features capable of causing wear acceleration, areas more than 25˚ below the equator were therefore removed from consideration for scanning.

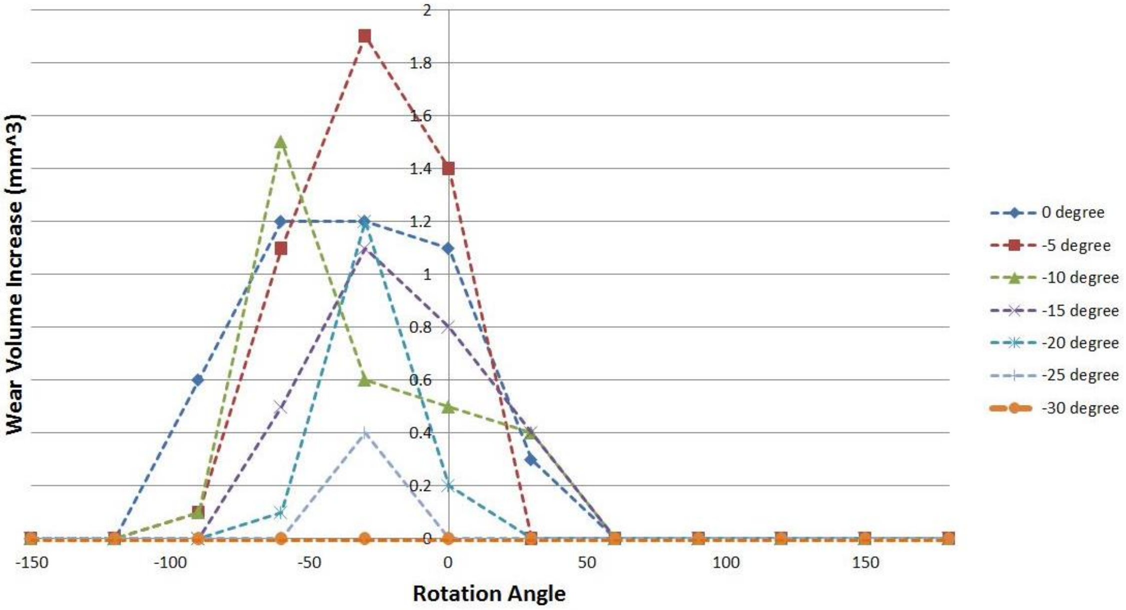

Figure 35: Results of parametric analysis to determine femoral head latitude locations capable of causing wear acceleration. The 0˚ rotation angle corresponded to the damage patch being oriented on the trunnion to be located at the superior-most location. The damage patch was rotated either anteriorly (+ rotation) or posteriorly (- rotation) about the trunnion axis.

Automated image alignment

In the preliminary stages of the retrieval analysis (see Chapter 4, below), femoral heads were selected on this basis of having only relatively minor levels of damage, to provide relatively “easy” cases conducive to development of this analysis. OP scanning of large areas of head damage had never been done before, so the total damage area that could be tractably analyzed was unknown. As development of the work progressed, analyses were conducted on femoral heads with progressively larger damage areas, in some instances covering in excess of 25% of the articular surface. The OP setup proved to be able to efficiently analyze large areas with relatively good efficiency. However, the process of manually aligning each scan to its respective location on the global photographs was tedious and time consuming. OP analysis of entire femoral head damage areas often involved hundreds of individual OP scans. A pre-processing pipeline was therefore developed (1) to automatically designate regions of femoral head damage to scan, (2) to align those OP scans to their respective positions in global-level photographs, and (3) to export the location and severity information to implant-specific FEA wear models.

Also, modifications were made to the biaxial indexing stage, to allow the specimen to be quickly positioned to a desired location in polar coordinates (Figure 36) ‡. The precision of this instrument was 1˚, which for a 28 mm head equates to less than 250 μm of linear distance. A zero mark made at the base of each femoral head served as a position datum for analyzing the femoral head in both the diffused-light photography and OP setups.

---

‡ This modified biaxial indexing stage was also designed and built by Thomas Baer with evaluation of the device in the OP set-up completed by Dr. Anneliese Heiner and the author.

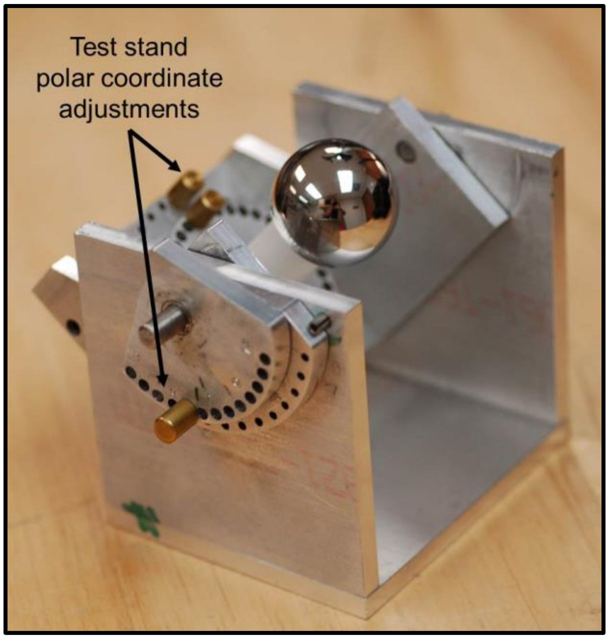

Figure 36: Updated biaxial indexing stage, featuring course and fine polar adjustments to allow for 1˚ position precision.

The zero mark on the femoral head was aligned to the 0˚ coordinate on the rotary table in the diffused light photography setup. Polar and circumferentially incremented images, as discussed above, were then captured. The damage detection program was applied to the global photographs to identify locations of damage features and to classify those features as either discrete scratches or as scrape/deposit regions. The femoral head was then divided into potential OP scan sectors, with each sector approximately the size of single of OP scan (Figure 37). Regions to scan were flagged, with each scan region identified by the polar coordinates at the center of the scan. Scratches were discretized into straight-line segments as described above. The endpoint coordinates of the scratch segments were saved, to be used when measuring their lip heights later in the analysis.

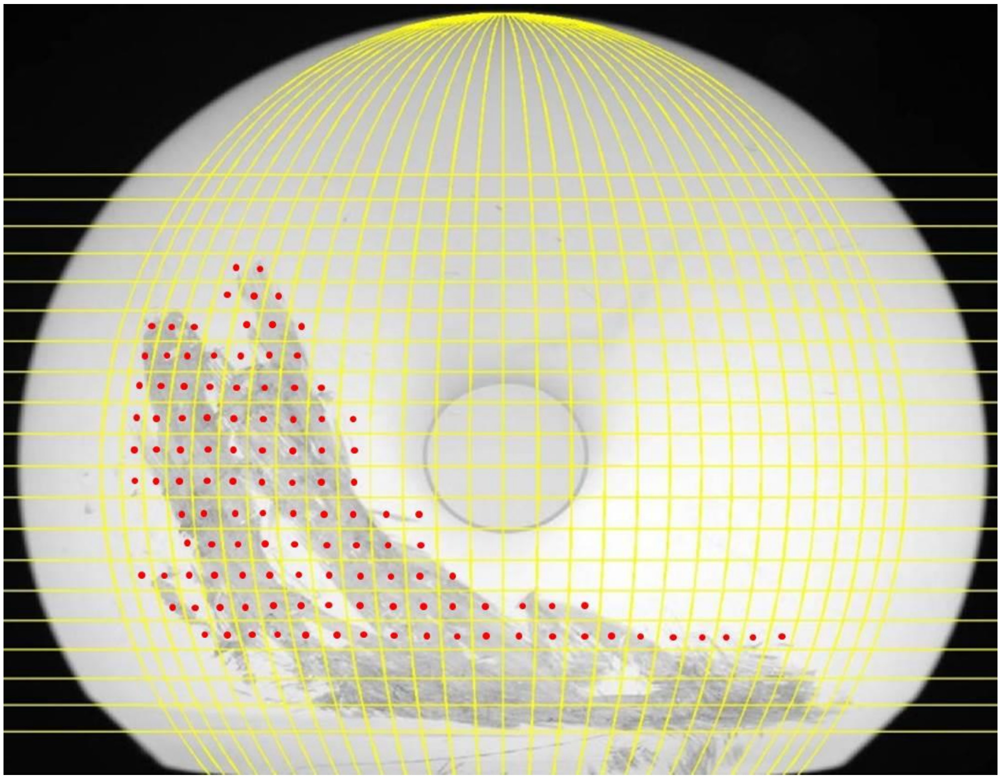

Figure 37: Global level femoral head photograph with grid indicating potential scan locations. The red dots indicate scan sectors that the damage detection program identified as containing damage. (Damaged areas above the indicated grid were captured in a polar view photograph.)

Sectors containing global-level damage were then OP scanned. The zero mark on the femoral head was aligned to the 0˚ longitude coordinate on the positioner. For each reported scan sector, the indexing stage was set to the coordinates of that sector. Additional fixturing was built for the OP scan stage to position the indexing stage so that the highest point of the femoral head was positioned directly under the OP scan lens. The site of interest was then scanned. If exceptionally tall (over ~20 µm) features were located in the scan region, the backscan (length the objective lens traversed while scanning) was increased to accurately measure the features. Each scan was saved as an ASCII file, which stored the 3D data as a matrix, with x and y coordinates indicated by the row and column numbers and the z coordinate indicated by the cell value. This file format allowed the scan to be later imported to MATLAB for further processing. Position setup and scan time averaged 3-4 minutes per scan.

Following completion of all scans, an automated program was then used to align these OP scans to their respective positions on the global-level photographs. The program measured the damage severity of each scratch and scrape feature identified during the original image analysis. There was potential for a small amount of error in the longitude coordinate when aligning the zero mark on the base of the femoral head to the corresponding zero line on the indexing stage. This error was assumed to be constant for all scans completed in a single scan session, provided the head was not removed from the positioning stage. To quantify this alignment error, three or four easily distinguishable points were identified on a global photograph and corresponding OP scan (Figure 38). The longitude coordinates of the points on each coordinate system were measured and the average difference defined the alignment error. This value was assigned to all OP scans obtained during that scan session. If multiple scan sessions were required to scan all femoral head damage, the process was repeated for each session. Alignment errors were generally less than 5°, and the error was consistent for all scans recorded in a single session.

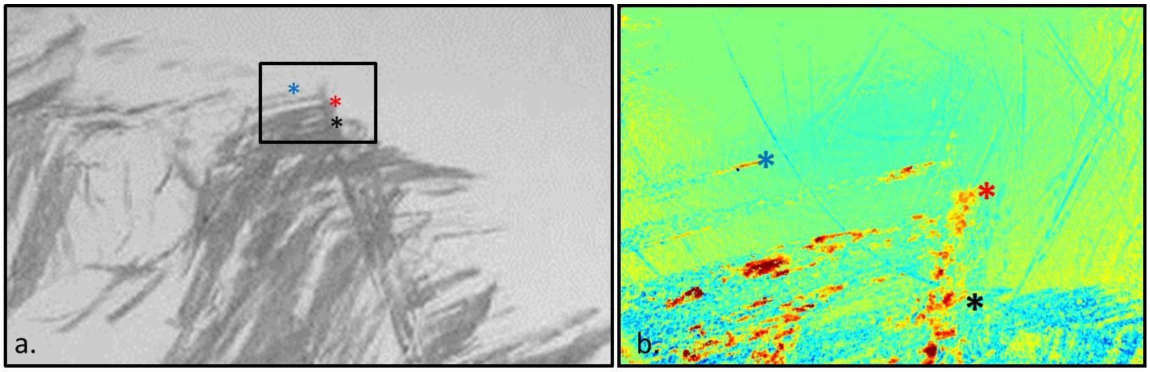

Figure 38: Identification of control points. a. Global photograph with visually distinguishable points identified to determine the alignment error. b. OP scan with corresponding points identified.

Two separate automation programs were developed, one to automatically measure scratch features and the other to automatically measure scrape damage features. For scratches (Figure 39), a list of scans taken in designated scratch regions was imported to MATLAB. Each OP scan was defined by the global location of the scan center (the biaxial indexing stage coordinates for that scan). The reported alignment error for that scan set was added to the longitude coordinate of each OP scan to ensure it was could be properly aligned to its global photograph location. To align each individual scan to its corresponding global location, the OP scan center was first identified on the global photograph. Each OP scan represented a 1.2 mm x 0.94 mm area of the femoral head. The appropriate scaling and translation factors were computed to relate these two coordinate systems, thus defining the area of the global photograph contained within the scan (Figure 40).

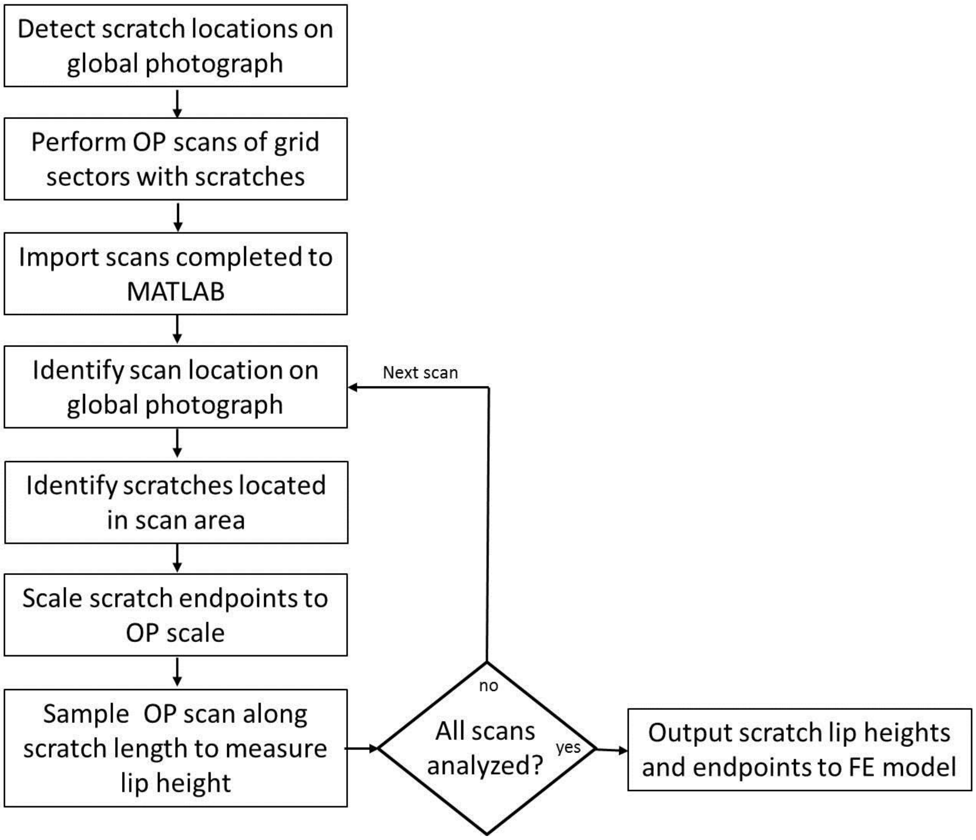

Figure 39: Flowchart of automated alignment program to measure scratch lip heights.

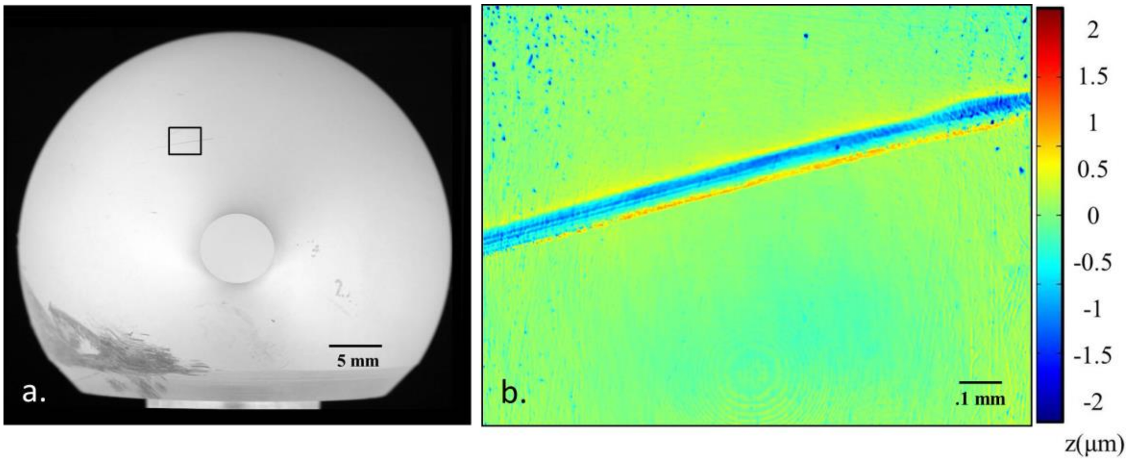

Figure 40: The area analyzed by a particular OP scan is identified in the global-level photograph (a). The black box indicates the area analyzed by the specified OP scan (b).

The coordinates of the global-photograph-detected scratches identified earlier in the analysis were imported, and the scratch segments located in this scanned region were determined. Scratch segments were identified as being located in the scanned region if their start, mid, or endpoint fell within the region of that particular OP scan. The global coordinates of each identified scratch were scaled and translated to the OP scale. As discussed earlier, OP scans were then sampled along each scratch's length to measure its lip height. The lip height in turn was used to calculate the scratch's wear coefficient scaling factor (k_{inc}). The scratch coordinates and wear coefficient increases were then written to a file to be input to the FE model. This process was repeated for all OP scans taken in scratch-identified locations.

A separate but conceptually related program was used to sample OP scans containing scrape damage (Figure 41). Similar to the scratch program, the OP scan area was first located in the global photograph (Figure 42a). An analyst-designated threshold was applied to this area on the global photograph to segment the scrape damage in that area (Figure 42b). The scrape-identified area was used to generate a mask, which was scaled and translated to the OP scale (Figure 42c).

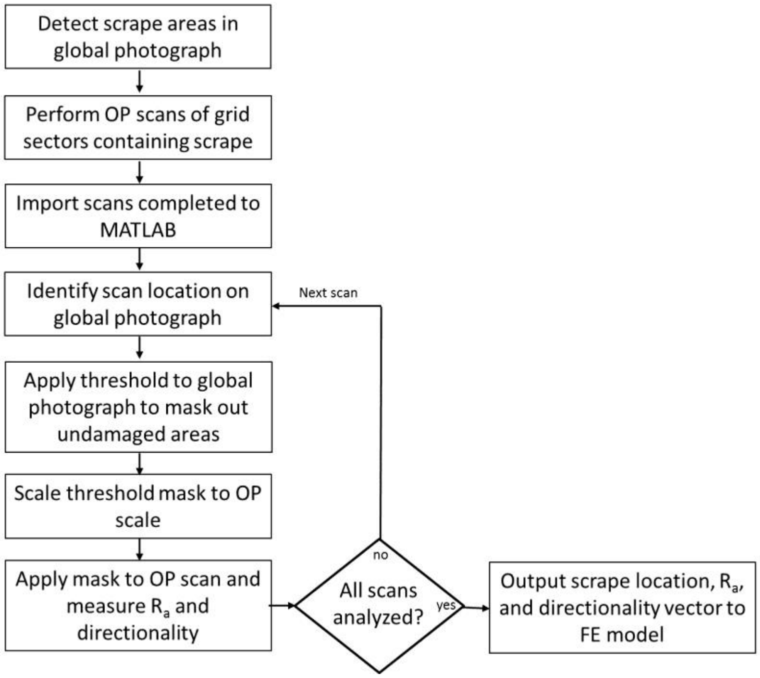

Figure 41: Flowchart of automated alignment program to measure scrape R_a and directionality.

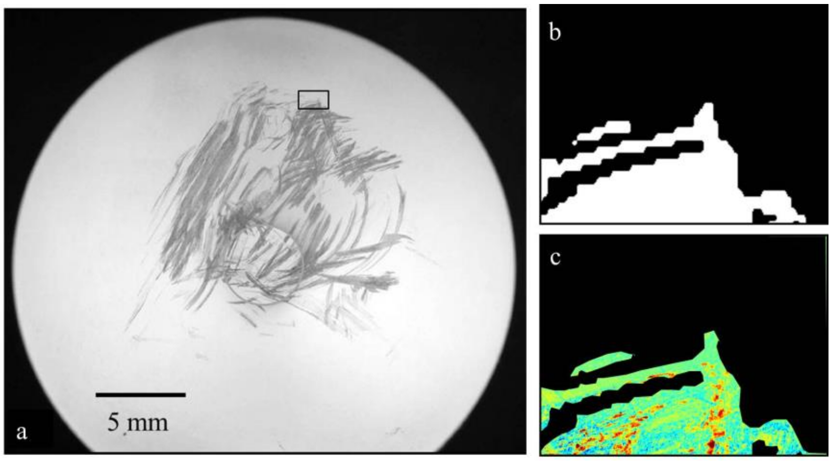

Figure 42: Scrape area identification. a. Global photograph indicating OP scan area. b. Threshold result from global photograph to identify scrape area of that scan. c. OP scan with threshold mask applied, which was used to compute the R_a value of the scan.

This mask was applied to the OP scan, and the non-masked area was sampled to calculate the R_a and corresponding k_{inc} values of that scrape region, along with the predominant scrape directionality. A Delaunay triangulation generated a mesh of this scrape area to be input to FE models (Figure 43). At the conclusion of running these two programs, the global coordinates of each scratch and scrape and their corresponding k_{inc} values were output to be imported into the FE wear models.

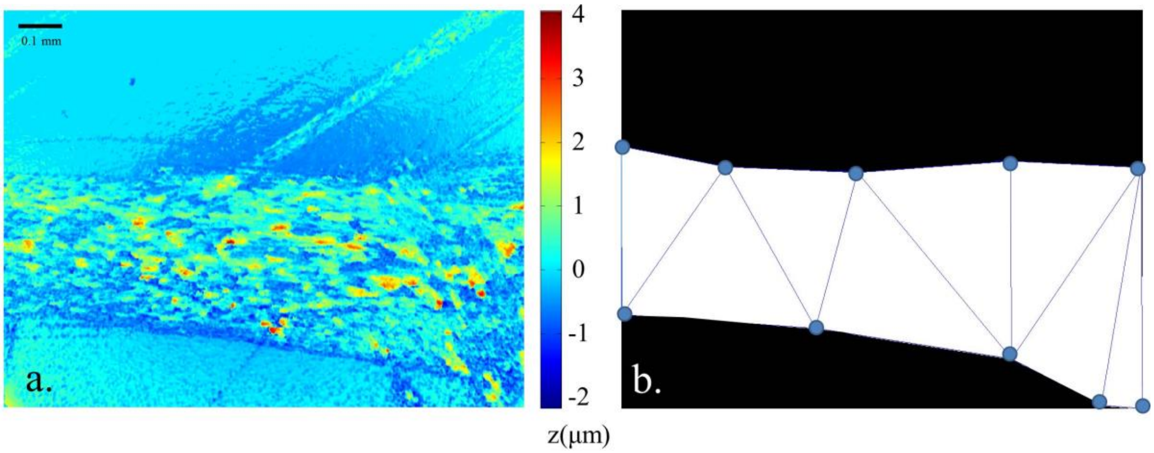

Figure 43: Mesh of scrape area. a. OP scan of scrape region. b. A Delaunay triangulation is performed on the threshold mask of the damage region to generate a triangular mesh to be input to the FE model.

While automated preprocessing was not completed on the large transfer deposits discussed above, the scrape program could be applied to automatically identify the transfer deposit areas and align OP scans to their respective locations. The dramatic visual darkening of the transfer deposits makes automated segmentation of the damage region even more straightforward than the scrape segmentation. The only necessary addition to a transfer deposit analysis program would be the ability to automatically measure the deposit height relative to the undamaged surface. To make this calculation, OP scans would need to be obtained that contain both transfer deposit and undamaged regions.

Performance of automated damage preprocessor

To confirm appropriate performance of this automated image alignment process, the scratch and scrape automation programs were run on two femoral heads which had been analyzed using the previous manual registration technique. The automatically measured scratch lip height and scrape R_a values were compared to damage severity information that had been previously assessed using manual alignment for these same two femoral heads. For the reported scrape R_a values, the values reported by the manual technique (which required analyst polygon delineation of the scrape region) were compared to those from the automated technique (Figure 44, Figure 45). The output of the two alternative methods allowed for a direct scan-to-scan comparison. Therefore, a paired t-test was used to compare the two datasets. The results showed no statistically significant difference between the distribution of scrape sector roughness of the two methods (Table 5).

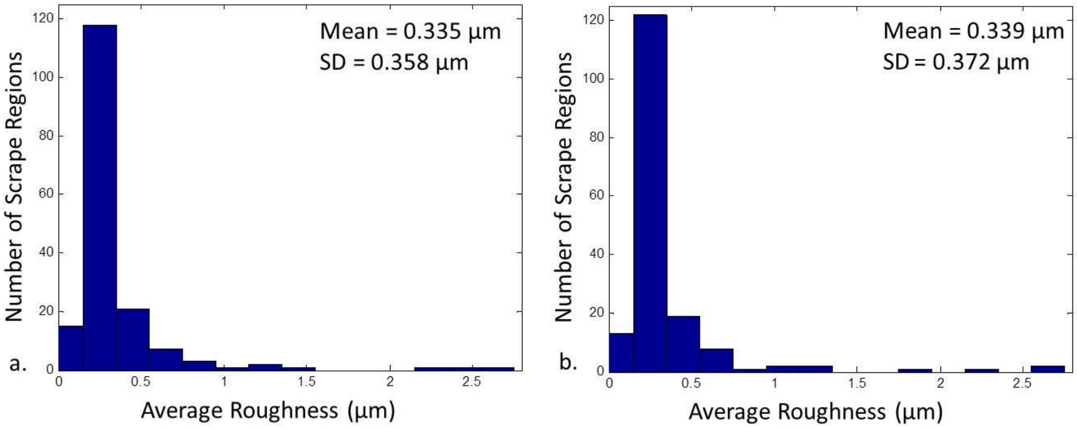

Figure 44: Scrape R_a measured for Specimen A using (a) manual alignment and (b) automated alignment.

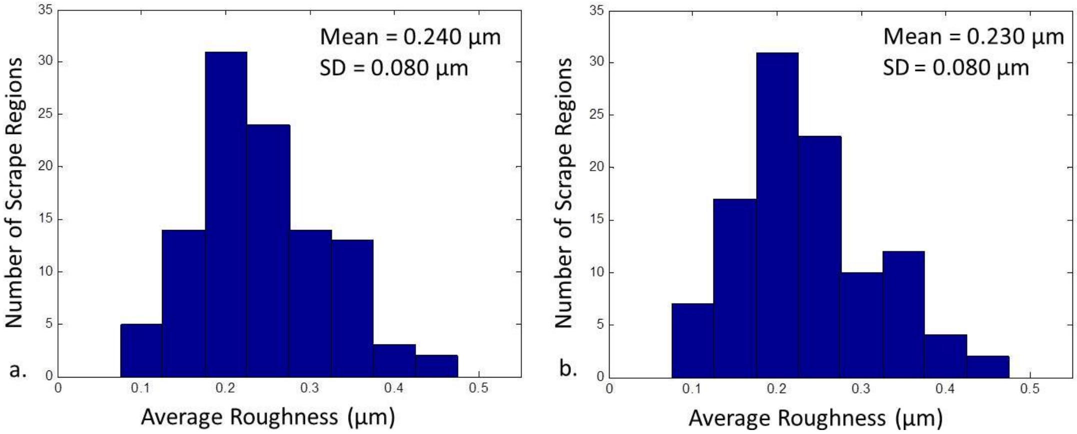

Figure 45: Scrape R_a measured for Specimen B using (a) manual alignment and (b) automated alignment.

In the case of scratches, there was no control in place to ensure every detected scratch was measured. This meant that the sampling order of the individual scratches might not be the same for the two methods, and therefore that a direct scratch-to-scratch comparison was not possible. Instead, the distributions of measured scratch lip heights from the manual registration and from the automated alignment processes were compared using a student's t-test (Figure 46, Figure 47). While the shape of the distributions varied slightly between the two measurement techniques, the results showed no statistically significant differences (Table 5). The automated damage preprocessor captured 97.7% and 99.1% of the scratches in samples A and B, respectively.

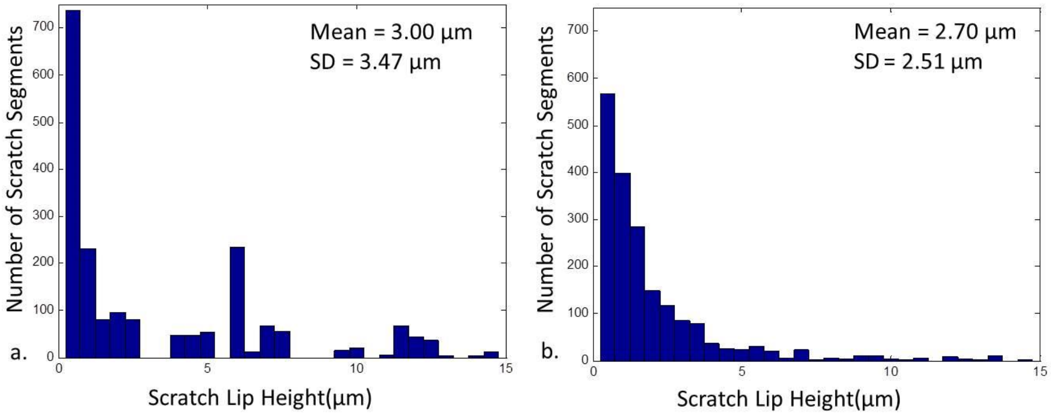

Figure 46: Scratch lip heights measured for Specimen A using (a) manual alignment and (b) automated alignment.

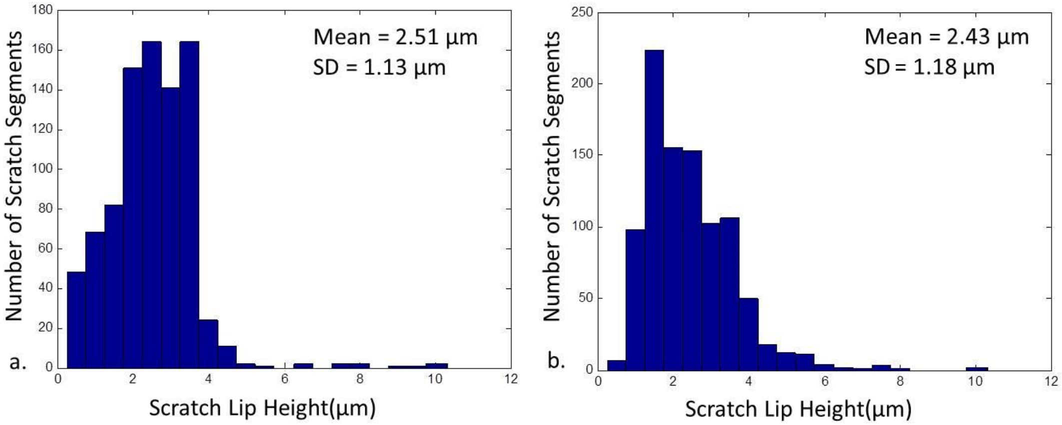

Figure 47: Scratch lip heights measured for Specimen B using (a) manual alignment and (b) automated alignment.

Table 5: Damage severity information

Head	Average Ra (µm)		p-value	Scratch Lip Height (µm)		p-value
	Manual	Automated		Manual	Automated	
A	0.335	0.339	0.62	3.000	2.700	0.103
B	0.240	0.230	0.06	2.510	2.430	0.119

Most importantly, the respective corresponding FE models (Figure 48) showed average wear differentials of only 1.3% and 5.5%. These small differentials provided substantiation that the automated damage preprocessing routines were reliable.

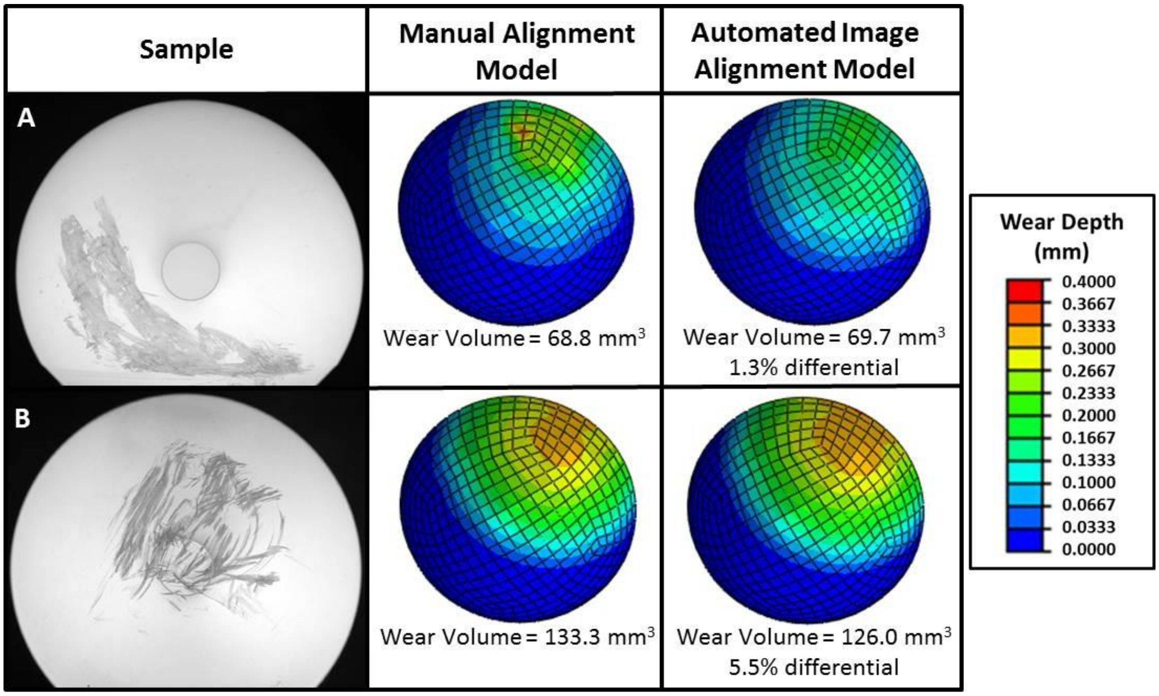

Figure 48: Results comparing the wear volume with damage severity information measured using the manual alignment method (left) and automated alignment method (right).

CHAPTER 4: DAMAGE-BASED WEAR COMPUTATIONS IN A REVISION RETRIEVAL POPULATION

Retrieval femoral head damage was hypothesized to be highly variable, thus leading to substantially different wear rates. To test this hypothesis, the potential wear acceleration of clinically occurring damage was analyzed using the above-described procedures.

The University of Iowa Orthopaedic Biomechanics Laboratory has a collection of over 200 retrieval THA implants. A set of 22 CoCr retrieval femoral heads (Figure 49) was selected from the current retrieval collection. They were chosen to illustrate a wide variety of damage features and severity levels. A sample set of this size is typical for retrieval analyses which use 3D profilometry [56, 102], rather than just a small number of 2D line profiles as is the case with most large-scale retrieval analyses. These illustrative retrievals had been implanted for between 0.2 and 18.9 years (Table 6).

Each retrieval head was photographed and image analyzed as discussed above (Chapter 3). OP scans were taken of each damaged region [§] and the results were used to generate patient-specific FE wear models. Each FE model was run for one million cycles of level walking gait. The volume of polyethylene removed was computed for each specimen and compared to a baseline simulation for an otherwise identical undamaged femoral head (R_a=0.007 μm).

The retrievals in this series had one major limitation, in that most were modular components whose femoral head had been removed during the retrieval process. Unfortunately, most often, surgeons performing retrievals do not record this circumferential orientation. The sensitivity of computed wear to this head-on-trunnion orientation is explored below. For purposes of this series, the wear acceleration reported

---

[§] A vast majority of the OP scans for this work were performed by Dr. Nishant Tikekar at Ohio State University. The remainder were performed by the author and Dr. Anneliese Heiner.

is the orientation of maximum wear. For consistency across this series, the angle between the femoral neck and stem was taken as 135˚ and femoral anteversion taken as 0˚ for all retrieval cases.

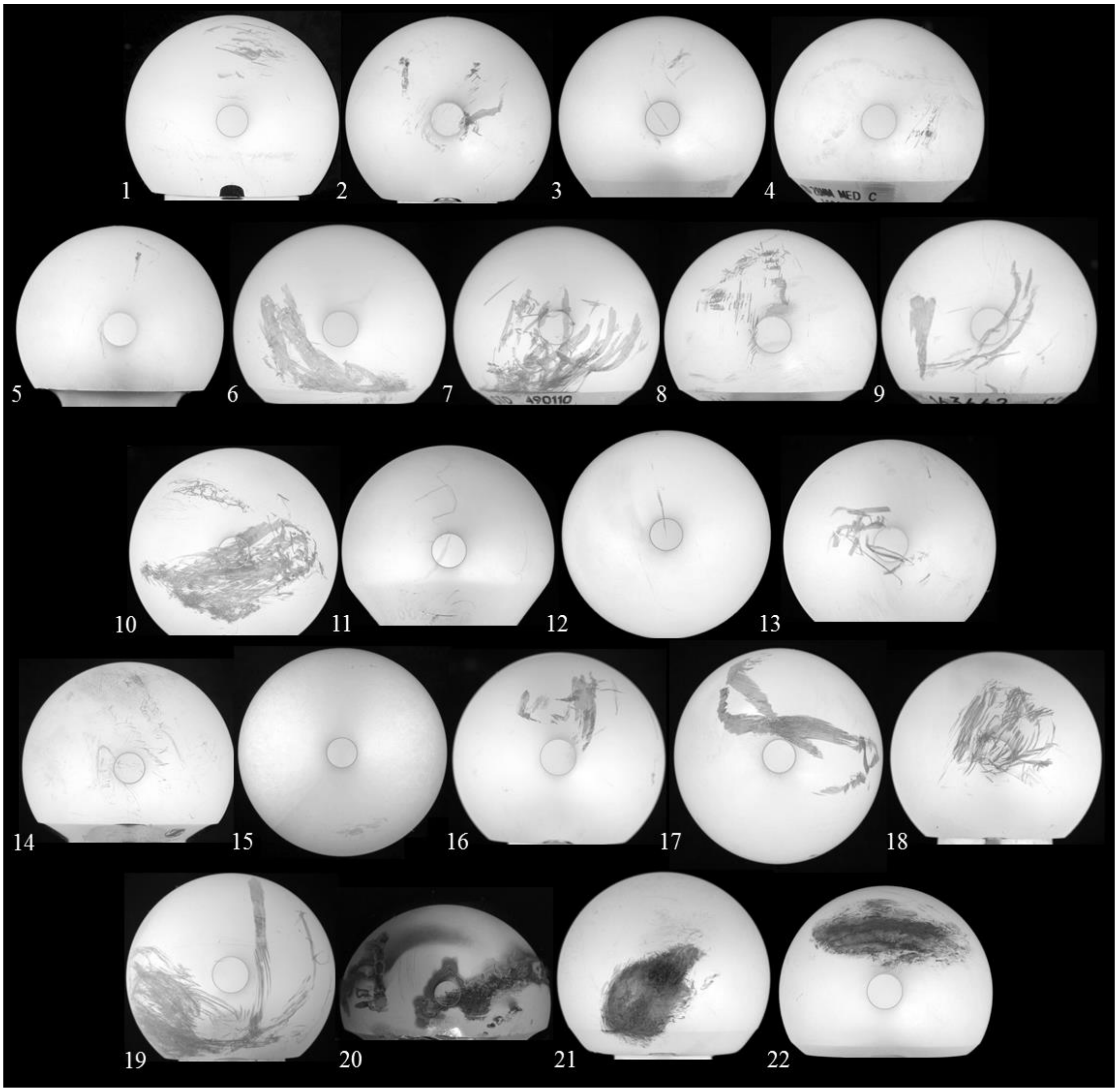

Figure 49: Retrievals modeled displaying the visually most critical damage features. Polar views are shown of retrievals 12 and 15. Circumferential views are shown of the remaining retrievals.

Table 6: Retrieval femoral head demographics

Retrieval Number	Time to Revision (years)	Reason for failure	Head Size (mm)	Visible debris embedded in liner
1	6.7	Aseptic Loosening	28	Yes
2	0.4	Dislocation	28	No
3	5.1	Septic Loosening	26	No
4	10.5	Aseptic Loosening	28	No
5	13.5	Aseptic Loosening	28	No
6	3.0	Dislocation	32	No
7	5.4	Dislocation	28	No
8	5.6	Recurrent Subluxation	28	Yes
9	7.4	Dislocation	28	No
10	1.5	Dislocation	32	Yes
11	14.8	Wear	32	No
12	6.2	Dislocation	28	No
13	0.8	Dislocation	32	No
14	18.9	Dislocation	28	No
15	0.2	Dislocation	36	No
16	0.4	Dislocation	28	No
17	8.9	Wear	26	No
18	9.8	Dislocation	28	Yes
19	0.2	Dislocation	28	No
20	17.1	Dislocation	22	No
21	4.4	Aseptic Loosening and Dislocation	28	Yes
22	16	Wear	28	No

Additional wear analysis was completed to study the effects each damage type's contribution to wear acceleration. Samples 1-20 displayed varying levels of scratch and scrape damage. For each of these samples, two separate FE models were run. One model contained only the scratch damage present on that retrieval, and the other only the scrape damage present. These results were used to estimate the percentage of wear acceleration due to each respective damage type.

A similar methodology was used to study the specific mechanisms responsible for wear acceleration due to transfer deposits. For sample 22, three FE models were developed to isolate the individual effects of deposit roughening, edge-gouging, and height.

Results

The image processing routine detected discrete scratches on 17 of the 22 specimens (Table 7). As would be expected, those specimens exhibiting scratch damage all showed large variability in the severity of individual scratches. Series-wide, retrieval number 10 showed the highest scratch lip height, 28.52 μm. To the author's knowledge, this registry represents the first-ever retrieval study to combine and document the severity of individual scratches.

In the interest of completeness, the present set of results included scratches with lip heights as low as 0.07 μm. This may have been unnecessarily exhaustive, however, since there is experimental evidence [50] that the lip height threshold for detectable wear acceleration from individual scratches is substantially higher, on the order of 1 μm. If desired for purposes of computational efficiency, wear-inconsequential scratches obviously could have been disregarded from further consideration in downstream wear modeling, simply by Boolean masking on the basis of lip height.

Table 7: Scratch properties

Retrieval Number	**Number of Scratch Segments**	**Scratch Lip Height (µm)**		
		Average ± S.D	**Min**	**Max**
1	246	2.19 ± 1.79	0.24	7.82
2	677	8.82 ± 4.25	0.84	14.85
3	101	1.72 ±0.95	0.08	4.75
4	70	1.72 ± 0.46	0.56	2.48
5	171	2.31 ± 1.29	0.32	7.01
6	415	3.00 ±3.55	0.25	14.55
7	1603	5.28 ± 3.84	1.03	17.74
8	190	2.39 ± 0.81	0.94	4.38
9	211	1.64 ± 0.40	1.01	2.87
10	1925	5.49 ± 4.14	2.52	28.52
11	430	2.76 ± 1.73	0.07	10.00
12	62	1.70 ± 1.13	0.62	5.38
14	1754	1.52 ± 0.67	0.84	3.41
15	6	0.93 ± 0.33	0.49	1.34
18	333	4.89 ± 0.97	3.91	8.51
19	1999	2.76 ± 0.12	1.03	6.33
20	824	9.65 ± 4.18	3.09	17.74
Series Total	11017	1.97 ± 0.81	0.07	28.52

Scraped regions were observed in 16 of the specimens analyzed (Table 8). The corresponding R_a values also showed extreme variability. Series-wide, the highest scrape-average roughness value was 8.51 µm (appearing on Specimen #18), a three-order-of-magnitude elevation relative to the typical R_a values for undamaged implant surfaces [49].

Table 8: Scrape properties

Retrieval Number	**Number of Scrape Sectors**	**R_a (µm)**		
		Average ± S.D.	**Min**	**Max**
1	16	0.62 ± 0.28	0.33	1.50
2	15	0.84 ± 0.51	0.33	2.01
4	21	0.28 ± 0.27	0.03	1.21
6	171	0.33 ± 0.27	0.07	2.74
7	39	0.55 ± 0.18	0.33	1.18
8	44	0.26 ± 0.15	0.04	0.65
9	68	0.21 ± 0.08	0.04	0.39
10	19	0.48 ± 0.10	0.33	0.64
13	91	0.17 ± 0.11	0.03	0.55
14	29	0.12 ± 0.06	0.05	0.34
15	7	0.24 ± 0.12	0.09	0.41
16	28	0.22 ± 0.07	0.19	0.52
17	71	1.12 ± 1.25	0.03	4.20
18	108	0.24 ± 0.08	0.09	0.46
19	11	0.80 ± 0.50	0.15	1.96
20	56	1.99 ± 0.32	0.71	7.48
Series Total	794	0.51 ± 0.75	0.03	7.48

Two of the retrieval specimens in this series (Specimens #21 and 22) showed titanium deposits, which lacked the characteristic directionality of scrape damage. The OP showed these regions to be raised on average 9.00 µm from the surrounding undamaged area. The average R_a values in the deposit areas were found to be 0.35 ± 0.58 µm and 0.54 ± 0.21 µm for Specimens #21 and 22, respectively (Table 9).

Table 9: Average roughness (R_a) values from transfer deposit regions as detected by optical profilometry.

Region	**Specimen #21** **R_a (μm)**	**Specimen #22** **R_a (μm)**
1	0.286	0.395
2	0.319	0.882
3	0.342	0.468
4	0.320	0.887
5	0.362	0.385
6	0.313	0.433
7	0.360	0.426
8	0.477	0.440
Average	0.347	0.540
Standard Deviation	0.058	0.214

The FE wear results showed increases in wear volume for all specimens when compared to a baseline simulation for an identical diameter undamaged femoral head having an R_a value on the order of 0.01 μm (Figure 50). Some increases were small, such as for Specimen #4, which had only minor amounts of damage. Others, however, such as the severely scraped Specimen #17 (Figure 51), showed multi-fold wear increases. The average wear acceleration was 4.24-fold, s.d. = 3.05-fold. Abaqus Viewer allowed UFIELD variables to be displayed on the deformed contour. The field variable wear depth was reported for all cases in this series and had been computed at each node on the acetabular liner bearing surface. The UMESHMOTION subroutine automatically adjusted nodes below this bearing surface to preserve element quality. Due to this function, wear depth is displayed in locations other than only the bearing surface, as displayed in Figure 51.

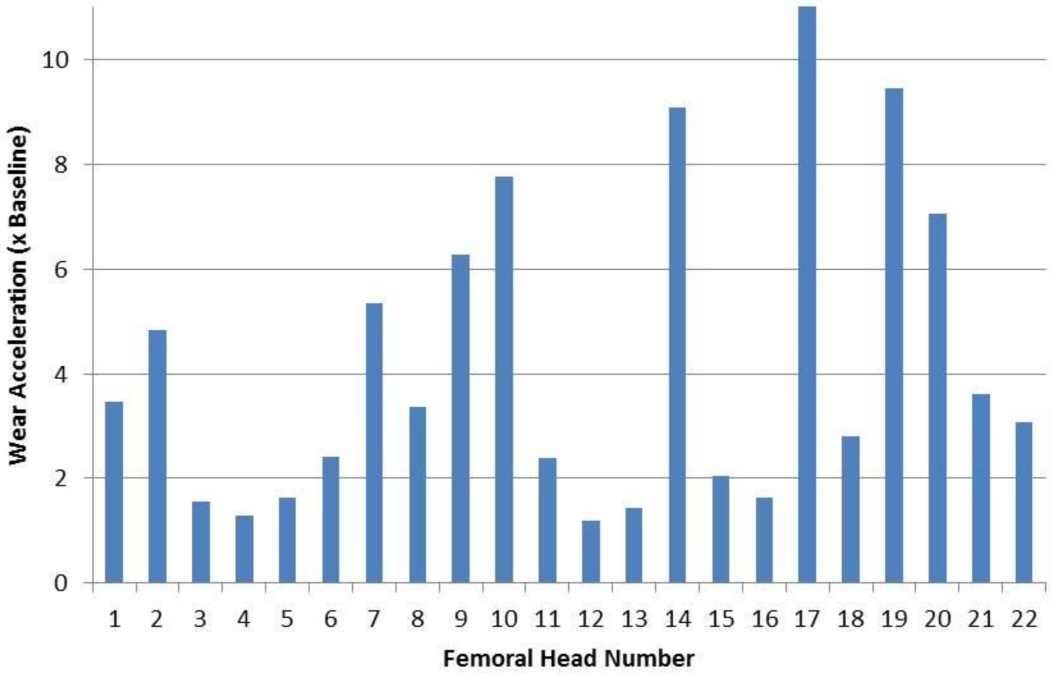

Figure 50: Wear acceleration for retrieval series. Each retrieval FE model was compared to a baseline simulation of an identifcal diameter undamaged femoral head.

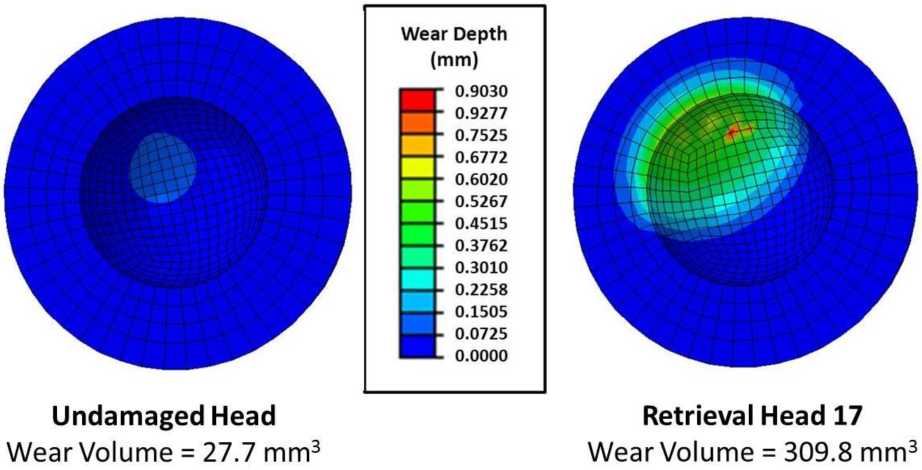

Figure 51: Comparison of wear depths for undamaged and representative retrieval femoral heads.

When the effects of scratching and scraping were isolated, it was shown that scratching alone caused wear acceleration in four of the samples and scraping alone in three of the samples. In the remaining samples, a combination of the two contributed to the total wear increase. On average, 63% of wear acceleration was caused by scratching and 37% by scraping (Figure 52).

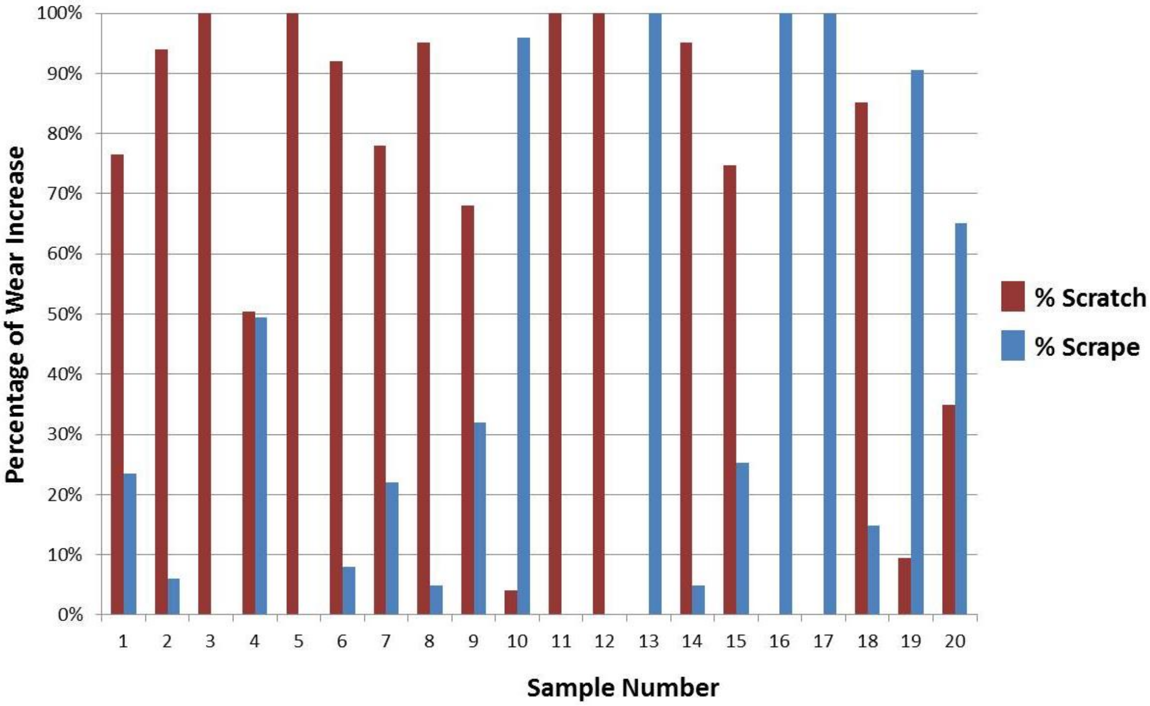

Figure 52: Results of FE analysis to isolate the wear acceleration potential of scratches versus scrapes on 20 retrievals.

For the large transfer deposit that was further analyzed on Specimen 22, a total wear acceleration of 3.6-fold was computed. Of this wear increase, 92.2% was due to the roughening effect, 7.3% was due to the edge-gouging effect, and 0.5% was due to the “mesa” height effect.

Orientation dependence

A modular head-neck junction allows replacement of the bearing in the presence of wear [178]. Most of the retrievals in this series were modular femoral heads, which had been removed from the stem component during the revision surgery. Oftentimes (in fact, typically), surgeons performing retrievals do not record circumferential orientation. Orientation is usually known only for monoblock components or for retrievals from autopsies. While the anatomic orientation of a retrieval femoral head obviously would have an impact on the PE liner wear rates [130], the variability of wear due to uncertainty of head orientation has not been explored. The retrieval femoral heads modeled for this work were therefore used to study this relationship [109]. The assumed rotational orientation of the femoral head about the femoral neck axis was perturbed in 30° increments, thus providing a total of 12 wear estimates for each retrieval specimen. Wear simulations for each of these assumed orientations were run to one million standard gait cycles.

Results

As expected, the resulting wear models showed significant variations in wear accelerations between the maximum- versus minimum-wear orientations for each individual retrieval (Figure 53). In general, the uncertainty of the wear rate due to not knowing femoral head orientation was greater than the nominal elevation of the wear acceleration due to the damage itself. As an example, for Sample #11 the maximum-wear orientation showed a 140% increase versus undamaged simulations, while the minimum-wear orientation showed only a 19% increase (Figure 54).

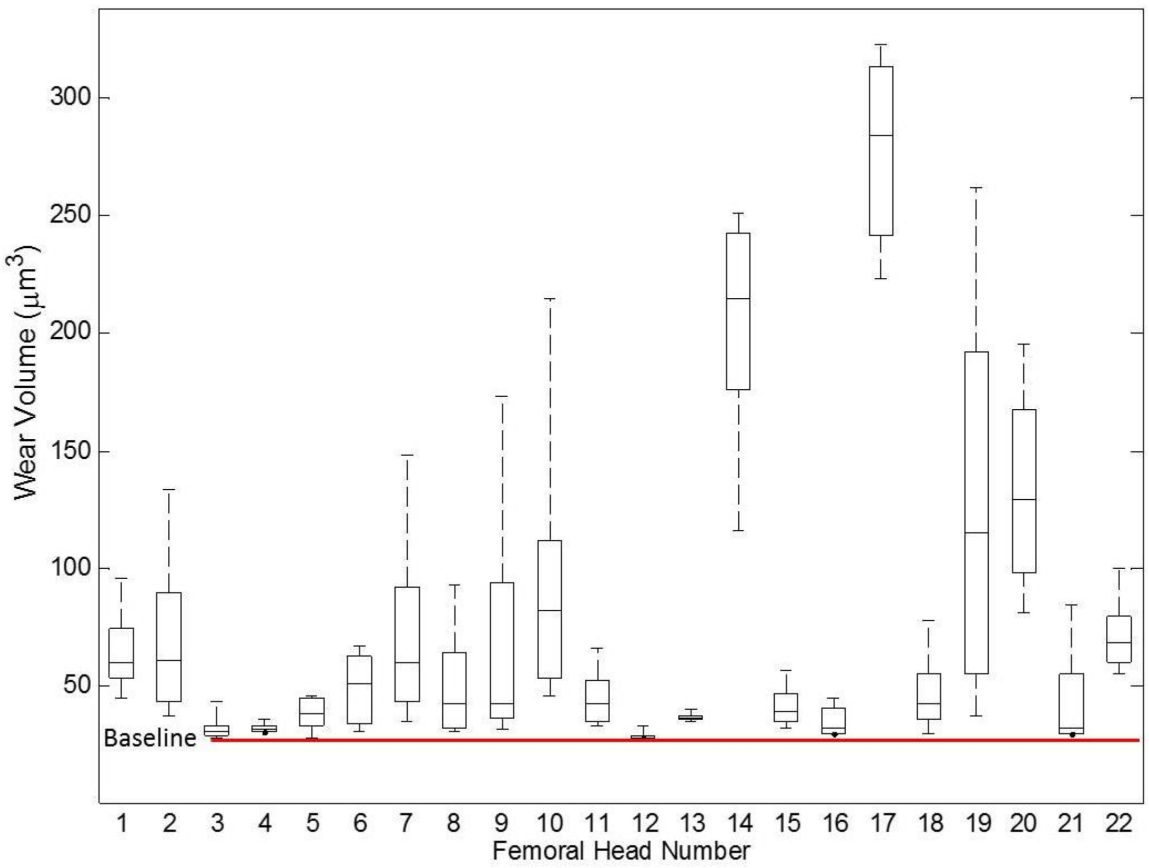

Figure 53: Box-and-whiskers plots of volumetric wear rates of damaged femoral heads, for 30° increments of rotational orientation of the femoral heads about the femoral neck axis. The baseline wear volume for an undamaged head simulation is indicated by the red line. For each box, the central mark is the median, the edges of the box are the 25th and 75th percentiles, and the whiskers (dashed lines) extend to the most extreme data points.

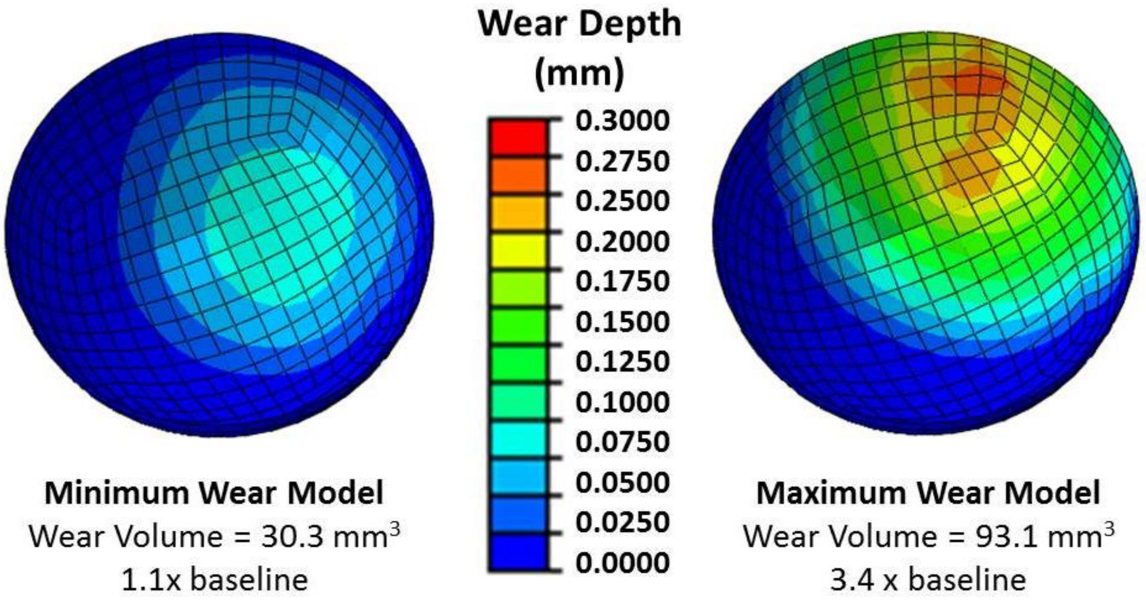

Figure 54: Volumetric wear depth plots for Specimen #8, for the rotational orientations having minimum (left) and maximum (right) volumetric wear.

In general, the difference between the FE models reporting the maximum and minimum wear acceleration was substantial (Table 10). The average difference was 250%. Specimen #19 reported the highest differential, with wear increases reported ranging from 35% to 845%, an 810% differential. The different orientations for this particular retrieval could be the difference between wear rates of little concern or of major concern.

Table 10: Wear rates of FE models reporting the minimum and maximum wear rate increase for each retrieval analyzed.

Specimen Number	**Minimum Wear Model Acceleration**	**Maximum Wear Model Acceleration**	**Difference**
1	61%	247%	186%
2	34%	382%	349%
3	0%	57%	57%
4	9%	28%	19%
5	0%	64%	64%
6	9%	142%	132%
7	24%	435%	411%
8	9%	236%	227%
9	12%	527%	515%
10	65%	675%	610%
11	19%	140%	120%
12	2%	19%	18%
13	26%	44%	17%
14	320%	807%	487%
15	16%	105%	90%
16	7%	64%	56%
17	707%	1067%	360%
18	7%	181%	174%
19	35%	845%	810%
20	195%	604%	409%
21	7%	206%	199%
22	98%	261%	163%

Scratch and scrape morphology

Metal ion release is an ongoing problem in total hip arthroplasty, causing catastrophic failures due to adverse soft tissue reactions. While this problem is most often associated with metal-on-metal implants, several reports have been published on pseudotumors caused by metallic debris in metal-on-polyethylene implants [16, 119, 170]. This issue had most commonly been associated with fretting and corrosion at the head-trunnion interface [15, 190]. Little attention, however, has been given to metallic debris that may have been removed from the femoral head or acetabular shell following scratching and/or scraping events.

Scratching is commonly thought of as primarily a ductile deformation event, with material from the metallic femoral head being “plowed” to create a valley, or furrow, with a majority of the displaced material being piled up along both sides of the valley. The OP scans obtained from the retrievals analyzed were used to determine to what extent this was indeed the case.

A MATLAB program was developed to compute the total volume of negative deviation in the OP scan (scratch valley volume) and the total volume of positive deviation (scratch lip volume) (Figure 55). Each 3D OP scan was imported to MATLAB as a matrix, with each cell value equal to the z (height) coordinate in µm, and the x and y coordinates identifying that cell’s location. First, the scratch area was manually identified, and all cells having negative values were isolated from this matrix. Each negative cell height value was multiplied by the pixel area (2 µm x 2 µm for the scans in this analysis) to compute the cell volume. All negative cell volumes were summed to determine the total volume of material plowed out of the valley. The same process was repeated with positive value cells to compute the volume of material piled up on the scratch’s lips. These values were used to compute the ratio between the scratch lip and valley volumes, along with the total volume of metal liberated from the femoral head.

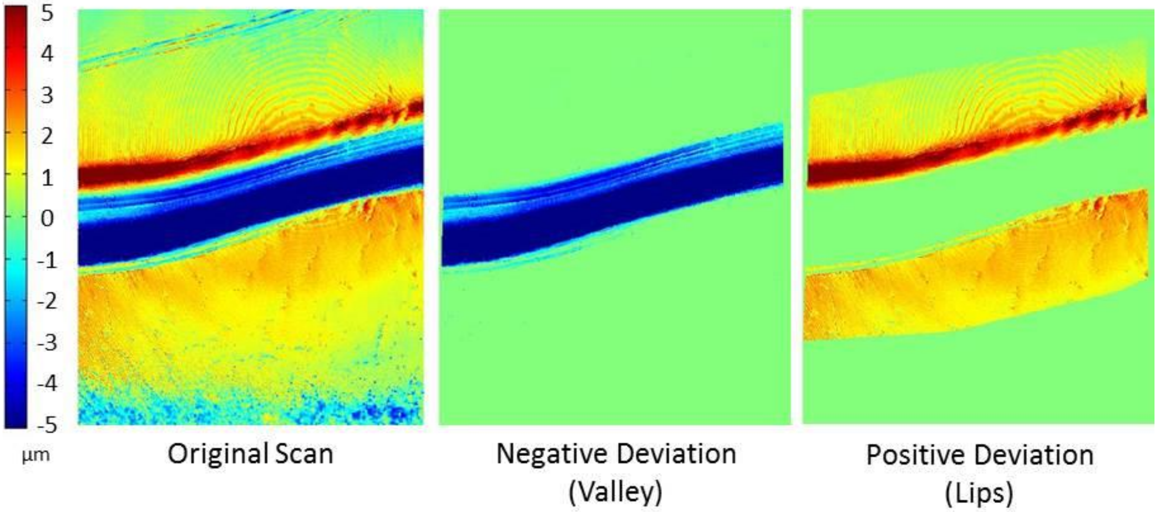

Figure 55: OP scan segmented into regions of negative (valley area) and positive (lip area) deviation.

Four retrievals which showed isolated scratches (Specimens #3, 5, 11, and 12) were selected to quantify the total volume of displaced metal piled up on the scratch lips. For each of these specimens, all OP scans that displayed isolated scratches (15, 20, 50 and 35 scans for each respective retrieval specimen) were analyzed. The total valley volume, total lip volume, and the ratio of the two were reported for each scan.

The results of this analysis showed net material removal in nearly all instances (Figure 56). Specimen #3 had the lowest single scan ratio of lip volume to valley volume, with a value of 0.04, indicating that nearly all of the material plowed from the valley in that local area was either liberated during the initial scratching event or subsequently smoothed down during normal joint articulation. Specimen #12 had the highest single scan ratio of lip volume to valley volume, 1.62, indicating net material deposition. One cause of this net deposition could have been that some of the material plowed away early during scratch formation was piled up later along the scratch, since several scratches spanned 10 or more single OP scans. This particular head specimen had also dislocated 17 times. While this specimen did not display the typical scrape features characteristic of dislocation damage, some metal transfer might have occurred followed acetabular shell contact. Some of the net deposition instances may have also been caused by error in the OP system, either in the initial scan resolution (although documented as 0.01 nm), or during the (spherical) form removal procedure.

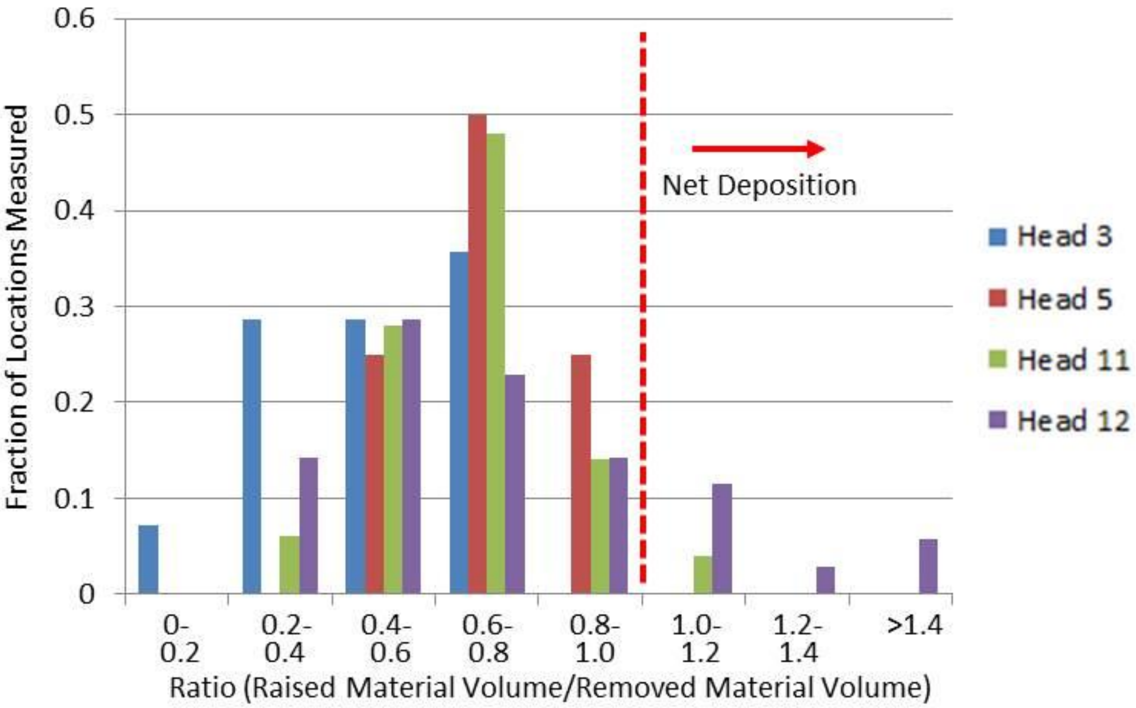

Figure 56: Ratios of scratch lip volume to scratch valley volume as measured from individual OP scans. Data to the right of the red line indicate net deposition in that OP scan.

The percent material removal was defined as the difference between the valley volume and lip volume, divided by the valley volume. The average material removal from all samples was 35%, s.d. = 20%. These results indicate that a large portion of the material removed from the scratch valleys (over half in many instances) was no longer present on the scratch lips. This finding is consistent with previous scratch analysis in retrievals. Swan et al. reported negative skewness to scratches measured on CoCr humoral heads [180], indicating that the sampling profiles had more valley area than lip area.

As with all retrievals, this information represents only a snapshot in time of the implant life. The reported material release could have occurred either at the time of scratch creation, or by gradual scratch lip wear-down. Previous literature reports have supported that possibility for both of these phenomena. In a study of retrieval metal-on-metal femoral heads, Sieber et al. [175] reported on the metal surfaces' "self-polishing" effect and capability for scratches to be worn down by further joint motion. No reports have been published on this same effect for metal-on-polyethylene implants *in vivo*. As a point of reference, however, there has been an *in vitro* wear study involving total knee replacements [4] that addressed the tendency of CoCr scratches to be worn away through normal articulation against the polyethylene insert. That study concluded that 210 km of sliding distance (~10 years *in vivo*) would be required to wear away scratches similar to those measured on the present retrievals.

Dowson et al. reported the ratio between lip area and valley area for single scratch profiles measured on diamond-tip stylus-created scratches immediately following scratch creation on stainless steel plates [50]. The average ratio between lip area and valley area was 46%, indicating over half of the material displaced from the valley was liberated during the initial scratching event. The amount of material liberated during the initial scratch event could be affected by relative sliding speed, the shape of the object scratching the surface, and material type. It was also noted in that study that scratches were rarely symmetric. Lack of symmetry between lips on the same scratch was also noted on the retrievals analyzed for this work (Figure 57).

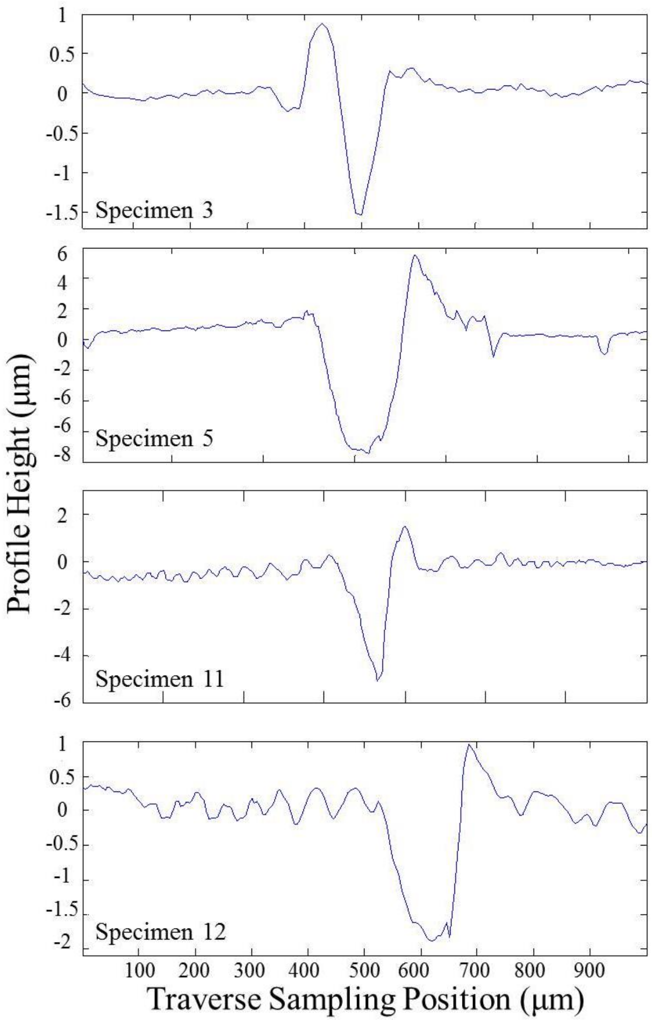

Figure 57: Example scratch profiles measured on each retrieval specimen displaying significant difference between lip heights measured on a single scratch.

It needs to also be borne in mind that when scratches measured on retrievals are displayed, most often each axis is on a different scale, to accentuate scratch severity for purposes of visual emphasis. When each axis is on the same scale, the slopes on the sides of the pile-up material are much less steep than most scratch profile illustrations suggest (Figure 58).

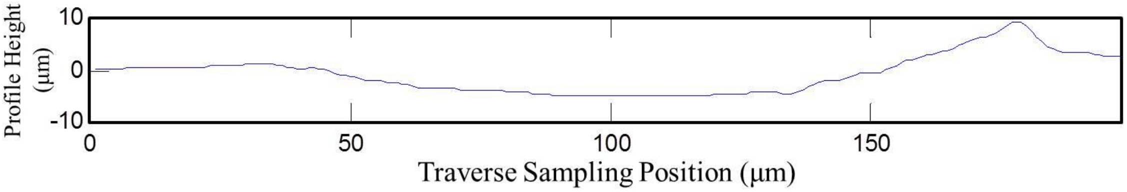

Figure 58: Scratch profile plotted with each axis on the same scale to display the actual scratch shape.

The total volumes of metal released from the femoral heads were 2.37 mm^3, 1.11 mm^3, 5.31 mm^3, and 0.56 mm^3 for the four respective samples over the course of the implant lifetime (5.1, 13.5, 14.8, and 6.2 years, respectively). Typical metal-on-metal volume loses have been reported to range from 0.3 mm^3/year to 6 mm^3/year in retrieval analyses [141, 175]. Langton et al. reported adverse tissue reactions to occur with bearing surface wear rates as low as 3mm^3/year [120]. Results of *in vitro* wear tests showed serum ion levels to increase 1,192 – 3,119 µg/L per mm^3 of metal wear volume if ions are not cleared from by the kidneys [85]. These concentrations well exceed thresholds proposed for monitoring when adverse reactions to metal debris may be occurring [76].

This process was also completed on four retrievals that displayed scrape damage (Specimens #1, 7, 13, and 18), to determine if the scrape events were primarily deposition events or if net material removal had taken place. The same MATLAB program was executed for each of the OP scans recorded for those four retrievals, reporting the total volume of metal piled up and the total volume scraped away. A total of 40, 41, 75, and 92 OP scans were analyzed for each respective retrieval. The raised material could have been either CoCr micro-scratch lips or titanium alloy transfer material, since the OP scans alone were unable to differentiate between the two.

Those results (Figure 59) showed that while scrapes most often tended to be net deposition events, material removal also occurred during many of these events, as was most evident in Specimens #13 and 18. On average, there was 19% (s.d. = 65%) more raised material than removed material in this set of scrape OP scans.

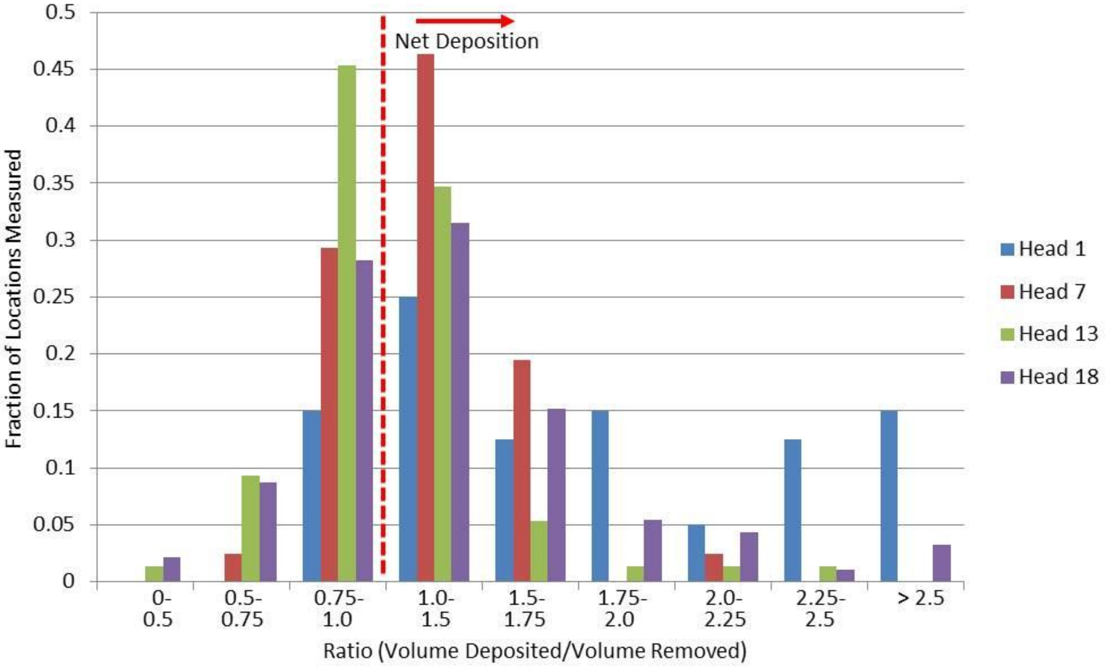

Figure 59: Ratios of material volume deposited to volume removed for representative scrapes as measured from OP scans. Data to the right of the red line indicate net deposition in that OP scan.

While this lip-vs.-valley volumetric analysis provides no basis to distinguish between material released at the time of scratch creation versus material released by gradual scratch lip wear-down, either form of release would have the effect both of liberating third bodies and of providing high-surface-to-volume-ratio particulates that would be of concern as source material for metal ion release or metallosis [38]. The analysis of deposition volume on scrapes shows the potential for metal transfer to the femoral head to occur (presumably from acetabular shell contact). These deposits would similarly have the potential to be subsequently worn down and released into the joint space. This wearing-down process would likely occur faster for titanium than for the CoCr lips, due to the softer metal composition. Some of this material could also be smoothed down but not released into the joint space, potentially tending to form the smoother “mesa-like” deposits observed on other retrievals.

Discussion

For total joint replacements with a polyethylene bearing surface, dramatically accelerated wear is often associated with accrual of damage to the hard-surface counterface. Moving from qualitative to quantitative assessments of this interaction requires a basis for representing hard-surface damage in a manner conducive to performance of physics-based wear analyses. The present formulation introduces a multiscale experimental/computational framework for making such damage representations. Global-level and micro-level imaging are coupled, to computationally register the severity and directionality of scratch, scrape, and transfer deposit damage present on entire implant bearing surfaces. This damage registry framework proved practical for use for typical retrieval total hip implants, thus opening the way for quantitative analyses of damage-related polyethylene wear rate acceleration on a case-specific basis.

Many previous literature studies have reported femoral head damage with the potential to cause wear acceleration. The results of such retrieval studies have often been the basis for femoral head damage creation for *in vitro* wear testing. The present study represents the first instance of lip heights of individual scratches being systematically cataloged on retrieval heads, as opposed to spot-specific reports of standard surface roughness parameters. Of the metrics reported in retrieval series in the literature, peak height, R_p, has been the most commonly used parameter to quantify scratch lip height. R_{pm} has also sometimes been reported in retrieval studies. It is calculated by dividing the evaluation length into five equal sections, measuring the highest peak in each section, and averaging those peaks [78, 146]. Peak height values have previously been reported to be on the order of 10-20 μm on CoCr heads [19, 106], up to 30 μm on ceramic heads [148], and up to 100 μm on Oxinium® heads [95, 106]. The maximum scratch lip heights reported in the present study, 28.5 μm, showed good general consistency with those previously reported values. In previous literature reports, peak heights of this severity have been reported in dislocation retrieval series. Similarly, the most severe scratches in the present series were observed on implants that had experienced dislocation.

Lip heights of scratches attributable to third body damage have typically been less severe, on the order of 2-4 μm [11, 91]. Efforts are ongoing in our laboratory to identify the tools and steps during the THA surgery itself that hold the possibility for introducing third body particles into the joint space. More details of this process and an automated image processing program for particle sizing in that work are included in Appendix A.

Previous literature studies have been unable to relate the R_p values measured on retrievals to corresponding *in vivo* wear rates [77, 181]. As defined, the R_p value represents only the single maximum asperity height in the area analyzed. In clinical situations, the amount of material build-up may vary substantially along even a single scratch. Also, multiple scratches of varying severities may appear in close proximity, a situation which R_p and R_{pm} are unable to meaningfully represent. The present study's scratch-based wear algorithm thus constitutes an advancement on previous work, in that it allows for multiple scratches to be modeled using a deterministic relationship that has already been shown to have a direct correlation to wear rate increase in pin-on-disc situations [50, 144].

In scraped regions of the present retrieval specimens, average R_a values were on the order of 0.5 μm. These values agree with average R_a values of retrieval femoral heads in the literature [78, 92, 94]. Maximum R_a values up to 4.3 μm have been reported by Tipper et al [186]. The maximum values detected in this study were of the same order of magnitude but, at 7.48 μm, slightly exceeded previous reported values. The difference in profilometry sampling technique may have accounted for some of that difference in R_a

values. When R_a values obtained via profilometry are reported in literature, they necessarily are reported as output by the profilometer software. When measured that way, they may include some undamaged portions of the implant surface in the analysis area, particularly in the case of 3D profilometry. This has the effect of lowering the reported R_a value for the damage region. The post-processing programs developed for the present work, however, allow for the damaged region to be segmented from the undamaged region in the OP scan, and thus allow for the R_a value to be measured in only the damage region. This allows for more meaningful reporting of damage R_a, which necessarily would be higher when measured only for damaged areas, as opposed to when undamaged regions are also included.

Generally, the R_a values measured on the transfer deposits agreed with the results of previous studies involving head-shell contact [17, 106, 132, 155]. While these transfer deposits showed R_a increases of 30- to 50-fold when compared to baseline values, they were substantially less severe than many of the reported scrape R_a values. Both of these damage types have been attributed to head-shell contact. Transfer deposits have also been associated with cases of liner wear-through and dissociation. The large, darkened transfer deposits may be the result of scrape damage that has been worn down and smoothed through acetabular articulation over time, thus lowering the average roughness and attenuating the directional nature of individual scrapes.

The image processing program detected nearly 2000 individual scratch segments in some of the more severely damage head in this series. These heads had damage covering up to 25% of the articular surface. In preliminary work with this scratch-based formulation, simulations with up to 12,000 scratch segments were successfully executed. The capability to model many thousands of scratch segments allows for even more severely damaged femoral heads to be modeled using this approach. The Abaqus research edition currently allows an unlimited number of nodes to be included in each simulation. The number of nodal locations able to be processed by user subroutines was not documented, but was the limiting factor in performing analyses with larger numbers of scratches. Preliminary work with the subroutines using the Abaqus v.6.6.1 edition would not allow for more than 12,000 scratches to be modeled. A higher threshold might have been possible with later Abaqus versions.

The present FE results included wear acceleration values up to only 11.6-fold. These wear acceleration values were lower than the highest reported values in literature. Clinical ranges of volumetric wear have been reported as 1.9-236.8 [6], 8-284 [97], and 1-131.3 [182] mm^3/year, representing 125-, 36-, and 131-fold variations, respectively, within individual patient cohorts. One reason for the present lower wear rates may have been that only repetitive level walking gait cycles were simulated for this wear series. In a previous FE study, the addition of stair-climbing challenge to a walking simulation showed a 57% increase in wear when compared to a walk-only simulation under roughened conditions [91]. Other studies have similarly reported additional wear increases when occasional stair descents [12] and stumbling and jogging [20] have been included in the analysis. When identical duty cycles are used, wear tends to be self-limiting due to "troughs" being cut into the PE surface. Damage features causing wear acceleration will continue to overpass only the trough (Figure 60).

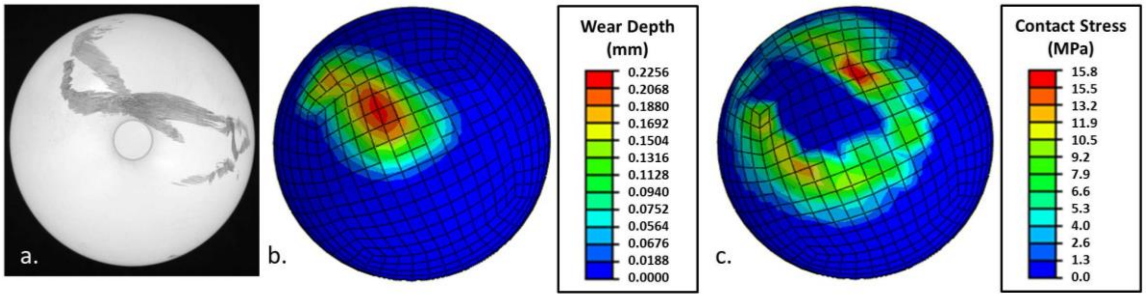

Figure 60: Trough effect example. a. Retrieval femoral head 17. b. Computed wear depths after 1 mesh update. c. Contact stress following the first mesh update, showing decreased stress in trough area already worn away.

Another fundamental problem with retrievals is that they most often come from revision surgeries, and thus reflect worst-case scenarios. Studies of well-functioning implants (retrieved at autopsy) are much less common [32, 40, 181]. Another major limitation of working with retrieval specimens, as noted above, is of course that the damage apparent forensically is just a one-time snapshot of status as of the time of the revision surgery. Typically, no information is available as to how long the detected damage may have been present, or to what extent acutely created damage may have been worn down with subsequent articulation over time.

The results of the orientation-on-trunnion analysis underscore the importance of knowing the actual femoral head orientation when analyzing the effects of femoral head damage on THA wear. Knowing the locations of component damage, relative to component orientation *in vivo* (and relative to the other THA components), greatly enhances the information obtainable from retrieval analysis. Surgeon documentation of anatomic orientation on all THA retrieval components would allow investigators to better connect component damage to pathological processes such as bearing surface wear, subluxation, and dislocation. Lack of head orientation documentation is a widespread problem in retrieval collections. Retrieval program coordinators and participating surgeons need to give enhanced attention to this issue, and to mark the anatomic orientation of the femoral head. To help raise consciousness on this issue, our group made a presentation at ORS specifically stressing this point [84].

To the author’s knowledge, the present datasets constitute the first-ever compilations of whole-bearing-surface damage features on orthopaedic total joint replacements. Besides their usage in the context of enabling wear computations, such datasets will likely prove useful in other contexts, such as for forensic assessment of specific surface damage events, and for “reverse engineering” of implant designs, to minimize wear-consequential counterface damage.

The ability to map microscopic-level implant damage over entire femoral heads offers new possibilities for quantifying third body and other adverse effects. Determination of damage patterns and severities observed on specific retrieval femoral heads can serve as a maximally clinically grounded basis for modelling clinically-realistic damage in laboratory wear simulations. The present damage-feature-based FE formulation expands upon the capabilities of previous computational wear models, by allowing simulation of wear acceleration due to actual *in vivo* damage patterns.

CHAPTER 5: WEAR INCREASE DUE TO DISLOCATION AND CLOSED REDUCTION

Many of the most severe damage features from the retrieval series (discussed in Chapter 4) were observed on femoral heads that had experienced one or more dislocations. A larger series of dislocated retrievals was therefore analyzed in its own right, using the above-described procedures to generate FE wear models to determine the wear acceleration propensity of damage due to dislocation and closed reduction. This dislocation series also addressed the ability of global-level photographs to predict relative wear acceleration propensity between retrievals. The results of the global photograph and FE analyses were used to determine how strong the relationship was between visually apparent damage severity and actual computed wear rates. It was hypothesized that the estimated wear accelerations accompanying dislocation would be substantial, and that there would be a strong quantitative association of wear acceleration with apparent severity of global-scale head damage.

Methods

Retrieval components from 27 metal-on-polyethylene THAs that had undergone dislocation(s) were available in the Laboratory's retrieval collection. Each retrieval specimen was photographed using diffused-light photography. The corresponding set of photographs was provided to five analysts (experienced orthopaedic bioengineers working in the same laboratory as the author), who were asked to rank the heads from least to most damaged, based on appearance in the reflection-masked global images. The analysts were not given any instructions as to how specifically to judge damage severity. Agreement between the individual rank orderings of the five evaluators was assessed by calculating the concordance between each set of pairs [81].

Once the ranks from all the analysts had been established, they needed to be combined in some way to reduce the five sets of rankings into an overall damage severity ordering. Ordinal sequencing allows for rank order (1st, 2nd, 3rd, etc.) by which individual data points can be sorted, but it does not allow determination of relative degree of difference between them. This system works well for data that consist only of rank or position, rather than actual quantitative measurements [116]. The ordinal system achieved this by majority "vote". To start this process, the femoral head with the majority of first place votes from the analysts (i.e., the specimen judged to be the least damaged) was determined. This process was continued for each sequential place until all femoral heads had been assigned a final rank. In the case of a tie, the ordinals given to each of the tied femoral heads from all analysts were added together.

After this ordinal ranking was complete, a representative subset of thirteen of these femoral heads was then selected for wear simulation (Table 11). Retrievals were selected so that they were evenly spread throughout the distribution. An effort was made to include as many as possible of the retrievals that had already been analyzed. Further information providing clinical context for these thirteen specific cases is presented in Table 12.

Table 11: Dislocation femoral head demographics (1=least severe, 13=most severe damage).

Visual Rank Order	Sex	BMI	Head Size (mm)	Age at Primary Surgery	Time to Revision (years)	# of Dislocations
1	F	29.8	36	68	0.2	3
2	M	30.5	28	68	6.6	17
3	F	28.3	28	70	0.7	2
4	F	26.8	32	71	0.8	3
5	F	46.1	28	60	0.4	3
6	F	23.8	28	75	7.4	4
7	M	32.1	32	70	3.0	3
8	F	27.8	28	72	8.0	4
9	M	24.4	28	34	19.2	5
10	M	22.8	28	38	5.4	5
11	F	27.5	32	89	1.5	2
12	F	22.5	28	54	0.2	1
13	F	29.8	22	38	17.1	2

Table 12: Dislocation series case data.

Visual Rank Order	Times(s) to Dislocation (Months)	Dislocation Direction	Dislocation Action
1	1.2	Posterior	Stumbled and fell
	1.4	NR	NR
	1.6	Anterior	NR
2	36.0	NR	Removing socks
	67 (6X)	NR	Often while asleep
	78 (9X)	NR	Often while asleep
	79.4	Posterior	Sleeping (especially soft mattress)
3	2.5	Posterior	NR
	7.1	Posterior*	NR
4	3.2	Posterior	Sitting, bent all the way over and twisted to the right
	4.6	Posterior*	NR
	8.4	Posterior*	Standing and turned foot inward
5	1.9	NR	Reaching for stove
	1.9	NR	NR
	2.2	NR	Getting out of car (possibly this was only a subluxation)
6	NR	Posterior	Patient had recurrent dislocation of both hips, which involved noncompliant activities such as deep flexion at the hip
	NR	Posterior	
	31.5	Posterior	
	86.5	Posterior	Felt pop in hip
7	10.1	Posterior	NR
	31.3	Posterior	Moving a planter, flexed and internally rotated hip
	34.5	Posterior	NR
8	87.4	Posterior*	NR, possibly pivoting
	87.4	Posterior*	NR, possibly pivoting
	95.9	NR	NR
	95.9	NR	NR
9	NR	Posterior*	For all dislocations, patient was in low seated Position (knees higher than hips) or stooped down and with a turn to the left
	NR	Posterior*	
	160.2	Posterior*	

Table 12 – continued

	208.2	Posterior*	
	226.3	Posterior*	
10	2.0	Posterior*	NR
	62.0	Posterior*	Carrying heavy bucket, got off balance
	62.0	Posterior*	Sitting on toilet, felt hip go out
	62.0	Posterior*	NR
	62.1	Posterior*	NR
11	11.5	NR	NR
	11.5	NR	NR
12	2.1	Posterior	NR
13	155.9	NR	NR, but recurrent subluxation and hip feeling wobbly
	205.0	NR	NR, but recurrent subluxation and hip feeling very sloppy

NR = Not reported
*Surgeon’s best inference of dislocation direction.

The above-described procedures (Chapter 3) were used to register and measure individual damage feature locations and severity. Patient-specific FE models were then generated of each retrieval specimen. As noted above, orientation of the femoral head on the trunnion was generally unknown for this set of retrievals. However, in the case of dislocations, the scrape damage due to acetabular shell contact tends to occur at characteristic locations. The global femoral head photographs were used to locate the centroid location of that scrape damage region, based on its global-scale visual appearance. This damage centroid location was used to estimate the *in vivo* orientation of that retrieval, as follows.

A previous set of computational models from our laboratory had investigated the scraping wear occurring during dislocation-prone maneuvers [59]. These models showed wear scars consistent with those of femoral heads revised for dislocation (Figure 61) **. Models were available for various acetabular cup orientations, BMI levels, and dislocation-prone challenges (gait, pivot, squat, sit-to-stand (low), sit-to-stand (normal), and stoop). For each retrieval head, the model set most closely matching its acetabular cup orientation (which had been reported during the retrieval surgery) was used to estimate the orientation of that retrieval head on the trunnion. Based on a brief review of the damage patterns for the various challenges modeled, the results of the sit-to-stand (normal) best matched those of the retrievals. Therefore, those results were used for the orientation estimation. The results from the base BMI of 25 were used.

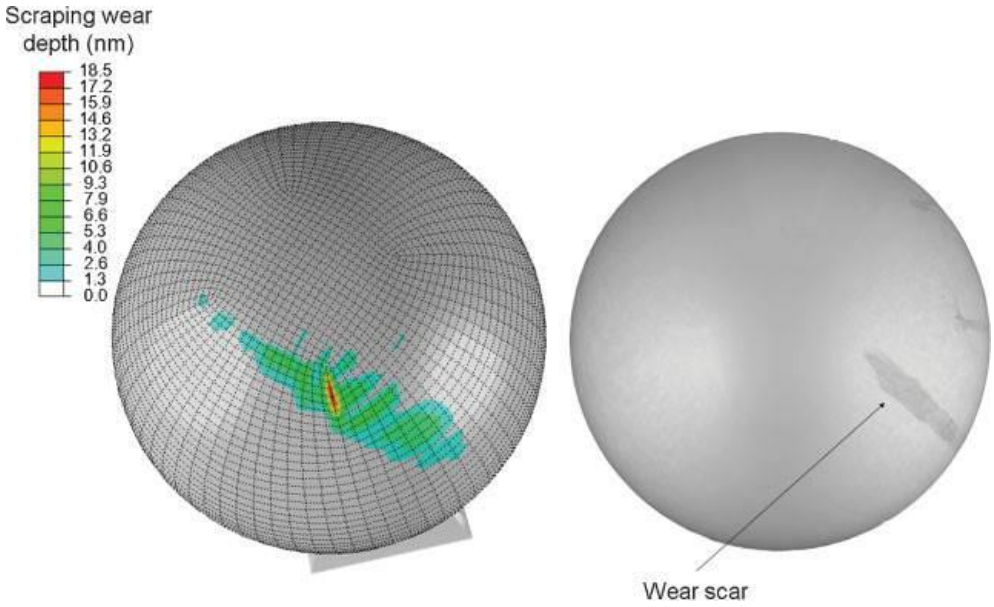

Figure 61: Scraping wear scar (left) computed on the femoral head for a 40˚ inclined, 6˚ anteverted cup. A similar damage feature (right) is apparent on a femoral component head (with similar trunnion taper axis orientation) from an implant that was revised at 2 months due to dislocation[59].

** These simulations were completed by Dr. Jacob Elkins, who provided the necessary Abaqus ODB files to make this orientation estimation possible.

In the selected FE model for each retrieval case, the coordinates of nodes reported as containing damage were output from the Abaqus output database (ODB) file and were used to compute the wear scar centroid (Figure 62a). On the retrieval, the damage area was segmented from the global photograph using an analyst-set threshold in MATLAB. The centroid of this defined damage area was computed via the *regionprops* function (Figure 62b). The orientation of the retrieval on the trunnion was then perturbed about the trunnion axis until the distance between its damage centroid and the FE model's damage centroid was minimized, using Microsoft Excel's optimization function. This least-distance orientation provided an estimation of the retrieval's *in vivo* orientation on the trunnion, thus presumably reducing the uncertainty of computed wear due to otherwise unknown head orientation. The angle between the femoral neck and stem was assumed to be 135° in all cases, and the femoral anteversion (which had also been reported at the time of revision) was customized to each retrieval case.

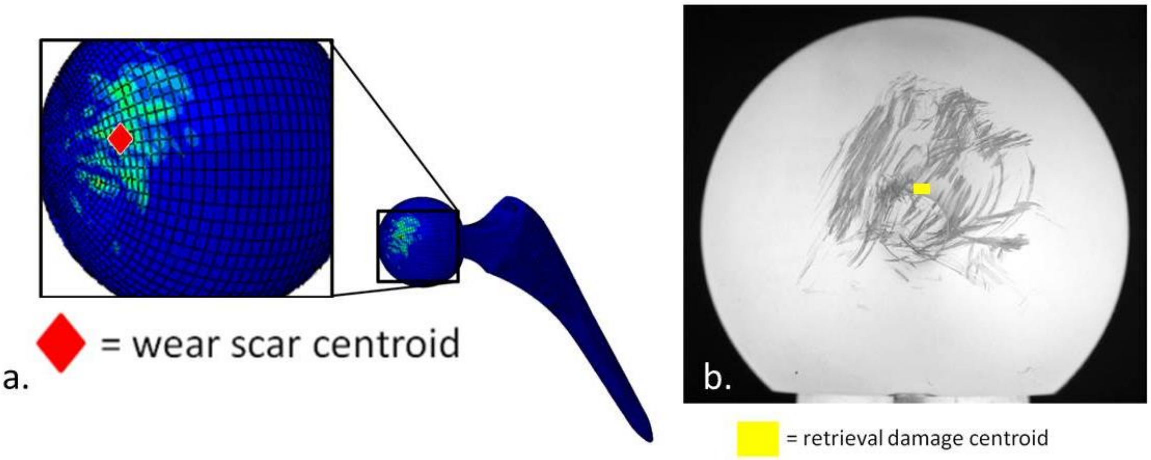

Figure 62: Centroid locations are indicated on (a) an example wear scar computed on a femoral head [59] and (b) a dislocation retrieval.

While the head-to-trunnion orientation had not been recorded for any of the heads retrieved due to dislocation in the laboratory's current collection, one femoral head that had been revised for aseptic loosening but displaying scrape damage similar to the dislocation retrievals (Figure 63a) happened to be stuck on the femoral neck, and therefore had known anatomic orientation. For purposes of providing a "reality check," this head was used to estimate how accurately this method for post facto orientation estimation could predict the actual *in vivo* orientation. On the stuck retrieval, the damage centroid was located 17˚ anterior to the sagittal midline. The damage centroid FE model most closely matching this retrieval (Figure 63b) predicted that the retrieval damage centroid would be positioned 9˚ anterior to the sagittal midline, an 8˚ differential. This level of agreement between the actual retrieval location and predicted location was very encouraging, and suggests this orientation estimation method may be able to replicate *in vivo* orientations reasonably well.

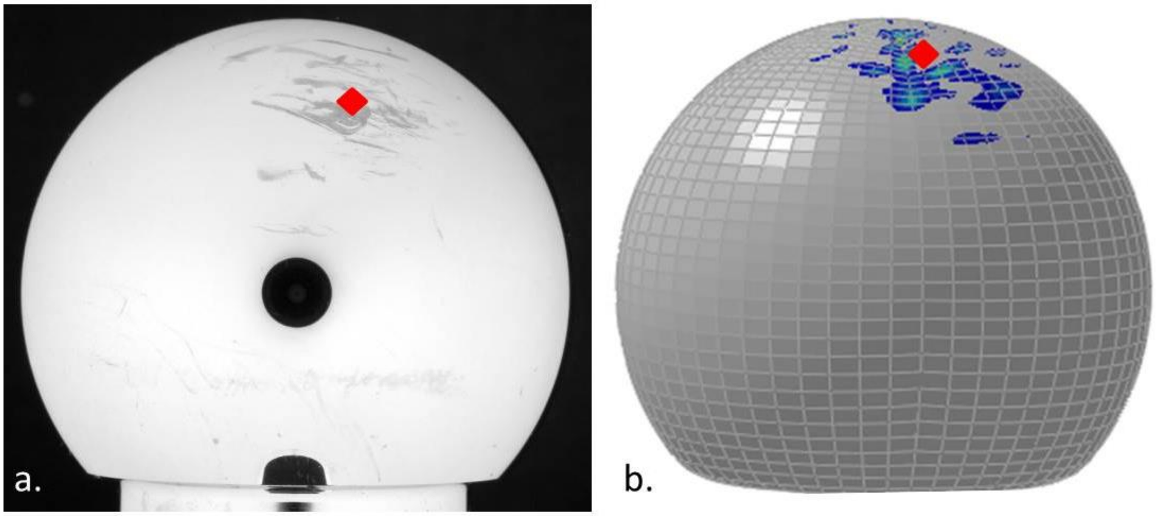

Figure 63: Damage centroid locations. a. Retrieval displaying characteristic scrape damage. The resultant centroid was 17˚ anterior to the sagittal midline. b. Wear scar result of FE model. The resultant centroid was 9˚ anterior to the sagittal midline, an 8˚ differential.

The wear simulations were run for one million cycles of level walking gait for each retrieval at its thus determined "least distant damage" orientation. The degree of association between the visual damage rank ordering and the computed wear rate was determined via concordance calculation [81]. The concordance calculation is useful in determining how well two diagnostic measures agree and can be used to evaluate reproducibility or inter-rater reliability.

Results

The concordance rates of the damage severity rankings for each pair of visual analysts ranged from 0.85 to 0.93 (Table 13). Across all five independent analysts, the concordance rate in ranking visual damage severity was 0.90, indicating relatively consistent assessments. Concordance correlation coefficient values of ±1 denote perfect concordance and discordance while a value of zero denotes a random relationship [124].

Table 13: Correlation coefficients of the damage severity rankings between each pair of analysts.

	AH	**VP**	**TS**	**GO**
KK	.88	.85	.86	.87
AH	-	.93	.93	.93
VP	-	-	.92	.92
TS	-	-	-	.93

The diffused light photographs (Figure 64, black-and-white images) and OP scans (Table 14) revealed dramatic levels of scratch and scrape damage to most of the femoral heads. Series wide, Specimen #13 showed the highest scrape-average roughness value, 3.47 µm. The most severely damaged regions on this and other heads corresponded to average roughness values in the range of several hundred times those of undamaged femoral heads [8]. OP scans showed individual scratches in this dislocation-specific series to have lip heights up to 21 µm. Across the series, wear acceleration varied widely (Figure 64, color-contour plots), depending on the damage location and severity. The FE results showed dramatic wear increases for almost all of the specimens modeled, when compared to baseline simulations of otherwise similar undamaged femoral heads (mean wear acceleration = 4.8-fold, S.D. = 3.5-fold).

Table 14: Results of OP damage assessment.

Visual Rank Order	**Average Roughness (µm)**			**Scratch Lip Height (µm)**			**Wear Acceleration (x Baseline)**
	Mean	**s.d.**	**Max**	**Mean**	**s.d.**	**Max**	
Baseline	0.01	0.01	n/a	0.09	0.08	n/a	n/a
1	0.24	0.12	0.41	0.93	0.33	1.34	2.0
2	n/a*	n/a*	n/a*	1.70	1.13	5.38	1.5
3	0.84	0.51	2.01	8.82	0.95	14.85	2.4
4	0.17	0.11	0.55	n/a**	n/a*	n/a*	1.2
5	0.22	0.07	0.52	n/a**	n/a*	n/a*	1.4
6	0.21	0.08	0.39	1.64	0.40	2.87	4.3
7	0.33	0.27	2.74	3.00	3.55	14.55	2.6
8	0.24	0.08	0.49	4.89	0.97	8.51	3.8
9	0.12	0.06	0.34	1.52	0.67	3.41	11.9
10	0.55	0.18	1.18	5.28	3.84	17.74	7.3
11	0.46	0.10	0.62	5.49	4.14	28.52	4.3
12	0.80	0.50	1.96	2.76	0.12	6.33	8.3
13	1.99	0.32	7.48	9.65	4.18	17.74	8.4

Note: The average roughness values were measured over all identified damage regions. Scratch lip heights were measured for each scratch cataloged.
* Only scratch damage was present
** Only non-scratch damage was present

The particular retrieval head whose apparent damage was ranked 9/13 by visual assessment showed the greatest effect, a volumetric wear acceleration of 11.9-fold. While this retrieval specimen appeared to have significantly less visually striking damage than several of the other specimens, various factors many have contributed to its higher wear rate. First, this specimen was recorded to have 1,754 individual scratch segments. While much of the scratching was relatively minor (average lip height=1.52 μm), the fact that this large number of scratches was spread out over a relatively large area minimized the wear-limiting “trough effect”. Also, these scratches were much more polarly located than much of the other damage noted in this series. Damage near the pole tends to cause higher wear rates than lower-latitude damage [130].

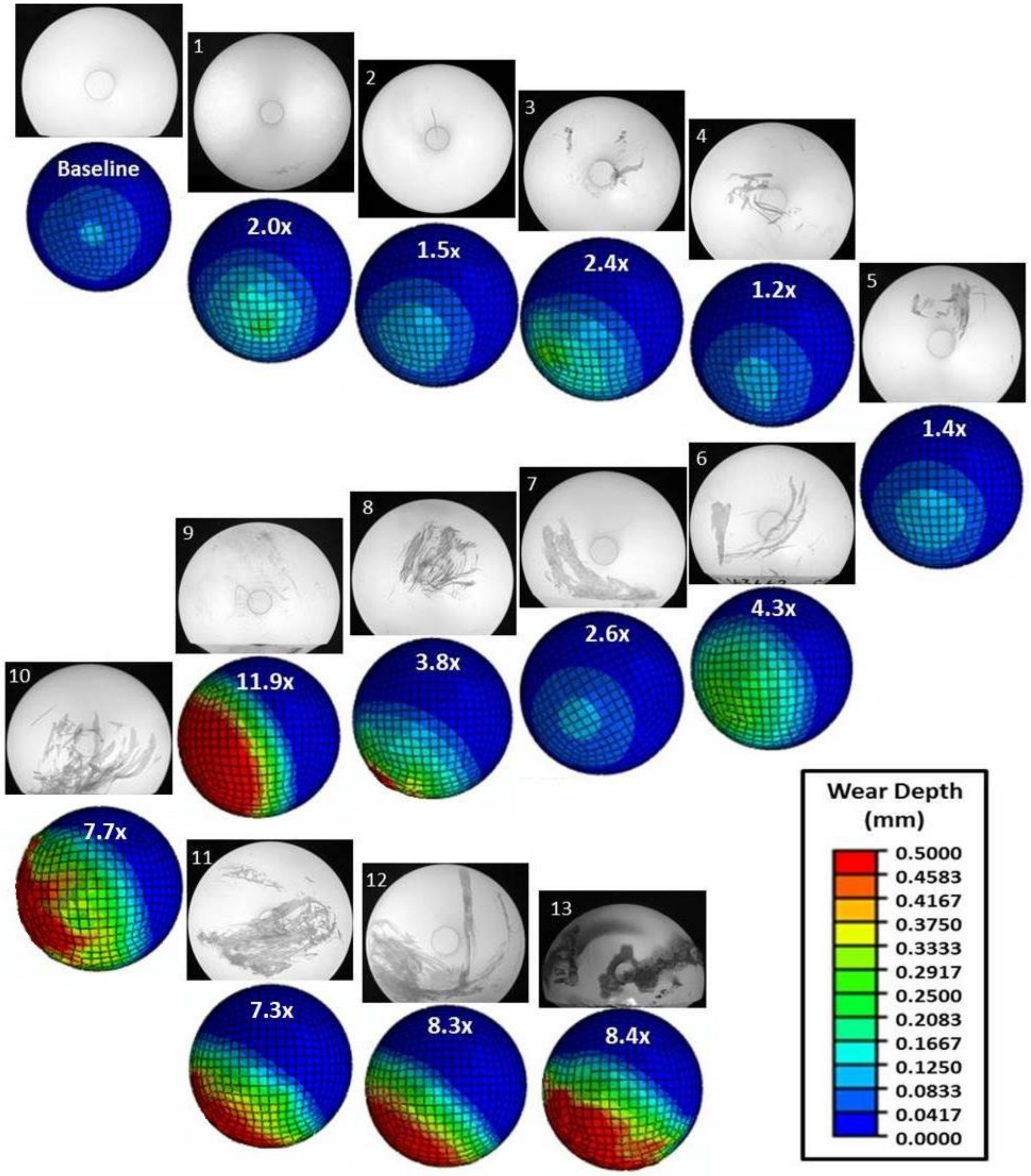

Figure 64: Diffused-light photographs and computed wear depths for each femoral head analyzed. Each diffused light photograph (polar views for heads 1 and 2, equatorial views for heads 3-13) displays the most severe damage features.

The concordance between the overall visual damage severity ranking and the computed wear acceleration ranking was 0.82 (Figure 65). This finding strongly supports the hypothesis that these two factors (visually evident head damage versus wear acceleration) would show consistent association. Interestingly however, there was no significant correlation of either visually apparent damage or of wear rate increase with either time to revision (R^2 =0.176 and 0.404, respectively) or with the number of dislocations sustained (R^2= 0.162 and 0.055, respectively).

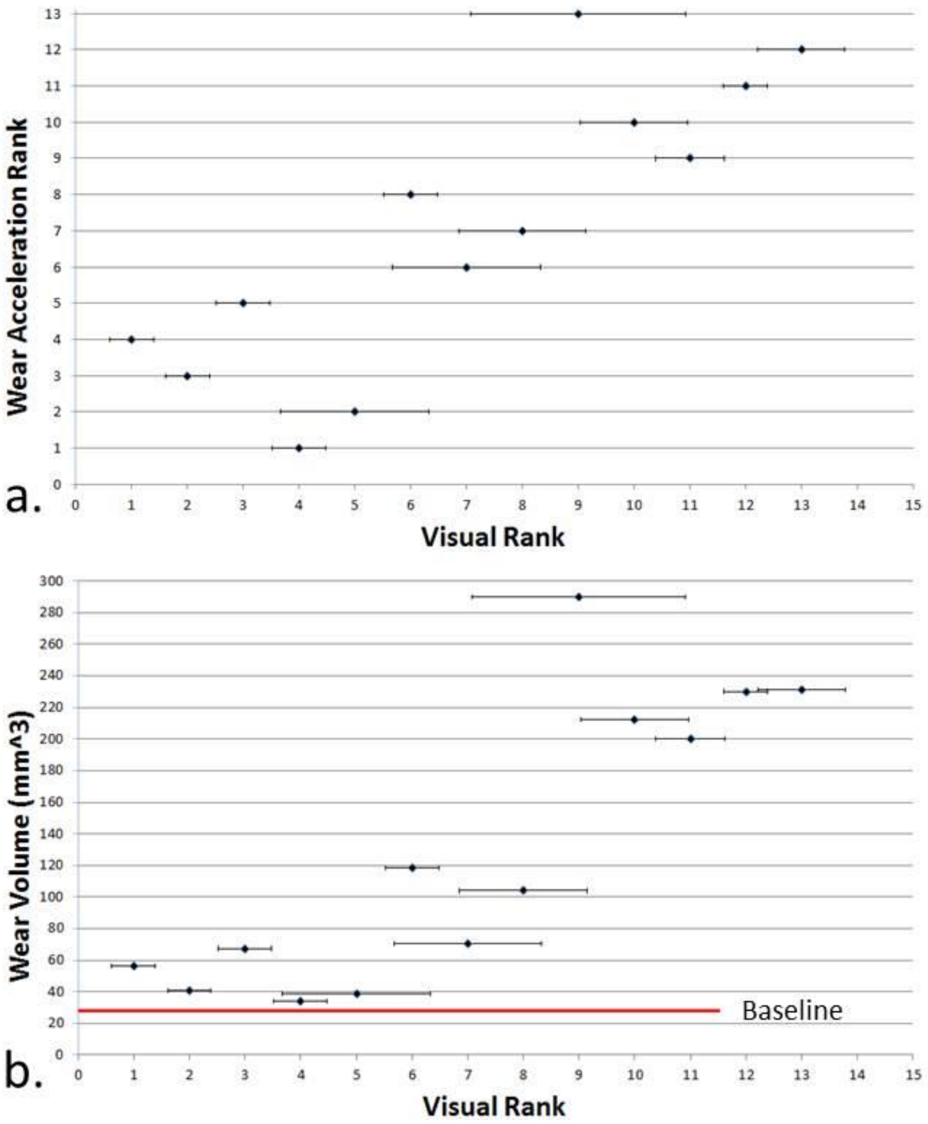

Figure 65: Comparison of femoral head ranking by visual assessment (95% confidence intervals) and computed wear acceleration. The concordance between the two rank orderings (b) was 0.82, indicating relatively strong rank association.

Discussion

While femoral head damage due to dislocation and subsequent closed reduction (or closed reduction attempts) has often been remarked upon, there have been only few and widely conflicting anecdotal reports as to the potency of such damage for accelerating bearing surface wear. In the case of Oxinium® heads, which have a thin ceramic-like oxidized zirconium layer atop bulk zirconium alloy, scraping-induced gouges on retrieval dislocation specimens have been especially dramatic visually. One study (with financial support from a competing manufacturer) found closed-reduced dislocated Oxinium® heads to produce up to 50 times more polyethylene wear than undamaged heads [95]. Another study (by Oxinium®'s manufacturer) [24], however, reported that retrieval Oxinium® femoral heads damaged from dislocation head wear increases of at most only 1.7 times higher than unused Oxinium® heads. Head-on-trunnion orientation was not addressed in either of these studies.

Until now, no formal basis has existed for systematically quantifying the effect of head dislocation upon PE wear. The present model utilized experimentally based relationships between wear acceleration and the location, orientation, and severity of scratch, scrape, and transfer deposit damage features, to allow for wear acceleration estimates on a specimen-specific basis. Global-level visual rank ordering was able to predict the rank ordering of wear acceleration reasonably well, with a concordance of 82%. Some of the differences in the two orderings are probably attributable to the subjective nature of global damage severity judgments, and to the fact that the global-level photographs sometimes rendered particular damage features to appear either more or less severe than the corresponding OP scans showed. For several specimens, scrapes that appeared to be very severe in the global-level photographs turned out to exhibit far less than expected increases in OP-based R_a values. For example, for two femoral heads with near-median damage (Specimens #6 and 7) that were ranked similarly by global visual assessment and that had similarly-appearing maximal scrape damage, representative OP scans of the most severely scraped regions in Specimen #7 showed R_a values approximately 3.5 times higher than the most severely scraped regions of Specimen #6 (Figure 66).

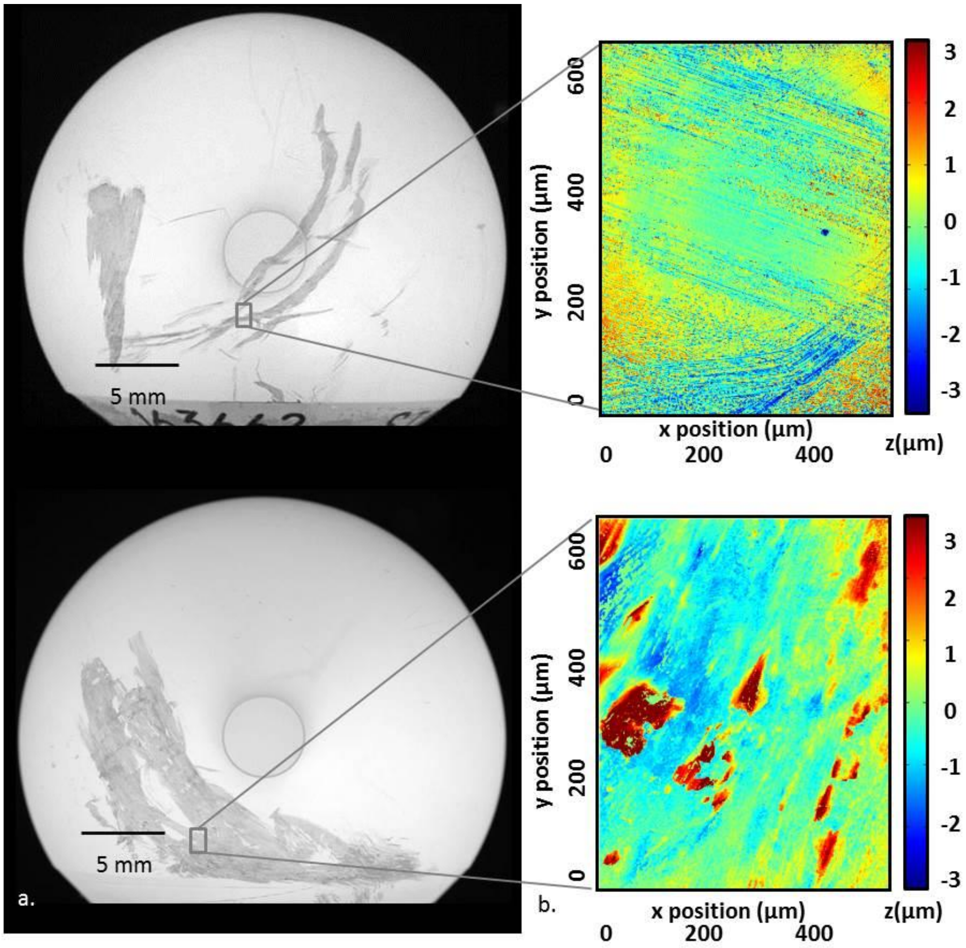

Figure 66: Differing R_a values example. (a) Global diffused light photographs of near-median-damage femoral heads (visually ranked #6/13 (top) and #7/13 (bottom)) and (b) OP scans of a representative severe damage region in each photograph. Corresponding R_a values of the indicated region were 0.22 µm (#6) and 0.76 µm (#7), respectively. The reported R_a values were computed in only the damage region of each OP scan.

In addition to severity, the damage location obviously affects wear rates. A prior FE wear study of generic damage features [130] had shown that damage located superiorly on the head near the sagittal midline was particularly deleterious in terms of accelerating PE wear. The importance of damage location can be appreciated from the differing computed wear rates of two specimens (#9 and #10) that had been visually assessed to have similar damage severity (Figure 67). While Specimen #10 was judged visually and measured by OP to have the more severe scratching and scraping, Specimen #9 showed nearly double the wear acceleration in the FE model. The more superiorly-located damage in Specimen #9 was probably responsible for this much higher wear rate. While it is intuitive that superiorly-located damage would tend to be more wear-consequential than near-equatorial damage, such "relationships" are at most nominal, and they need to be viewed against the backdrop of highly idiosyncratic individual specimen damage distributions and wear scar morphologies.

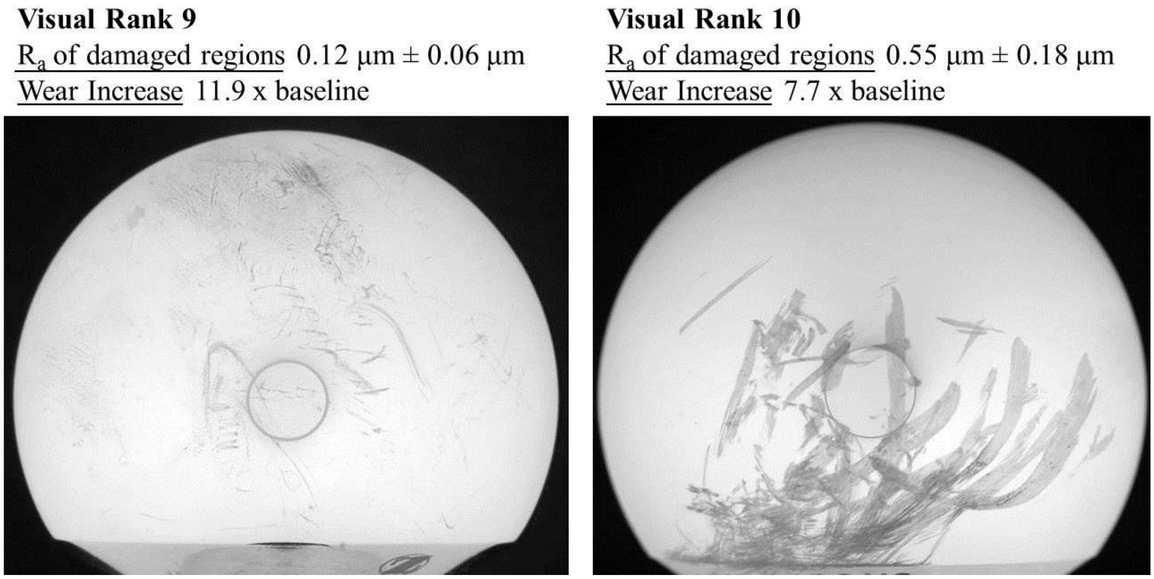

Visual Rank 9
R_a of damaged regions 0.12 µm ± 0.06 µm
Wear Increase 11.9 x baseline

Visual Rank 10
R_a of damaged regions 0.55 µm ± 0.18 µm
Wear Increase 7.7 x baseline

Figure 67: The femoral heads ranked #9 and #10 by visual assessment demonstrate the importance of damage location. While Specimen #10 was judged visually and measured by OP to have the more severe damage, Specimen #9 showed nearly double the wear acceleration in the FE model. The more superiorly-located damage in Specimen #9 was probably responsible for this much higher wear rate.

In this series, the number of dislocations experienced had no correlation with either visually apparent damage or wear acceleration. For example, the specimen ranked as having next-to-least damage by visual assessment, and which showed only small amounts of damage and minimal wear increase, had been clinically documented to have dislocated 17 times. By contrast, the three retrievals judged to be most severely damaged by visual ranking had only dislocated once or twice. Mai et al. reported similar findings [132], with no correlation between R_a and time *in vivo* or with the number of dislocations. The lack of correlation between the number of dislocations sustained and damage or wear severity underscores the fact that every single dislocation must be approached clinically with the presumption that it can cause significant damage and therefore hold the potential for substantial wear acceleration.

As previously stressed, a major limitation of working with retrieval specimens is that the damage apparent forensically is just a one-time snapshot of damage status as of the time of the revision surgery. In the case of dislocation retrievals, each major feature of head damage can reasonably be presumed to have occurred in concert with a specific dislocation/relocation episode. However, for patients experiencing multiple dislocations, it is obviously impossible to judge how long the forensically apparent damage from individual dislocations may have been present *in vivo*.

For the current set of retrievals, no orientation information was known for the great majority of specimens. While the “minimum centroid distance” orientation estimation method presented here arguably provides at least a reasonable first estimation for the head-on-trunnion orientation, actual physical knowledge of this orientation would still be the gold-standard for documenting damage feature locations and predicting wear acceleration.

As part of our institution’s new retrieval program launched in 2012, surgeons have been asked to mark the orientation of the femoral head before it is removed from the trunnion. The procedure suggested was to draw a line or spot on the femoral head intraoperatively using a surgical marking pen such as Surgi-Mark, with the corresponding orientation noted on a retrieval information sheet. Alternatively, the orientation can be written on the femoral head itself (i.e., write a “P” to indicate posterior orientation). Once the anatomic orientation is permanently indicated, usually with a scribed line on the bottom ring of the head, the intraoperative marker can be washed off. To date, this initiative has been gratifyingly successful: 36 modular femoral heads have been received, with orientation known for 21 (58%). The requested orientation was marked on 17 heads (47%), and four heads (11%) were received still attached to the stem.

With dislocations, this orientation knowledge could be used to try to determine if there is any link between dislocation direction (anterior versus posterior) and wear acceleration potential. The direction of dislocation is typically recorded in post-op reports. Different dislocation directions would presumably result in different damage locations, and possibly different levels of damage severity. A collection of dislocation retrievals for which the orientation is known could be used to build FE wear models and determine if a particular dislocation direction is more wear-consequential.

While obtaining a successful closed reduction with minimal manipulation of the hip is the ideal immediate treatment for dislocation, it should be borne in mind that closed reductions achieved only after lengthy/forceful/heroic manipulation attempts carry the potential for substantial amounts of iatrogenic head damage. The trade-off of increased likelihood of a complex and difficult late revision due to massive wear-induced osteolysis, versus the much less radical surgery of an open reduction of the dislocation, needs to be kept in mind in cases where success remains elusive with ever-more-forceful closed reduction attempts. The ideal standard of care [132] is for closed reductions to be performed with the patient under heavy intravenous sedation or in the operating room under general anesthesia, with dislocation direction confirmed (before reduction) by cross-table lateral radiographs, and with fluoroscopy used for guidance during the reduction maneuver itself. This allows extreme care to be taken to minimize contact between the femoral head and the acetabular rim during relocation maneuvers, to prevent additional damage to the head. Against that backdrop, it is important to recognize that a substantial fraction of closed reductions are performed by emergency room physicians (70% of admitted cases in one center [71]), who in many if not most instances are less attuned to the phenomena of head damage wear-induced osteolysis than are orthopaedic surgeons. Orthopaedic surgeon presence is therefore highly desirable for closed reductions whenever practical, and formal and informal dialog on this subject between orthopaedic surgeons and emergency medicine colleagues needs to be encouraged.

In summary, the present results indicate that typical dislocation (and/or closed reduction) damage is capable of producing order-of-magnitude wear rate increases (here, as high as 11.9-fold), and on average leads to several-fold increases (4.8-fold in this particular group). While it is not currently possible to make patient-specific *in vivo* assessments of damage occurring due to a given dislocation and/or closed reduction episode, wear accelerations in these ranges are obviously of major concern clinically. Heightened surveillance is therefore justified for patients with closed reduction of a dislocation.

CHAPTER 6: DAMAGED TEMPLATE IDENTIFICATION FOR PHYSICAL WEAR TESTS

While numerous physical wear tests have been conducted in academic and industrial laboratories to study the effects of third body and dislocation/subluxation damage, a consensus wear testing protocol for that purpose has so far not emerged. While virtually all investigators have stated that their particular test method is consistent with clinical observations, justification as to how they came to that conclusion has seldom been provided.

A clinically grounded method for damage creation holds attraction as a basis for standardizing physical wear testing. Toward that end, the damage registry from the retrievals analyzed in Chapter 3 was used to develop templates of femoral head damage statistically representative of clinically observed damage. These templates provide a basis to create functionally scratched and scraped femoral heads, upon which physical wear tests can be conducted. For purposes of such wear testing, only scrapes and scratches were considered. (Due to the complexity of transfer deposits and the fact that they are a relatively infrequent occurrence compared to scratches and scrapes, retrievals displaying transfer deposits were excluded from this analysis.) The results of the retrieval study were used to determine the range of clinically occurring scratch lip heights and scrape R_a values, their respective preferential locations, and their wear acceleration potentials. These data were used to generate damage templates that provide guidance for creating functionally damaged femoral heads. Alternative damage templates were created to simulate the effects of (i) only scratches, (ii) only scrapes, and (iii) both of these damage types on the same head. Corresponding FE models were created for each damage template to estimate the wear acceleration due to that damage pattern.

Methods

To develop a wear testing protocol capable of gaining widespread acceptance, there is need for ability to incorporate clinically-realistic counterface damage. The results from the retrieval study were used to develop statistically based templates for functionally damaged heads representative of the size, location, and severity of clinically occurring damage. A total of 20 retrievals (specimens 1-20 presented in Chapter 3), displaying a wide variety of damage severities and damage distributions were used for this purpose. The damage severity information measured on these retrieval femoral heads analyzed was compiled to determine the distributions of scratch lip heights (Figure 68) and scrape R_a values (Figure 69).

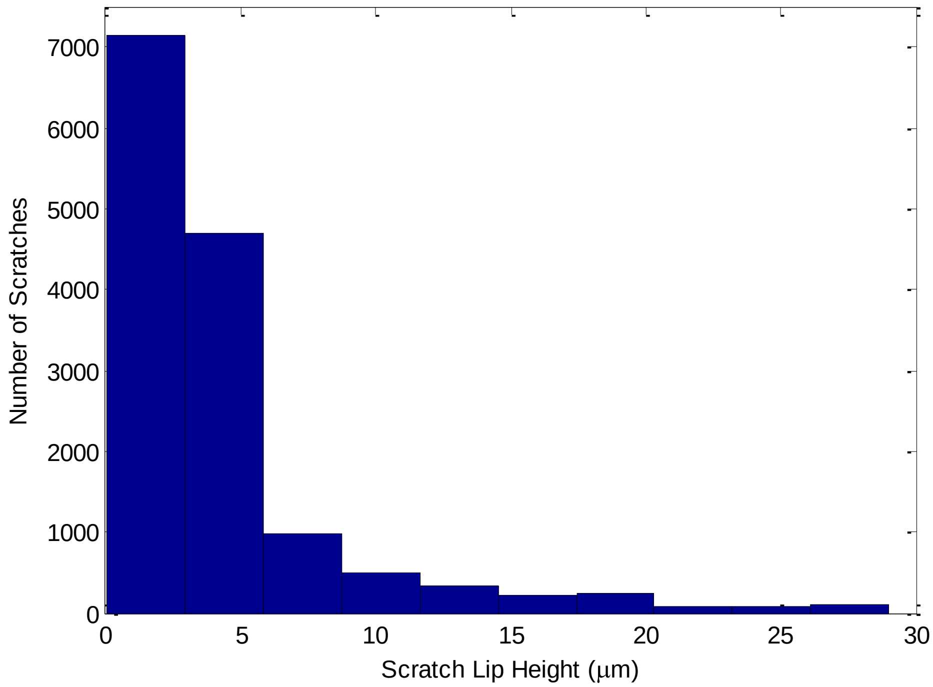

Figure 68: Histogram of scratch lip heights over all retrievals analyzed. The 25th percentile value is equal to 1.55 μm, the 50th percentile is equal to 3.09 μm, and the 75th percentile is equal to 4.97 μm.

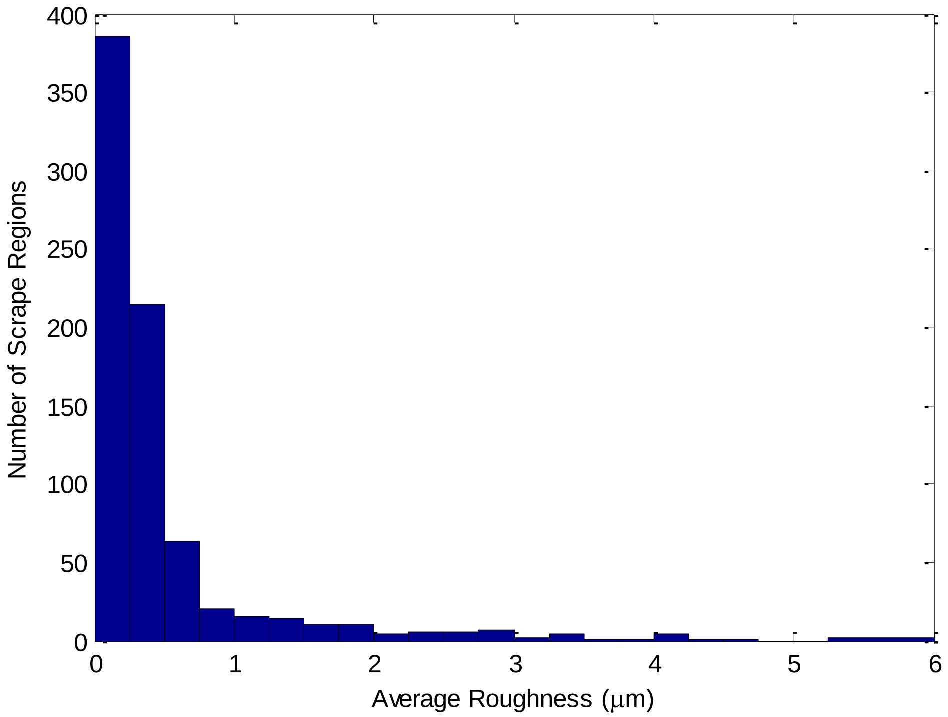

Figure 69: Histogram of scrape-average roughness values over all retrievals analyzed. The 25th percentile value is equal to 0.18 μm, the 50th percentile is equal to 0.25 μm, and the 75th percentile is equal to 0.47 μm.

Each retrieval analyzed obviously had a unique scratch and scrape population. A major goal of developing templates for creating functionally damaged heads is to replicate varying levels of clinically-realistic wear acceleration. As previously noted, no information was available on the *in vivo* orientation of the femoral head on the trunnion for this set of retrievals. While this was a limitation in the earlier context of assessing individual patients’ wear, it is an advantage in the context of providing additional relationships between damage scenarios and wear accelerations, for purposes of “clinical” database enhancement. Thus, the previously tabulated wear results for each femoral head (perturbations in 30° rotational increments about the trunnion for the retrieval study) were included as additional cases linking damage distributions with total wear acceleration potential (Figure 70). The twelve simulations that were run for each of the 20 femoral heads thus provided a total of 240 instances of damage-versus-computed wear.

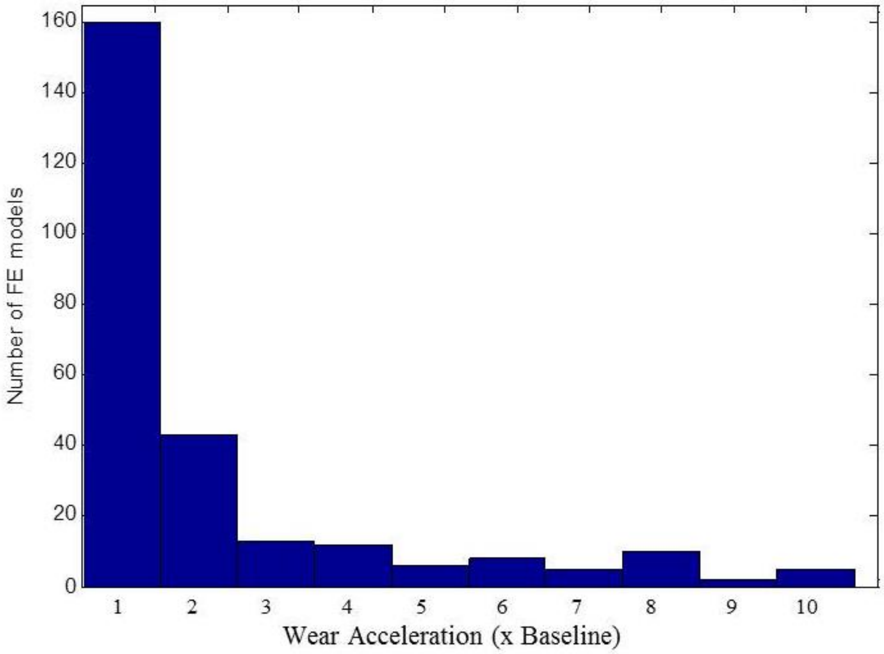

Figure 70: Histogram of wear acceleration values. The 20th percentile value is equal to 1.2x baseline, the 50th percentile is equal to 1.6x baseline, and the 80th percentile is equal to 3.5x baseline.

Target models were proposed for femoral heads of varying levels of wear elevation when compared to undamaged head simulations, in agreement with the retrieval series. The levels set were low (20th percentile, 1.2x baseline), moderate (50th percentile, 1.6xbasline), and severe (80th percentile, 3.5x baseline). Retrievals near each of these damage levels are shown in Figure 71.

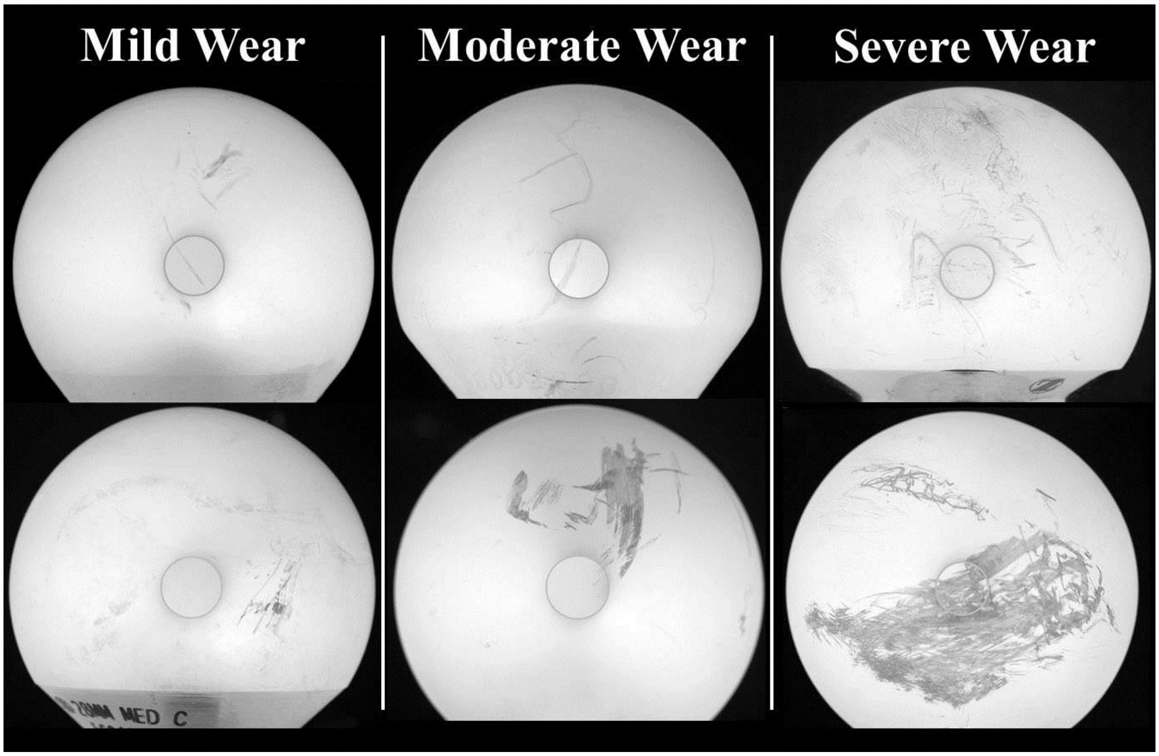

Figure 71: Example femoral heads producing mild (1.2x baseline), moderate (1.6x baseline), and severe (3.5x baseline) wear increases. Damage to femoral heads in the top row was largely scratch damage and damage to femoral heads in the bottom row was mainly scrape damage.

The damage-feature-based FE model was used to develop damage “targets” to be used for guidance when generating functionally damaged heads. Damage occurring slightly anterior to the sagittal midline has been shown to be one of the most kinetically critical sites of femoral head damage for wear acceleration [130]. To simplify generation of physical test specimens, it was decided that all damage would be centered near this location.

FE models were constructed using damage features consistent with clinically occurring damage. The scratch-only FE models were generated to nominally replicate the total scratch length and scratch lip heights evident on retrievals. For each damage level, various numbers of scratches were placed in the location of predominant scratching for the retrieval of that damage level shown in Figure 71, to replicate the approximate scratching density. A "reverse engineering" process was then completed to determine the severity and number of scratches required to reach the desired wear acceleration value.

For this process, several patterns of scratch damage were modeled. Those patterns contained 8-14 scratches for the moderate-wear model and 30-50 scratches for the severe-wear model. Various levels of scratch severity were simulated for each such pattern. Scratch severity levels were modeled at values consistent with each severity level reported in the retrieval collection (i.e., 40th to 60th percentile scratch lip heights for the moderate-wear case and 70th to 90th percentile scratch lip heights for the severe-wear case). For each damage level, the model most closely matching the desired wear acceleration was chosen as the damage template for that particular severity level.

For the moderate-wear target, 10 scratches approximately 6 mm in length were modeled (Figure 72a). Scratch lip heights were each 3.2 µm, which corresponded to the median height reported on retrievals. For the severe-wear was, 41 scratches ranging from 4 µm to 10 µm in length were modeled (Figure 72b). Scratch lip heights were each 5.2 µm, which correlated to the 75th percentile values reported on retrievals. The predicted wear increases for these models were 1.67x baseline for the moderate-wear case and 3.58x baseline for the severe-wear case (Figure 73). A zero longitude coordinate was indicated on each damage template. This mark should be made on each physical test specimen created from these damage templates and will indicate how the head should be oriented on the trunnion in the physical test set-up.

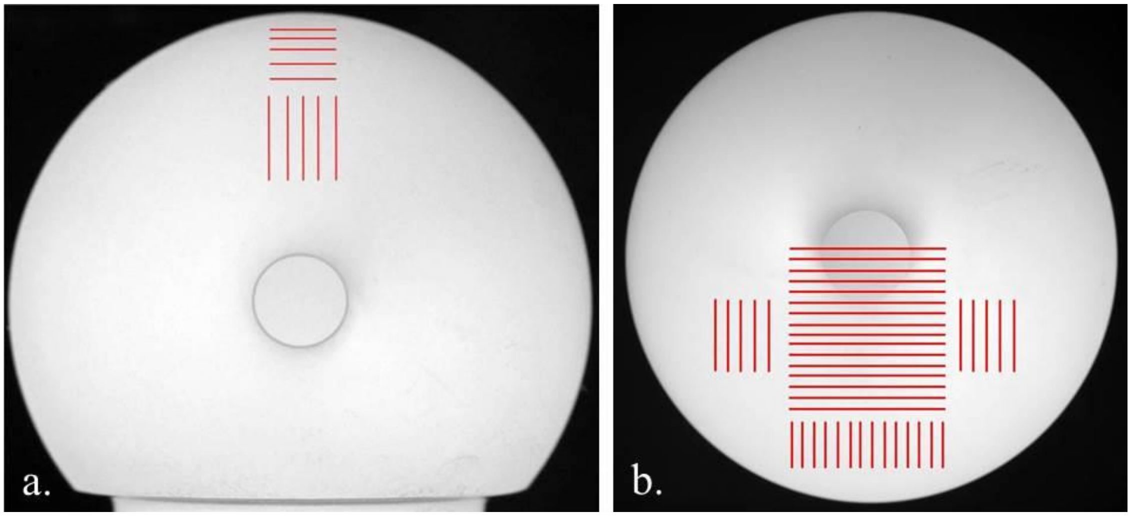

Figure 72: Targets for damage of functionally scratched femoral heads. a. 10 scratches, each having 3.2 µm lip heights, were predicted to cause moderate (50th percentile) wear increases. b. 41 scratches, each having 5.2 µm lip heights, were predicted to cause severe (80th percentile) wear increases. The zero longitudinal coordinate is 30˚ to the left of the centroid of each scratch pattern.

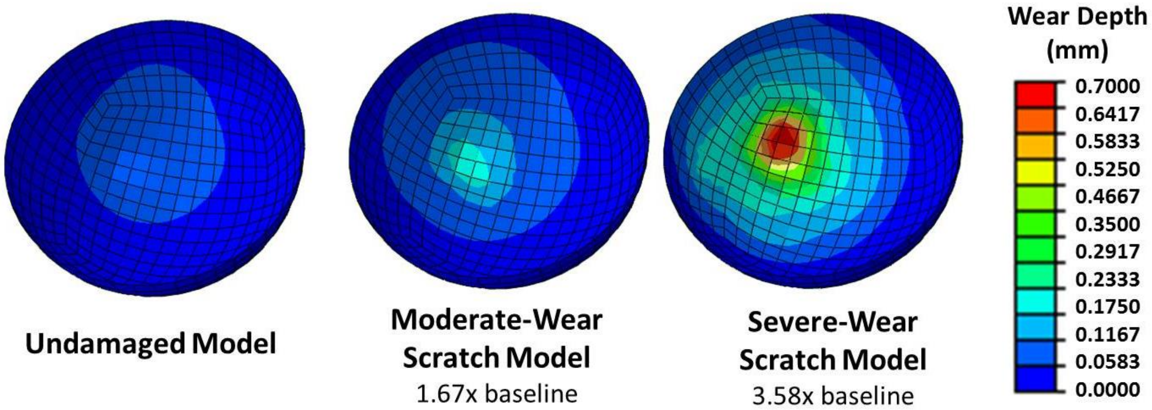

Figure 73: Wear contours for target functionally scratched femoral heads.

For the scrape-only models, a single scrape area was used to encompass the approximate scrape area of retrievals resulting in moderate (50th percentile) and high (80th percentile) wear levels. Similar to the methodology with the scratch-only models, the scrape was placed in the location of predominant scraping for the retrieval of that damage level shown in Figure 71. The size and roughness were perturbed until the desired wear acceleration in the FE model was reached.

Similar to the scratch reverse engineering process, a series of single scrape models of various sizes and severity levels were completed. Scrape severity levels were modeled at values consistent with each severity level reported in the retrieval collection (i.e., 40th to 60th percentile R_a for the moderate-wear case and 70th to 90th percentile R_a for the severe-wear case). For each damage level, the model most closely matching the desired wear acceleration was chosen as the damage template for that particular severity level.

In the moderate-wear model, a scrape approximately 6.5 mm x 13.5 mm in size and with an R_a value of 0.28 μm was used (Figure 74a). This R_a corresponded to the median value measured on retrievals. The high wear model contained a single scrape area approximately 12 mm x 24 mm in size with an average roughness of 0.55 μm, corresponding to the 80th percentile values measured on retrievals (Figure 74b). On both models, the predominant directionality of scraping was aligned along the vertical axis of the scrape. The predicted wear increases for these models were 1.65x baseline for the moderate case and 3.58x baseline for the severe case (Figure 75).

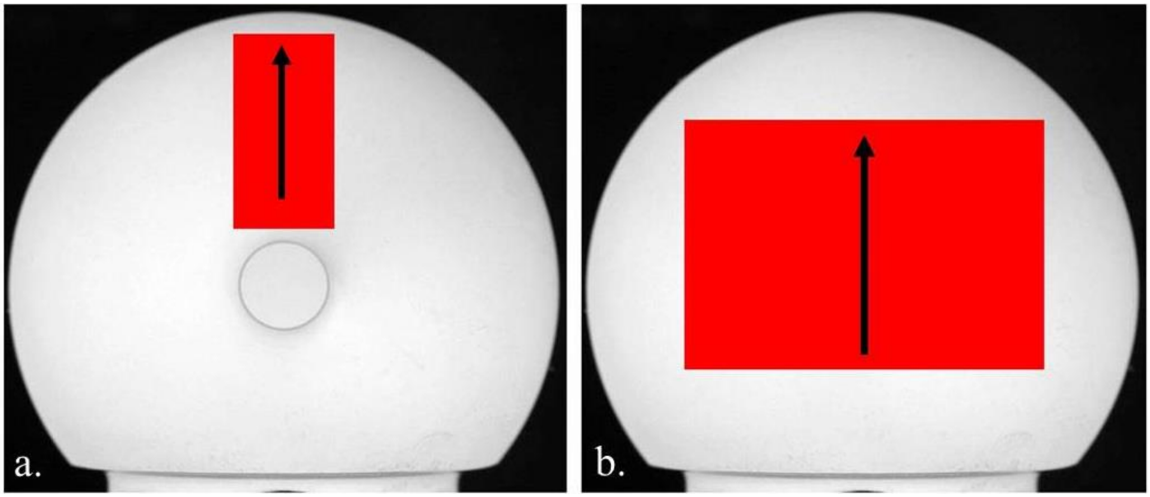

Figure 74: Targets for damage of functionally scraped femoral heads. a. a 6.5 mm x 13.5 mm scrape having an R_a of 0.28 μm, which was predicted to cause moderate (50th percentile) wear increases. b. a 12 mm x 24 mm scrape having an R_a of 0.55 μm, which was predicted to cause severe (80th percentile) wear increases. The predominant directionality of microscratches within the scrape is defined by the black arrow in each image. The zero longitudinal coordinate is 30˚ to the left of the centroid of each scrape.

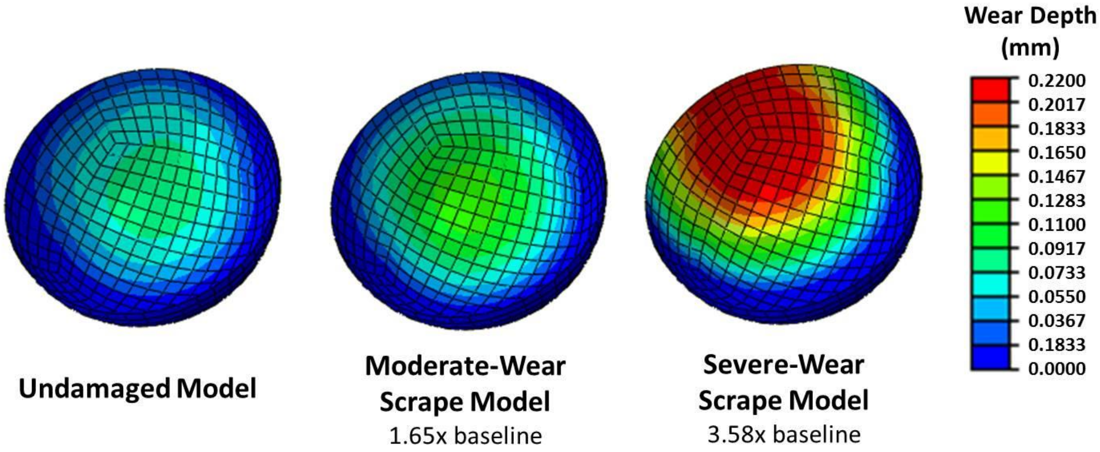

Figure 75: Wear contours for target functionally scraped femoral heads.

The target damage models containing both scratch and scrape damage were chosen such that the scratch and scrape damage contributions to wear acceleration were consistent with those for retrieval damage. The retrieval study had reported that on average, 63% of wear acceleration was due to scratch damage and 37% to scrape damage. The low-wear target model consisted of 4 scratches, each approximately 5 mm in length and with 1.3 μm lip heights, and a single 5 mm x 11 mm scrape having an R_a of 0.13 μm (Figure 76a). These scratch lip height and R_a values both corresponded to the 15th percentile measured on retrievals for each respective damage type. The moderate-wear target model consisted of 10 scratches, each approximately 5 mm in length and with 2.0 μm lip heights, and a 5 mm x 11 mm scrape having an R_a of 0.33 μm (Figure 76b). These scratch lip height and R_a values corresponded to the 30th and 60th percentiles, respectively. The severe-wear target model consisted of 15 scratches, each approximately 5 mm in length and with 9.0 μm lip heights, and a 12 mm x 22 mm scrape having an R_a of 1.2 μm (Figure 76c). These scratch lip height and R_a values both corresponded to the 90th percentile values of their respective damage types. The predicted wear increases for these models were 1.35x baseline for the low-wear case, 1.65x baseline for the moderate-wear case and 3.57x baseline for the severe-wear case (Figure 77). Methods for *in vitro* creation of these scratches and scrapes are discussed in Appendix B.

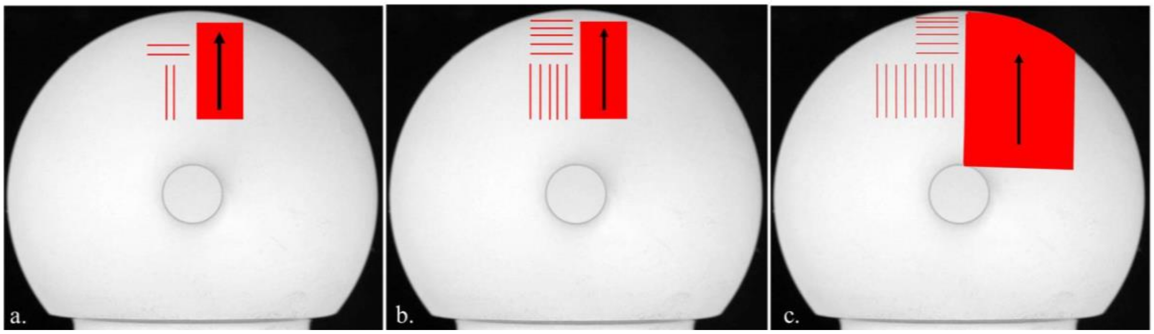

Figure 76: Targets for damage of functionally damaged femoral heads with both scratches and a scrape. a. 4 scratches with 1.3 µm lip heights and a 5 mm x 11 mm scrape having an R_a of 0.13 µm, were predicted to cause low wear increases. b. 10 scratches with 2.0 µm lip heights and a 5 mm x 11 mm scrape having an R_a of 0.33 µm, were predicted to cause moderate wear increases. c. 15 scratches with 9.0 µm lip heights and a 12 mm x 22 mm scrape having an R_a of 1.20 µm, were predicted to cause severe wear increases. The predominant directionality of microscratches within each scrape is defined by the black arrow in each image.

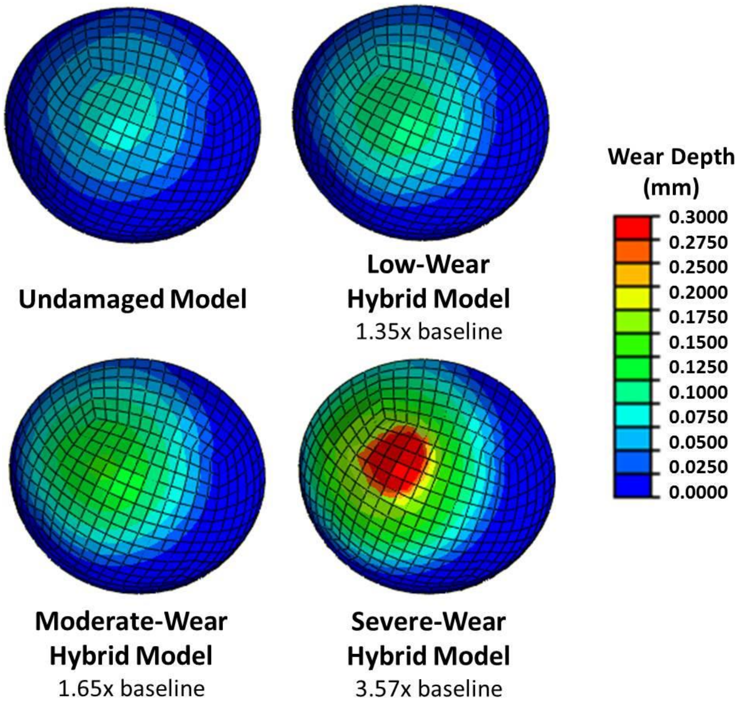

Figure 77: Wear contours for target functionally damaged femoral heads containing both scratch and scrape damage.

Discussion

Almost all available information regarding wear potential of femoral head damage has come from laboratory wear simulations. The link of such testing to *in vivo* reality, however, has not been well established. Previously published wear tests have reported wear rate increases ranging from nearly no increase [60] to more than a 100-fold increase [170]. Generation of third body damage for such laboratory wear simulations has lacked a standard protocol. Methods to induce damage for laboratory simulations have included regionally roughening a part of the bearing surface with SiC grit paper [20, 195], adding particles to joint fluid [91, 162], creating discrete scratches at prescribed locations [8, 122], and working with retrieval implants [57, 94].

Despite the striking heterogeneity of third body laboratory testing protocols and wear acceleration results, investigators almost always have justified their specific experimental design as being realistic due to its having resulted in bearing surface damage that is consistent with damage observed clinically. A large reason for justification of this wide variety of damage is that retrieval damage is highly variable and difficult to describe and quantify using currently established procedures. Previous techniques to classify damage have been subject to a wide amount of variability, and quantitative assessments of damaged areas have relied only on isotropic surface roughness parameters, which do not accurately represent the scratching/scraping damage observed in retrievals [77].

The inability to catalog retrieval damage on a scratch-population basis had been a large reason for this impasse. *In vivo* femoral head damage varies from implant to implant, and from site to site on any given implant. The multi-scale image procedures described in Chapter 3 now allow these clinically occurring micron-level damage features to be globally quantified. The damage-feature-based FE formulation described in Chapter 2 now allows for the wear potential of these damage features to be computed on an implant-level basis. Together, these two new capabilities enable femoral head damage to be cataloged in a manner capable of providing meaningful relationships with wear acceleration. The femoral head damage templates for physical wear testing here identified encompass both the severity of damage features observed clinically and the corresponding expected wear acceleration predictions. Damage templates such as these can therefore serve as a basis for a clinically-grounded testing protocol for third body and subluxation/dislocation damage wear testing.

CHAPTER 7: CONCLUSION

Polyethylene wear in total hip arthroplasty is a strong clinical concern, particularly beyond the second decade of use when aseptic loosing caused by osteolysis remains a leading cause of failure. Development of HXPEs have substantially reduced wear rates, but there remain a number of extreme outliers experiencing wear volumes an order of magnitude higher than cohort means. While femoral head damage has been long recognized for its potential to accelerate wear, previous analyses were unable to establish a quantitative link between the degree of damage and wear acceleration, largely due to the heterogeneity of damage implant-to-implant and also site-to-site on a given implant.

The damage-feature-based FE model introduced in this work allows for wear acceleration computations due to micron-level asperities to be performed on a global implant scale. Previous computational models of implant damage had only been able to model either single asperities in a small, local area[144, 156], or global-scale areas of homogeneous isotropic roughening, neither of which are representative of clinical damage[28]. The new damage-feature-based approach allows implant-level wear simulation of thousands of clinically occurring damage features, enabling wear simulation for even severely damaged femoral heads.

The multi-scale image procedure utilized diffused-light-photography and optical profilometry, thus allowing for microscopic damage features to be globally mapped and quantified for given individual implants. The diffused-light photography technique avoids extraneous room feature reflections that distort femoral head damage, historically a common problem in visual analysis of metallic femoral heads. The photographs taken using this technique highlighted damage in a manner that enabled image analysis to automatically identify damage locations. Optical profilometry allowed for all such damage-identified locations - often covering substantial portions of the femoral head - to be analyzed. This method relies far less upon subjective analyst judgments regarding damage types and appropriate scan locations than has been the case with previous damage assessment work, thus making the present approach a more appealing route for inter-study comparisons. The automated image processing procedure allowed for damage severity information to be quickly and accurately measured from the scans obtained.

The damage registry developed during this work represents the first systematic compilation of femoral head damage on an individual damage feature basis. Using the developed methods, the damage on 22 retrieval femoral heads was cataloged, and FE wear models computed the wear acceleration due to each implant-specific damage pattern. This damage registry encompassed the lip heights of over 11,000 individual scratch segments and the R_a values of nearly 800 scrape regions. This included scratches with lip heights as high as 28.5 μm and scape region R_a values up to 7.5 μm, a three-order-of-magnitude increase from values typical of pristine femoral heads. The corresponding FE models showed this clinical damage was capable of producing multi-fold wear increases when compared to undamaged femoral head simulations.

Dislocation and closed reduction events were linked to the most severe damage features reported. FE wear models of a series of dislocation retrievals were developed to determine the wear acceleration propensity of this damage. The diffused-light photographs were rank-ordered based on their visual damage severity. This visual ranking was able to predict the relative computed wear volumes reasonably well, with a concordance of 0.82. The FE results showed that dislocation and closed reduction damage is capable of producing significant wear increases when compared to undamaged femoral heads, on average 4.8-fold, and as high as 11.9-fold in this series.

The data obtained from the retrieval analysis and FE models were used as a clinically-grounded basis for laboratory creation of standardized head damage. The locations and severities of each individual scratch and scrape feature recorded in this dataset were used to create templates of femoral head damage to represent clinically observed damage. These templates arguably serve as a basis for physically testing third body and dislocation damage effects consistent with clinically-occurring damage.

Path forward

The damage-feature-based wear model and multi-scale imaging procedure have allowed seemingly random retrieval damage to be assessed, and a quantitative link to be established between damage and wear acceleration. Using these advances, further work can be contemplated to more fully understand femoral head damage and its long term wear consequences.

In the future, the FE formulation could be modified to allow for the gradual wear-down of scratches that would be expected to occur. This could be implemented using the relationship reported by Alvarez et al.[4] to track the cumulative sliding distance of each scratch segment and lower its lip height based on that sliding distance. A major limitation of the Alvaerz et al. work is that the relationship was based on the results of pin-on-disc tests. This relationship may change somewhat when the duty cycle is modified to replicate multidirectional joint kinematics. However, OP scans of scratches before and after laboratory simulator wear testing could be used to quantify scratch lip height reduction and sliding distance under physiological conditions.

The FE models presented in this work modeled only conventional UHMWPE. While similar relative behavior would be expected from HXPE, a logical next step would be to model various types of HXPE. This would of course require baseline wear coefficients and the empirical relationships between scratch lip height/R_a and wear coefficient elevation for each polyethylene version of interest.

The automated image alignment of the local OP scans to their respective global positions greatly improved the efficiency of damage severity quantification. Further modifications to the OP test set-up could provide further efficiency and precision to this process. A positioning stage utilizing stepper motors to rotate the femoral head to desired scan locations (rather than the current manual method) would allow the user to easily reposition the femoral head to desired scan locations without the need to remove the positioner from OP stage.

As discussed above, for the current set of retrievals, no orientation information is known for a majority of specimens. As part of a new retrieval program, surgeons are being asked to mark the orientation of the femoral head before it is removed from the trunnion, by marking the superior-most point of the femoral head base. This orientation mark will allow for FE models to be created without the orientation dependence uncertainty of the previous dataset. Cooperation thus far has been very encouraging.

For dislocations, this head-orientation knowledge could be used to try to determine if there is any link between dislocation direction and wear potential. The direction of dislocation is typically recorded in the post-op reports. Different dislocation directions would presumably result in different damage locations. A collection of dislocation retrievals for which the orientation is known could be used to build FE wear models and determine if a particular dislocation direction is more wear-consequential.

Finally, a major limitation of working with retrievals obtained at revision surgery is that they represent only the worst case situations. Analysis of autopsy retrievals post-mortem would allow for wear quantification of well-functioning implants, allowing for insight into potential long-term wear consequences of these implants. This information will be increasingly valuable as the need for increased implant lifetime continues to rise.

APPENDIX A: THIRD BODY DEBRIS ANALYSIS

In both primary and revision cases, there are numerous tools and steps during the surgery itself that hold the possibility for introducing metal and/or bone debris into the surgical field, debris which subsequently could find its way into the bearing space. Potential sources for debris generation include knife blades, acetabular reamers, the process of drilling for screw insertion, and many others. A part of our laboratory's larger effort in third body wear study involves particulate debris from the peri-articular tissues and joint fluid from cadaver preparations and from human THA surgeries being harvested and cataloged. An end goal of those efforts is to determine which stages of the THA procedure have the most propensity to generate third bodies capable of producing wear-consequential femoral head damage. This work involves data sharing between surgeries performed at the University of Iowa, and particle isolation work occurring at the University of Leeds in the UK. In the protocols currently used in Leeds, the counting and sizing of particles following the isolation procedure requires manual analyst segmentation of each individual particle in a large series of scanning electronic microscopy images, an extremely tedious and time-consuming process. An automated image processing program was therefore developed, in the interest of expediting that process.

Pilot studies are underway to determine if the Leeds enzymatic isolation protocol alters the size of particulate debris and to determine if small numbers of particles can be reliably isolated from tissues. Earlier laboratory tests have shown that metallic particles 40 μm in diameter are capable of producing wear-consequential scratch lips 1-2 μm in height [165]. Mirghany and Jin[147] showed that creation of detectable scratch lips from bone cement and ZrO_2 particles 20 μm in diameter could occur under physiologic loads. Bone particles of this size, however, caused no significant bearing surface deformation.

Using these results as a basis for determining the size and material type of particles most likely to cause wear-consequential femoral head scratching, samples of metal and bone cement particles have been produced. These samples were created with small (n≈32 particles) and large (n≈128 particles) quantities of debris (Figure A1). Metal particles with two size distributions (mean=24.6 µm, s.d.=6.5 and mean=170.8 µm, s.d.=17.9, respectively) and bone cement particles with one size distribution (mean=234.8 µm, s.d.=41.5) were generated from commercially purchased particles by sifting the particles over a mesh screen whose opening size was selected to match the desired particle size. Particles were placed on filter paper, where they were photographed before being placed in bijou bottles with bovine synovial membrane tissue. These samples were then sent to Leeds for particle analysis.

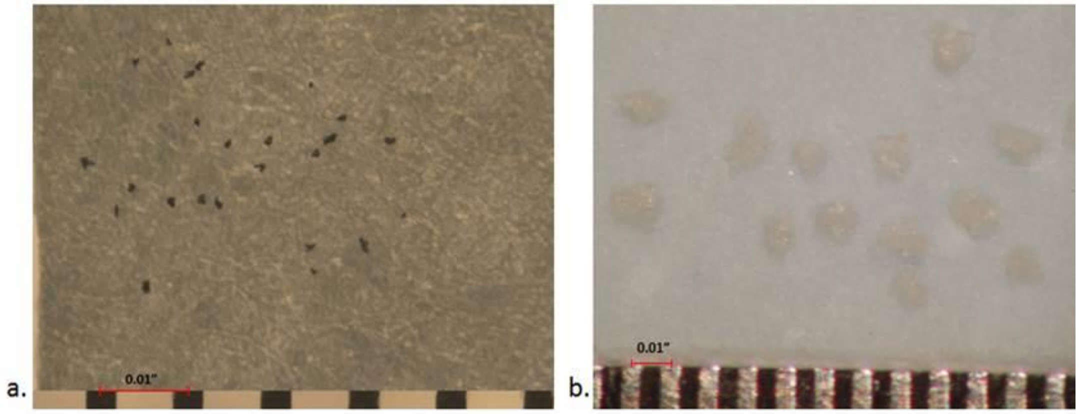

Figure A1: Particles used for pilot study - a. metal particles and b. bone cement particles.

An image processing program was used to count and size the particles in each sample from photographs taken of the particles on filter paper. A median filter was first used to eliminate small artifacts on the filter paper. A morphological top hat filter then isolated the particles from the background. This filter computes the morphological opening of the image and then subtracts the result from the original image. Following this operation, each isolated object was designated as a particle (Figure A2). The following characteristics for each individual particle were measured: width (W), height (H), length (d_{max}), breadth (d_{min}), fiber length (FL), fiber breadth (FB), perimeter (P), and area (A). These data were used to calculate the five morphologic parameters specified by ASTM F1877-05 [90]: equivalent circle diameter (ECD), aspect ratio (AR), elongation (E), roundness (R), and form factor (FF). A morphological filter was used to eliminate particles whose size fell below an analyst-set threshold. This program allowed for particles to be counted and sized with minimal analyst intervention.

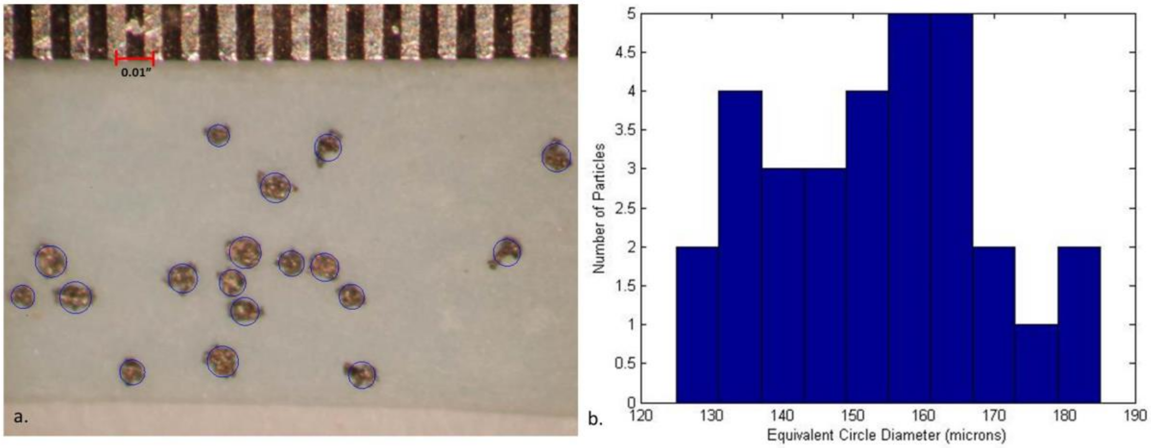

Figure A2: Equivalent circle diameter measurement. (a) Photograph of a typical set of particles on filter paper, and the corresponding particles detections (blue circles, of equivalent circle diameter)and (b) histogram of the detected particle sizes, reported in terms of equivalent circle diameter.

This analysis was also applied to the digital images captured by SEM following the isolation procedure (Figure A3). The current protocol for particle sizing at Leeds uses Image Pro Plus (Cybernetics, USA)[168, 185]. The program requires manual analyst segmentation of each individual particle, a time-consuming process. For a pilot study of metallic debris, particles appearing on SEM images were sized using both the established manual and the new automated procedures. The results showed only a 1.3% differential on average when the particles sizes measured on each image were compared. A paired t-test (α=0.05) showed no statistically significant differences between the two measurement techniques.

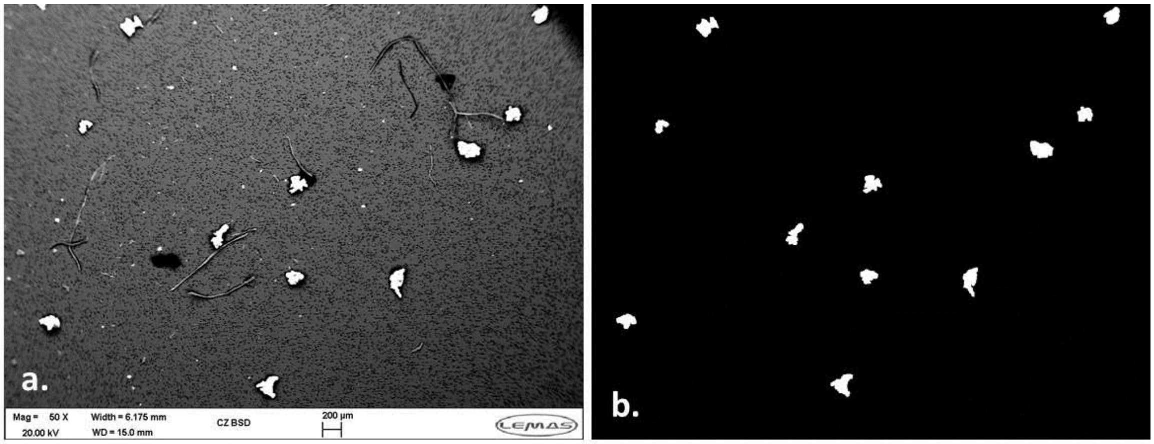

Figure A3: Metallic particles following particle isolation procedure - a. SEM image and b. binarized results after the image analysis program isolated particles for counting and sizing.

Automated particle counting and sizing at Leeds has been hindered in the past due to problems with particles clumping together. This has most often been an issue with polyethylene particles, which are on the order of 1 µm in size. Clumping is much less of an issue with the much larger metal, bone, and bone cement third body particles anticipated in the surgical experiments. The results of this pilot analysis show that the automated image sizing procedure is able to replicate the results of the manual procedure. This program will greatly increase the efficiency of the sizing for the reminder of the experiments to be completed.

APPENDIX B: METHODS FOR CREATING *IN VITRO* DAMAGE

Scratches

Scratches of specific lip heights can be created *in vitro* in a variety of ways. Ruling scratches on manufacturer-provided femoral heads using a diamond-tip stylus allows for control of the size and location of individual scratches. This method of scratch replication is well precedented for physical wear tests [8, 73] and is able to replicate material pile-up to form parametrically controllable scratch lip heights (Figure B1). A major advantage of this method is that scratches easily can be ruled in precise desired locations. A CNC mill allows prescribed patterns of scratches to be stylus-ruled at a given load along the spherical femoral head surface (Figure B2). The scratch lip heights produced can be controlled by the load applied to the diamond-tip stylus as it is drawn over the femoral head.

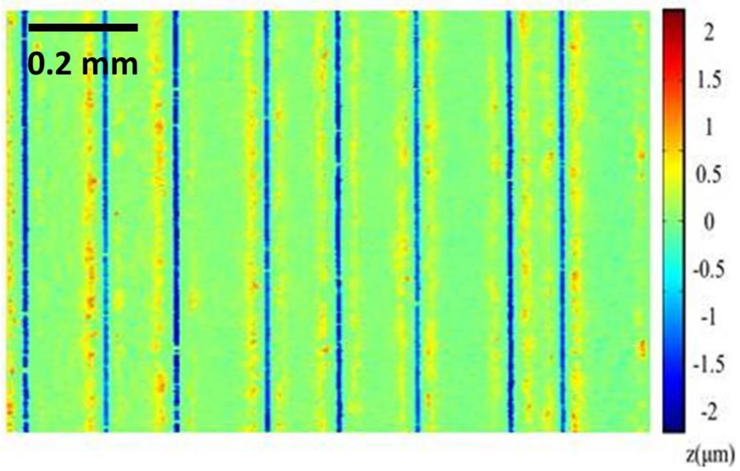

Figure B1: Optical profilometry scan of a series of parallel scratches made in our laboratory by a spring-loaded diamond-tip stylus.

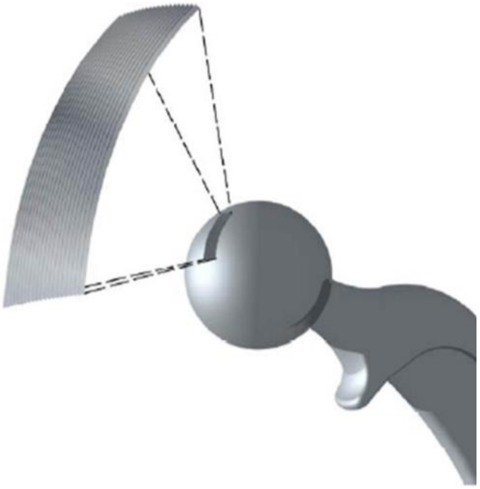

Figure B2: Conceptual schematic for ruled-scratch femoral head damage, produced by CNC machining.

Scrapes

Femoral head scraping and titanium transfer has previously been replicated *in vitro* by contacting a femoral head with a titanium alloy shell and moving the femoral head under a prescribed load [35, 95]. A similar method has been implemented in our laboratory (Figure B3). A block of titanium alloy was machined to have a concave surface with a radius to match the femoral head, to form a “scraper”. That scraper was held in place on a CNC mill. A spring was used to apply a prescribed load to the femoral head, and the femoral head was rotated while maintaining constant contact pressure with the scraper.

Figure B3: Titanium alloy scrape setup in CNC mill.

Preliminary trials of this method showed that scrapes of varying sizes could be created either by changing the scraper contact area or by performing multiple passes (Figure B4). These scrapes showed micro-scratches characteristic of *in vivo* scrapes (Figure B5a). OP scans along the scrape showed consistent average roughness values within individual scrapes, ranging from 0.20 μm to 0.67 μm, which agreed well with values commonly measured on retrievals (Figure B5b). Small areas of material deposition were also noted on the OP scans.

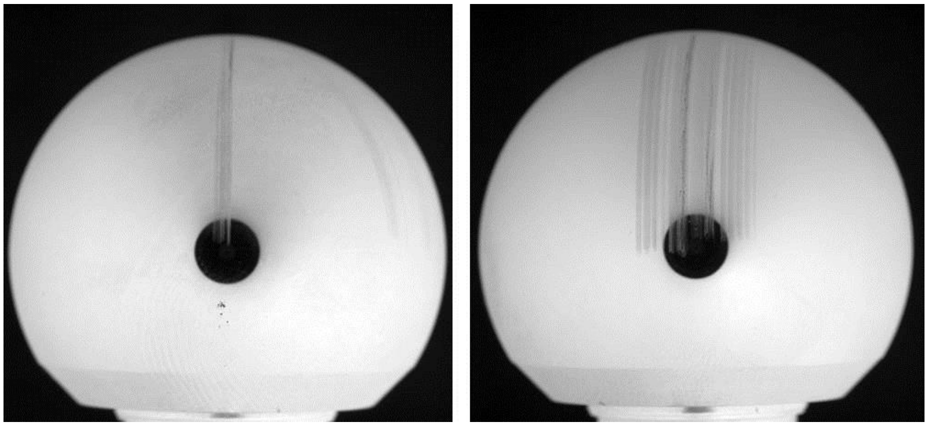

Figure B4: *In vitro* replication of femoral head damage.

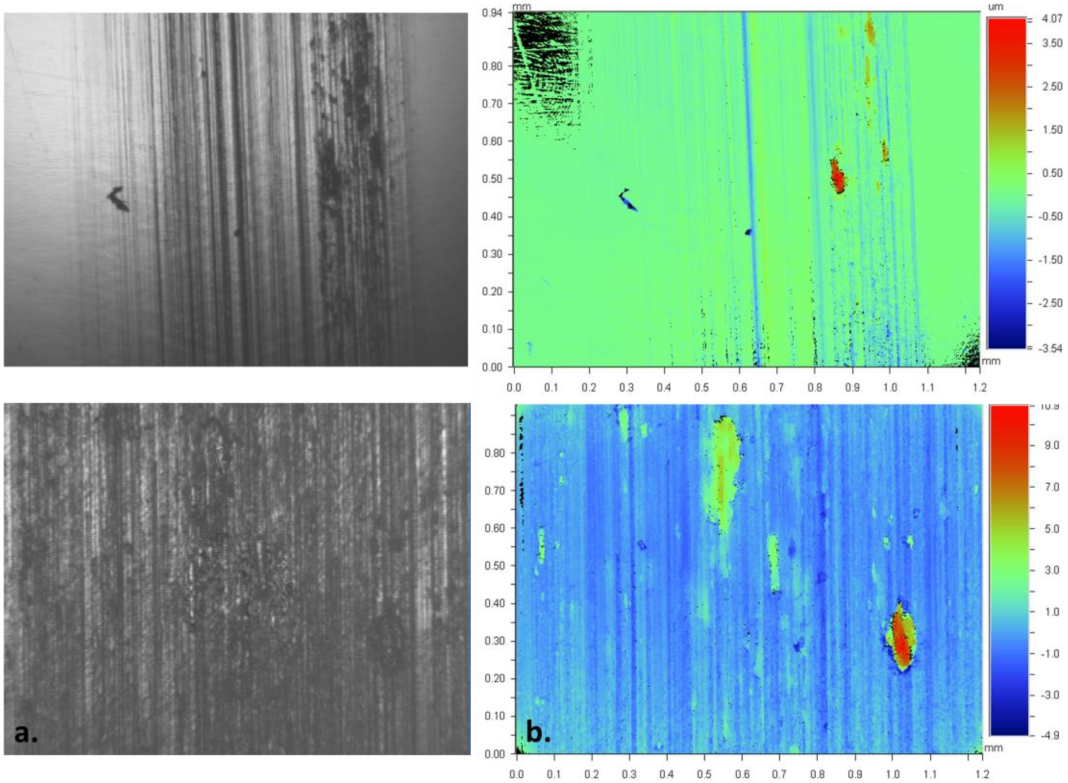

Figure B5: Laboratory-created scrapes. (a) Micrographs and (b) OP scans of selected scrape regions. Top images were recorded from a scrape produced by moving the scraper along the femoral head once, at a force of 427 N. The scrape on the bottom images was produced by moving the same scraper back and forth five times at a force of 534 N. The corresponding R_a values were 0.203 μm and 0.507 μm for the top and bottom OP scans, respectively.

A parametric analysis was conducted with this setup to produce a range of scrape R_a values by varying (i) the contact pressure between the scraper and femoral head and (ii) the number of scraping passes (Figure 86). Scrapes were created with a single pass of the scraper, up and down the length of the scrape, and up and down five times. Variations of the spring force on the scraper were 427 N, 534 N, and 925 N. Using this setup, scrape R_a values up to 0.67 μm were able to be produced. Scrapes of this severity corresponded to the 84th percentile of R_a values measured on the retrievals.

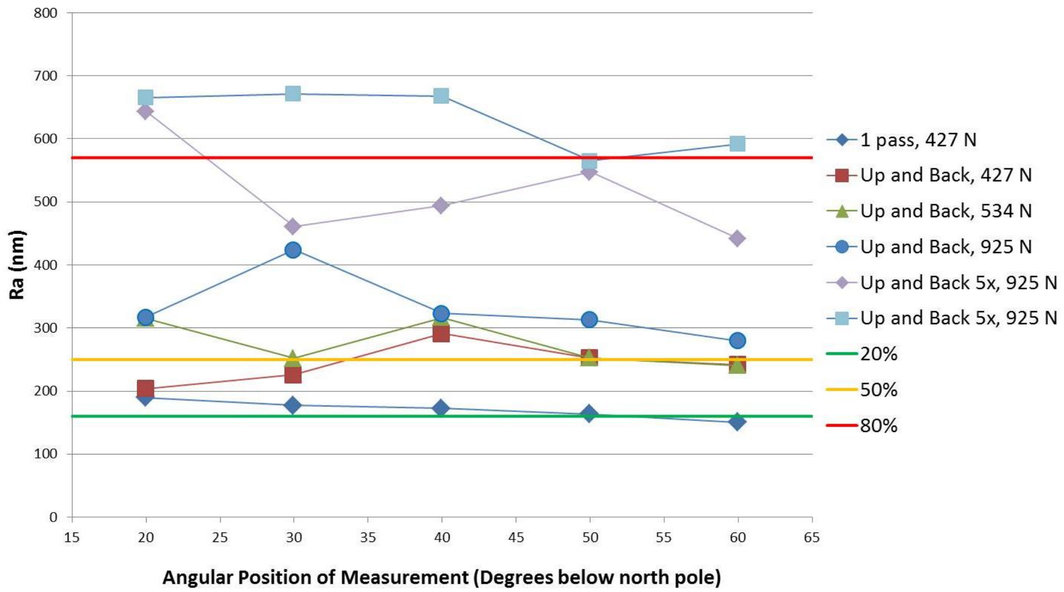

Figure B6: Results of a preliminary parametric analysis conducted to produce scrapes with various levels of roughness severity. The force on the scraper and the number of scraping passes were varied. The solid lines indicate the 20th, 50th, and 80th percentile R_a values from the retrieval series in Chapter 4.

REFERENCES

1 AAOS, 'Information About Hip Replacements' (2013).

2 Abdelgaied A, Liu F, Brockett C, Jennings L, Fisher J, Jin Z, 'Computational Wear Prediction of Artificial Knee Joints Based on a New Wear Law and Formulation', *J Biomech,* 44 (2011), 1108-16.

3 Allain J, Goutallier D, Voisin MC, Lemouel S, 'Failure of a Stainless-Steel Femoral Head of a Revision Total Hip Arthroplasty Performed after a Fracture of a Ceramic Femoral Head. A Case Report', *J Bone Joint Surg Am,* 80 (1998), 1355-60.

4 Alvarez E, DesJardins DJ, 'Scratch Morphology Evolution of Cocr Femoral Components: A Retrieval and Wear Simulator Study', *59th Annual Meeting of the Orthopaedic Research Society* (San Antonio, TX: 2013).

5 Archard JF, 'Contact and Rubbing of Flat Surfaces', *J Appl Phys*, 24 (1953), 981-8.

6 Atkinson JR, Dowson D, Isaac JH, Wroblewski BM, 'Laboratory Wear Tests and Clinical Observations of the Penetration of Femoral Heads into Acetabular Cups in Total Replacement Hip Joints: Iii: The Measurement of Internal Volume Changes in Explanted Charnley Sockets after 2–16 Years *In Vivo* and the Determination of Wear Factors', *Wear*, 104 (1985), 225-44.

7 ASME B46, 'Surface Texture', (American Society of Mechanical Engineers, 1995).

8 Barbour PS, Stone MH, Fisher J, 'A Hip Joint Simulator Study Using New and Physiologically Scratched Femoral Heads with Ultra-High Molecular Weight Polyethylene Acetabular Cups', *Proc Inst Mech Eng H*, 214 (2000), 569-76.

9 Barrack RL, Castro FP, Jr., Szuszczewicz ES,Schmalzried TP, 'Analysis of Retrieved Uncemented Porous-Coated Acetabular Components in Patients with and without Pelvic Osteolysis', *Orthopedics*, 25 (2002), 1373-8; discussion 78.

10 Barreto S, Folgado J, Fernandes PR, Monteiro J, 'The Influence of the Pelvic Bone on the Computational Results of the Acetabular Component of a Total Hip Prosthesis', *J Biomech Eng*, 132 (2010), 054503.

11 Bauer TW, Taylor SK, Jiang M, Medendorp SV, 'An Indirect Comparison of Third-Body Wear in Retrieved Hydroxyapatite-Coated, Porous, and Cemented Femoral Components', *Clin Orthop Relat Res* (1994), 11-8.

12 Benson LC, DesJardins JD, Harman MK, and LaBerge M, 'Effect of Stair Descent Loading on Ultra-High Molecular Weight Polyethylene Wear in a Force-Controlled Knee Simulator', *Proc Inst Mech Eng H*, 216 (2002), 409-18.

13 Bevill SL, Bevill GR, Penmetsa JR, Petrella AJ, and Rullkoetter PJ, 'Finite Element Simulation of Early Creep and Wear in Total Hip Arthroplasty', *J Biomech*, 38 (2005), 2365-74.

14 Bloebaum RD, Dupont JA, 'Osteolysis from a Press-Fit Hydroxyapatite-Coated Implant. A Case Study', *J Arthroplasty,* 8 (1993), 195-202.

15 Bobyn JD, Tanzer M, Krygier JJ, Dujovne AR, Brooks CE, 'Concerns with Modularity in Total Hip Arthroplasty', *Clin Orthop Relat Res* (1994), 27-36.

16 Bolland BJ, Culliford DJ, Langton DJ, Millington JP, Arden NK, Latham JM, 'High Failure Rates with a Large-Diameter Hybrid Metal-on-Metal Total Hip Replacement: Clinical, Radiological and Retrieval Analysis', *J Bone Joint Surg Br,* 93 (2011), 608-15.

17 Bourne RB, Barrack R, Rorabeck CH, Salehi A, Good V, 'Arthroplasty Options for the Young Patient: Oxinium on Cross-Linked Polyethylene', *Clin Orthop Relat Res,* 441 (2005), 159-67.

18 Bourne RB, Maloney JW, Wright JG, 'An AOA Critical Issue. The Outcome of the Outcomes Movement', *J Bone Joint Surg Am,* 86-A (2004), 633-40.

19 Bowsher JG, Donaldson TK, Williams PA, Clarke IC, 'Surface Damage after Multiple Dislocations of a 38-mm-Diameter, Metal-on-Metal Hip Prosthesis', *J Arthroplasty,* 23 (2008), 1090-6.

20 Bowsher JG, Shelton JC, 'A Hip Simulator Study of the Influence of Patient Activity Level on the Wear of Crosslinked Polyethylene under Smooth and Roughened Femoral Conditions', *Wear,* 250 (2001), 167-79.

21 Bozic KJ, Kurtz SM, Lau E, Ong K, Vail TP, Berry DJ, 'The Epidemiology of Revision Total Hip Arthroplasty in the United States', *J Bone Joint Surg Am,* 91 (2009), 128-33.

22 Bragdon CR, Jasty M, Muratoglu OK, O'Connor DO, Harris WH, 'Third-Body Wear of Highly Cross-Linked Polyethylene in a Hip Simulator', *J Arthroplasty,* 18 (2003), 553-61.

23 Bragdon CR, O'Connor DO, Lowenstein JD, Jasty M, Syniuta WD, 'The Importance of Multidirectional Motion on the Wear of Polyethylene', *Proc Inst Mech Eng H,* 210 (1996), 157-65.

24 Bragdon CR, KK Wannomaie, Lozynsky A, Micheli B, Malchau H, 'The Effect of in Vivo Damage of Oxinium Femoral Heads on the Wear of Highly Cross-Linked Polyethylene', in *55th Annual Meeting of the Orthopaedic Research Society* (Las Vegas, NV: 2009).

25 Brand RA, Pedersen DR, Davy DT, Kotzar GM, Heiple KG, Goldberg VM, 'Comparison of Hip Force Calculations and Measurements in the Same Patient', *Journal of Arthroplasty,* 9 (1994), 45-51.

26 Brand U, Hillmann W, 'Calibration of Step Height Standards for Nanometrology Using Interference Microscopy and Stylus Profilometry', *Precision Engineering,* 17 (1995), 22-33.

27 Brown TB, Lundberg HJ, Pedersen DR, Callaghan JJ, '2009 Nicolas Andry Award: Clinical Biomechanics of Third Body Acceleration of Total Hip Wear', *Clin Orthop Relat Res,* 467 (2009), 1885-97.

28 Brown TD, Stewart KJ, Nieman JC, Pedersen DR, Callaghan JJ, 'Local Head Roughening as a Factor Contributing to Variability of Total Hip Wear: A Finite Element Analysis', *J Biomech Eng,* 124 (2002), 691-8.

29 Buttery TC, Archard JF, 'Grinding and Abrasive Wear', *Proceedings of the Institution of Mechanical Engineers,* 185 (1970), 537-51.

30 Callaghan JJ, Bracha P, Liu SS, Piyaworakhun S, Goetz DD, Johnston RC, 'Survivorship of a Charnley Total Hip Arthroplasty. A Concise Follow-up, at a Minimum of Thirty-Five Years, of Previous Reports', *J Bone Joint Surg Am,* 91 (2009), 2617-21.

31 Callary SA, Field JR, Campbell DG, 'Low Wear of a Second-Generation Highly Crosslinked Polyethylene Liner: A 5-Year Radiostereometric Analysis Study', *Clin Orthop Relat Res,* 471 (2013), 3596-600.

32 Campbell P, Urban RM, Catelas I, Skipor AK, Schmalzried TP, 'Autopsy Analysis Thirty Years after Metal-on-Metal Total Hip Replacement. A Case Report', *J Bone Joint Surg Am,* 85-A (2003), 2218-22.

33 Canny J, 'A Computational Approach to Edge Detection', *Pattern Analysis and Machine Intelligence, IEEE Transactions* 8(1986), 679-98.

34 Caton J, Prudhon JL, 'Over 25 Years Survival after Charnley's Total Hip Arthroplasty', *Int Orthop,* 35 (2011), 185-8.

35 Chang CB, Yoo JJ, Song DS, Kim DJ, Koo KH, Kim HJ 'Transfer of Metallic Debris from the Metal Surface of an Acetabular Cup to Artificial Femoral Heads by Scraping: Comparison between Alumina and Cobalt-Chrome Heads', *J Biomed Mater Res B Appl Biomater,* 85 (2008), 204-9.

36 Charnley J, 'Arthroplasty of the Hip. A New Operation', *Lancet,* 1 (1961), 1129-32.

37 Charnley J, Cupic Z, 'The Nine and Ten Year Results of the Low-Friction Arthroplasty of the Hip', *Clin Orthop Relat Res* (1973), 9-25.

38 Cipriano CA, Issack PS, Beksac B, Della Valle AG, Sculco TP, Salvati AG, 'Metallosis after Metal-on-Polyethylene Total Hip Arthroplasty', *Am J Orthop (Belle Mead NJ),* 37 (2008), E18-25.

39 Clohisy JC, Calvert G, Tull F, McDonald D, Maloney WJ, 'Reasons for Revision Hip Surgery: A Retrospective Review', *Clin Orthop Relat Res* (2004), 188-92.

40 Collier JP, Bauer TW, Bloebaum RD, Bobyn JD, Cook SD, Galante JO, Harris WH, Head WC, Jasty MJ, MC Mayor, 'Results of Implant Retrieval from Postmortem Specimens in Patients with Well-Functioning, Long-Term Total Hip Replacement', *Clin Orthop Relat Res* (1992), 97-112.

41 Cuckler JM, 'If Hip Implant Retrievals Could Speak, What Would They Tell Us?', *J Bone Joint Surg Br,* 94 (2012), 11-3.

42 Currier JH, McHugh DJ, Tower DR, Barlow DR, Collier JP, Van Citters DW, 'Retrieved MOM Heads Show Damage from *in Vivo* Articulation and Bearing Contact.', in *58th Annual Meeting of the Orthopaedic Research Society* (San Francisco: 2012), p. 0081.

43 D'Antonio JA, Capello WN, Ramakrishnan R, 'Second-Generation Annealed Highly Cross-Linked Polyethylene Exhibits Low Wear', *Clin Orthop Relat Res* (2011).

44 Dallaire S, Dufour M, Gauthier B, 'Characterization of Wear Damage in Coatings by Optical Profilometry', (1993), 363-68.

45 Davidson JA, Poggie RA, Mishra AK, 'Abrasive Wear of Ceramic, Metal, and UHMWPE Bearing Surfaces from Third-Body Bone, PMMA Bone Cement, and Titanium Debris', *Biomed Mater Eng,* 4 (1994), 213-29.

46 Dharmastiti R, Barton DC, Fisher J, Edidin A, Kurtz S, 'The Wear of Oriented UHMWPE under Isotropically Rough and Scratched Counterface Test Conditions', *Biomed Mater Eng,* 11 (2001), 241-56.

47 Dowd JE, Sychterz CJ, Young AM, Engh CA, 'Characterization of Long-Term Femoral-Head-Penetration Rates. Association with and Prediction of Osteolysis.', *J Bone Joint Surg Am,* 82-A (2000), 1102-7.

48 Dowling JM, Atkinson JR, Dowson D, Charnley J, 'The Characteristics of Acetabular Cups Worn in the Human Body', *J Bone Joint Surg Br,* 60-B (1978), 375-82.

49 Dowson D, El-Hady Diab MM, Gillis BJ, Atkinson JR, 'Influence of Counterface Topography on the Wear of Ultra High Molecular Weight Polyethylene under Wet or Dry Conditions', in *Polymer Wear and Its Control* (American Chemical Society, 1985), pp. 171-87.

50 Dowson D, Taheri S, Wallbridge NC, 'The Role of Counterface Imperfections in the Wear of Polyethylene', *Wear,* 119 (1987), 277-93.

51 Drabu KJ, Michaud RJ, McCullagh PJ, Brummitt K, Smith RA, 'Assessment of Titanium Alloy on Polyethylene Bearing Surfaces in Retrieved Uncemented Total Hip Replacements', *Proc. Inst. Mech. Eng. H J. Eng. Med.,* 208 (1994), 91-95.

52 Duda RO, Hart PE, 'Use of the Hough Transformation to Detect Lines and Curves in Pictures', *Commun. ACM,* 15 (1972), 11-15.

53 Dumbleton JH, D'Antonio JA, Manley MT, Capello WN, Wang A, 'The Basis for a Second-Generation Highly Cross-Linked Uhmwpe', *Clin Orthop Relat Res,* 453 (2006), 265-71.

54 Dumbleton JH, MT Manley, Edidin AA, 'A Literature Review of the Association between Wear Rate and Osteolysis in Total Hip Arthroplasty', *J Arthroplasty,* 17 (2002), 649-61.

55 Eberhardt AW, McKee RT, Cuckler JM, Peterson DW, Beck PR, Lemons JE, 'Surface Roughness of Cocr and Zro2 Femoral Heads with Metal Transfer: A Retrieval and Wear Simulator Study', *Inr J Biomat,* 2009 (2009).

56 Elfick AP, Hall RM, Pinder IM, Unsworth A, 'The Influence of Femoral Head Surface Roughness on the Wear of Ultrahigh Molecular Weight Polyethylene Sockets in Cementless Total Hip Replacement', *J Biomed Mater Res*, 48 (1999), 712-8.

57 Elfick AP, Smith SL, Unsworth A, 'Variation in the Wear Rate During the Life of a Total Hip Arthroplasty: A Simulator and Retrieval Study', *J Arthroplasty*, 15 (2000), 901-8.

58 Elkins JM, Callaghan JJ, Brown TD, 'Stability and Trunnion Wear Potential in Large-Diameter Metal-on-Metal Total Hips: A Finite Element Analysis', *Clin Orthop Relat Res*, 472 (2014), 529-42.

59 Elkins JM, Callaghan JJ, Brown TD. 'The Frank Stinchfield Award: Redefining the "Safe Aone" for Optimal Wear and Stability in Total Hips. It's Smaller Than We Thought: A Computational Analysis.' in *20th Combined Open Meeting of the Hip Society and the American Association of Hip and Knee Surgeons*. (New Orleans, LA: 2014).

60 Endo MM, Barbour PS, Barton DC, Fisher J, Tipper JL, Ingham E, Stone MH, 'Comparative Wear and Wear Debris under Three Different Counterface Conditions of Crosslinked and Non-Crosslinked Ultra High Molecular Weight Polyethylene', *Biomed Mater Eng*, 11 (2001), 23-35.

61 Endo M, Tipper JL, Barton DC, Stone MH, Ingham E, Fisher J, 'Comparison of Wear, Wear Debris and Functional Biological Activity of Moderately Crosslinked and Non-Crosslinked Polyethylenes in Hip Prostheses', *Proc Inst Mech Eng H*, 216 (2002), 111-22.

62 Estok II EM, Bragdon CR, Plank GR, Huang A, Muratoglu OK, Harris WH, 'The Measurement of Creep in Ultrahigh Molecular Weight Polyethylene: A Comparison of Conventional Versus Highly Cross-Linked Polyethylene', *J Arthroplasty*, 20 (2005), 239-43.

63 Evangelista GT, Fulkerson E, Kummer F, Di Cesare PE, 'Surface Damage to an Oxinium Femoral Head Prosthesis after Dislocation', *J Bone Joint Surg Br*, 89 (2007), 535-7.

64 ASTM F2033-05, 'Total Hip Joint Prosthesis Bearings', (2013).

65 Fialho JC, Fernandes PR, Eca L, Folgado J, 'Computational Hip Joint Simulator for Wear and Heat Generation', *J Biomech*, 40 (2007), 2358-66.

66 Fisher J, Dowson D, 'Tribology of Total Artificial Joints', *Proc Inst Mech Eng H*, 205 (1991), 73-9.

67 Fisher J, Firkins P, Reeves EA, Hailey JL, Isaac GH, 'The Influence of Scratches to Metallic Counterfaces on the Wear of Ultra-High Molecular Weight Polyethylene', *Proc Inst Mech Eng H*, 209 (1995), 263-4.

68 Fregly BJ, Sawyer WG, Harman MK, Banks SA, 'Computational Wear Prediction of a Total Knee Replacement from in Vivo Kinematics', *J Biomech*, 38 (2005), 305-14.

69 Gencur SJ, Rimnac CM, Kurtz SM, 'Failure Micromechanisms During Uniaxial Tensile Fracture of Conventional and Highly Crosslinked Ultra-High Molecular Weight Polyethylenes Used in Total Joint Replacements', *Biomaterials*, 24 (2003), 3947-54.

70 Georgiades G, Babis GC, Hartofilakidis G, 'Charnley Low-Friction Arthroplasty in Young Patients with Osteoarthritis: Outcomes at a Minimum of Twenty-Two Years', *J Bone Joint Surg Am*, 91 (2009), 2846-51.

71 Germann CA, Geyer DA, Perron AD, 'Closed Reduction of Prosthetic Hip Dislocation by Emergency Physicians', *Am J Emerg Med*, 23 (2005), 800-5.

72 Gibon E, Scemama C, David B, Hamadouche M, 'Oxinium Femoral Head Damage Generated by a Metallic Foreign Body within the Polyethylene Cup Following Recurrent Dislocation Episodes', *Orthop Traumatol Surg Res*, 99 (2013), 865-9.

73 Glennon LP, Baer TE, Martin JA, Lack WD, Brown TD, 'Sliding Direction Dependence of Polyethylene Wear for Metal Counterface Traverse of Severe Scratches', *J Biomech Eng*, 130 (2008), 051006.

74 Goreham-Voss CM, Hyde PJ, Hall RM, Fisher J, Brown TD, 'Cross-Shear Implementation in Sliding-Distance-Coupled Finite Element Analysis of Wear in Metal-on-Polyethylene Total Joint Arthroplasty: Intervertebral Total Disc Replacement as an Illustrative Application', *J Biomech*, 43 (2010), 1674-81.

75 Goreham-Voss CM, Vicars R, Hall RM, Brown TD, 'Preferential Superior Surface Motion in Wear Simulations of the Charite Total Disc Replacement', *Eur Spine J*, 21 Suppl 5 (2012), S700-8.

76 Griffin WL, 'Metal Ion Levels: How Can They Help Us?', *J Arthroplasty*, 29 (2014), 659-60.

77 Hall RM, Siney P, A Unsworth, and Wroblewski BM, 'The Effect of Surface Topography of Retrieved Femoral Heads on the Wear of UHMWPE Sockets', *Med Eng Phys*, 19 (1997), 711-9.

78 Hall RM, Unsworth A, Siney P, Wroblewski BM, 'The Surface Topography of Retrieved Femoral Heads', *J Mater Sci Mater Med*, 7 (1996), 739-44.

79 Hall RM, Siney P, Unsworth A, Wroblewski BM, 'Wear in Retrieved Charnley Acetabular Sockets', *Proc Inst Mech Eng H*, 210 (1996), 197-207.

80 Haraguchi K, Sugano N, Nishii T, Sakai T, Yoshikawa H, Ohzono K, 'Influence of Polyethylene and Femoral Head Surface Quality on Wear: A Retrieval Study', *Int Orthop*, 25 (2001), 29-34.

81 Harrell FE, *Regression Modeling Strategies: With Applications to Linear Models, Logistic Regression, and Survival Analysis* (Springer-Verlag, New York 2001).

82 Heiner AD, Kruger KM, Baer TE, Brown TD, 'Enhancing Damage Visibility on Metallic Bearing Surfaces: A Simple Technique for Photography and Viewing', *J Arthroplasty*, Mar;28(3):543 (2013), e9-543.e12.

83 Heiner AD, Galvin AL, Fisher J, Callaghan JJ, Brown TD, 'Scratching Vulnerability of Conventional Vs Highly Cross-Linked Polyethylene Liners Because of Large Embedded Third-Body Particles', *J Arthroplasty*, 27 (2012), 742-9.

84 Heiner AD, Kruger KM, Tikekar NM, Lannutti JJ, Callaghan JJ, Brown TD, 'Uncertainty of Head Orientation on the Trunnion Undermines Reliability of Case-Specific Retrieval Wear Simulations', in *59th Annual Meeting of the Orthopaedic Research Society* (San Antonio, TX: 2013), Poster #1027

85 Heisel C, Streich N, Krachler M, Jakubowitz E, Kretzer JP, 'Characterization of the Running-in Period in Total Hip Resurfacing Arthroplasty: An in Vivo and in Vitro Metal Ion Analysis', *J Bone Joint Surg Am*, 90 Suppl 3 (2008), 125-33.

86 Hopkins AR, Hansen UN, Amis AA, Knight L, Taylor M, Levy O, Copeland SA, 'Wear in the Prosthetic Shoulder: Association with Design Parameters', *J Biomech Eng*, 129 (2007), 223-30.

87 Howie DW, McCalden RW, Nawana NS, Costi K, Pearcy MJ, Subramanian C, 'The Long-Term Wear of Retrieved Mckee-Farrar Metal-on-Metal Total Hip Prostheses', *J Arthroplasty*, 20 (2005), 350-7.

88 Ingham E, Fisher J, 'Biological Reactions to Wear Debris in Total Joint Replacement', *Proc Inst Mech Eng H*, 214 (2000), 21-37.

89 Ingham E, Fisher J, 'The Role of Macrophages in Osteolysis of Total Joint Replacement', *Biomaterials*, 26 (2005), 1271-86.

90 ASTM International, 'Standard Practice for Characterization of Particles. ', (West Conshohocken, PA: 2005).

91 Isaac GH, Atkinson JR, Dowson D, Kennedy PD, Smith MR, 'The Causes of Femoral Head Roughening in Explanted Charnley Hip Prostheses', *Eng Med*, 16 (1987), 167-73.

92 Isaac GH, Wroblewski BM, Atkinson JR, Dowson D, 'A Tribological Study of Retrieved Hip Prostheses', *Clin Orthop Relat Res* (1992), 115-25.

93 ISO7206-2, 'Implants for Surgery - Partial and Total Hip Protheses. Part 2: Articulating Surfaces Made of Metallic, Ceramic, and Plastic Materials', (Geneva, Switzerland: 2013).

94 Ito H, Maloney CM, Crowninshield RD, Clohisy JC, McDonald DJ, Maloney JW, 'In Vivo Femoral Head Damage and Its Effect on Polyethylene Wear', *J Arthroplasty*, 25 (2010), 302-8.

95 Jaffe WL, Strauss EL, Cardinale M, Herrera L, Kummer FJ, 'Surface Oxidized Zirconium Total Hip Arthroplasty Head Damage Due to Closed Reduction Effects on Polyethylene Wear', *J Arthroplasty*, 24 (2009), 898-902.

96 Jasty M, Bragdon CR, Lee K, Hanson A, Harris WH, 'Surface Damage to Cobalt-Chrome Femoral Head Prostheses', *J Bone Joint Surg Br*, 76 (1994), 73-7.

97 Jasty M, Goetz DD, Bragdon CR, Lee KR, Hanson AE, Elder JR, Harris WH, 'Wear of Polyethylene Acetabular Components in Total Hip Arthroplasty. An Analysis of One Hundred and Twenty-Eight Components Retrieved at Autopsy or Revision Operations', *J Bone Joint Surg Am*, 79 (1997), 349-58.

98 Jones VC, Williams IR, Auger DD, Walsh W, Barton DC, Stone MH, Fisher J, 'Quantification of Third Body Damage to the Tibial Counterface in Mobile Bearing Knees', *Proc Inst Mech Eng H*, 215 (2001), 171-9.

99 Kang L, Galvin AL, Jin ZM, Fisher J, 'A Simple Fully Integrated Contact-Coupled Wear Prediction for Ultra-High Molecular Weight Polyethylene Hip Implants', *Proc Inst Mech Eng H*, 220 (2006), 33-46.

100 Kang L, Galvin AL, Fisher J, Jin Z, 'Enhanced Computational Prediction of Polyethylene Wear in Hip Joints by Incorporating Cross-Shear and Contact Pressure in Additional to Load and Sliding Distance: Effect of Head Diameter', *Journal of biomechanics*, 42 (2009), 912-18.

101 Kempf I, Semlitsch M, 'Massive Wear of a Steel Ball Head by Ceramic Fragments in the Polyethylene Acetabular Cup after Revision of a Total Hip Prosthesis with Fractured Ceramic Ball', *Arch Orthop Trauma Surg*, 109 (1990), 284-7.

102 Kim YH, Ritchie A, Hardaker C, 'Surface Roughness of Ceramic Femoral Heads after in Vivo Transfer of Metal: Correlation to Polyethylene Wear', *J Bone Joint Surg Am*, 87 (2005), 577-82.

103 Kleinhans JA, Jakubowitz E, Seeger JB, Heisel C, Kretzer JP, 'Macroscopic Third-Body Wear Caused by Porous Metal Surface Fragments in Total Hip Arthroplasty', *Orthopedics*, 32 (2009), 364.

104 Knight LA, Pal S, Coleman JC, Bronson F, Haider H, Levine DL, Taylor M, Rullkoetter PJ, 'Comparison of Long-Term Numerical and Experimental Total Knee Replacement Wear During Simulated Gait Loading', *J Biomech*, 40 (2007), 1550-8.

105 Kohm A, Gaumer J, Ravula V, Urban R, Gilbertson L, Bos G, Dey T, Nelson L, Dyce J, Lannutti JJ, 'Three-Dimensional Laser Micrometry Characterization of Surface Wear in Total Hip Arthroplasty', *J Biomed Mater Res B Appl Biomater*, 82 (2007), 428-39.

106 Kop AM, Whitewood C, Johnston DJ, 'Damage of Oxinium Femoral Heads Subsequent to Hip Arthroplasty Dislocation Three Retrieval Case Studies', *J Arthroplasty*, 22 (2007), 775-9.

107 Kruger KM, Tikekar NM, Heiner AD, Baer TE, Lannutti JJ, Callaghan JJ, Brown TD, 'Encoding Scratch and Scrape Features for Wear Modeling of Total Joint Replacements', *Comput Math Methods Med*, (2013), 624267.

108 Kruger KM, Tikekar NM, Heiner AD, Baer TE, Lannutti JJ, Callaghan JJ, Brown TD, 'A Novel Formulation for Scratch-Based Wear Modelling in Total Hip Arthroplasty', *Comput Methods Biomech Biomed Engin*, 17 (2014) 1227-36.

109 Kruger KM, Tikekar NM, Heiner AD, Lannutti JJ, Callaghan JJ, Brown TD, 'Quantification and Wear Prediction Due to Femoral Head Damage in Total Hip Arthroplasty. ', in *11th International Symposium on Computer Methods in Biomechanics and Biomedical Engineering* (Salt Lake City, UT: 2013).

110 Kruger KM, Tikekar NM, Heiner AD, Lannutti JJ, Callaghan JJ, Brown TD,, 'Morphologic Factors Responsible for Elevated Wear from Bearing-Foreign Material Deposition in Total Hip Arthroplasty', in *Transactions of the 59th Annual Meeting of the Orthopaedic Research Society*. (San Antonio, TX: 2013).

111 Kurtz SM, Gawel HA, Patel JD, 'History and Systematic Review of Wear and Osteolysis Outcomes for First-Generation Highly Crosslinked Polyethylene', *Clin Orthop Relat Res,* 469 (2011), 2262-77.

112 Kurtz SM, Lau E, Ong K, Zhao K, Kelly M, Bozic KJ, 'Future Young Patient Demand for Primary and Revision Joint Replacement: National Projections from 2010 to 2030', *Clin Orthop Relat Res,* 467 (2009), 2606-12.

113 Kurtz SM, Ochoa JA, Hovey CB, White CV, 'Simulation of Initial Frontside and Backside Wear Rates in a Modular Acetabular Component with Multiple Screw Holes', *J Biomech,* 32 (1999), 967-76.

114 Kurtz CM, Ong K, Lau E, Mowat F, Halpern M, 'Projections of Primary and Revision Hip and Knee Arthroplasty in the United States from 2005 to 2030', *J Bone Joint Surg Am,* 89 (2007), 780-5.

115 Kusaba A, Kuroki Y, 'Femoral Component Wear in Retrieved Hip Prostheses', *J Bone Joint Surg Br,* 79 (1997), 331-6.

116 Labovitz S, 'The Assignment of Numbers to Rank Order Categories', *Am Socio Rev,* 35 (1970), 515-24.

117 Lampropoulou-Adamidou K, Georgiades G, Vlamis J, Hartofilakidis G, 'Charnley Low-Friction Arthroplasty in Patients 35 Years of Age or Younger. Results at a Minimum of 23 Years', *Bone Joint J,* 95-B (2013), 1052-6.

118 Langton DJ, Jameson SS, Joyce TJ, Gandhi JN, Sidaginamale R, Mereddy P, Lord J, Nargol AV, 'Accelerating Failure Rate of the ASR Total Hip Replacement', *J Bone Joint Surg Br,* 93 (2011), 1011-6.

119 Langton DJ, Jameson SS, Joyce TJ, Hallab NJ, Natu S, Nargol AV, 'Early Failure of Metal-on-Metal Bearings in Hip Resurfacing and Large-Diameter Total Hip Replacement: A Consequence of Excess Wear', *J Bone Joint Surg Br,* 92 (2010), 38-46.

120 Langton DJ, TJ Joyce, Jameson SS, Lord J, Van Orsouw M, Holland JP, Nargol AV, and De Smet KA, 'Adverse Reaction to Metal Debris Following Hip Resurfacing: The Influence of Component Type, Orientation and Volumetric Wear', *J Bone Joint Surg Br,* 93 (2011), 164-71.

121 Learmonth IS, Young C, Rorabeck C, 'The Operation of the Century: Total Hip Replacement', *Lancet,* 370 (2007), 1508-19.

122 Lee R, Essner A, Wang A, Jaffe WL, 'Scratch and Wear Performance of Prosthetic Femoral Head Components against Crosslinked Uhmwpe Sockets', *Wear*, 267 (2009), 1915-21.

123 Li L, Patil S, Steklov N, Bae W, Temple-Wong M, D'Lima DD, Sah RL, Fregly BJ, 'Computational Wear Simulation of Patellofemoral Articular Cartilage During in Vitro Testing', *J Biomech*, 44 (2011), 1507-13.

124 Lin LI, 'A Concordance Correlation Coefficient to Evaluate Reproducibility', *Biometrics*, 45 (1989), 255-68.

125 Linder L, Lindberg L, Carlsson A, 'Aseptic Loosening of Hip Prostheses. A Histologic and Enzyme Histochemical Study', *Clin Orthop Relat Res* (1983), 93-104.

126 Liu F, Galvin A, Jin Z, Fisher J, 'A New Formulation for the Prediction of Polyethylene Wear in Artificial Hip Joints', *Proc Inst Mech Eng H*, 225 (2011), 16-24.

127 Liu F, Leslie I, Williams S, Fisher J, Jin Z, 'Development of Computational Wear Simulation of Metal-on-Metal Hip Resurfacing Replacements', *J Biomech*, 41 (2008), 686-94.

128 Lundberg HJ, Liu SS, Callaghan JJ, Pedersen DR, O'Rourke MR, Goetz DD, Vittetoe DA, Clohisy JC, Brown TD, 'Association of Third Body Embedment with Rim Damage in Retrieved Acetabular Liners', *Clin Orthop Relat Res*, 465 (2007), 133-9.

129 Lundberg HJ, Pedersen DR, Baer TE, Muste M, Callaghan JJ, Brown TD, 'Effects of Implant Design Parameters on Fluid Convection, Potentiating Third-Body Debris Ingress into the Bearing Surface During THA Impingement/Subluxation', *J Biomech*, 40 (2007), 1676-85.

130 Lundberg HJ, Stewart KJ, Callaghan JJ, Brown TD, 'Kinetically Critical Sites of Femoral Head Roughening for Wear Rate Acceleration in Total Hip Arthroplasty', *Clin Orthop Relat Res* (2005), 89-93.

131 Lundberg HJ, Stewart KJ, Pedersen DR, Callaghan JJ, and Brown TD, 'Nonidentical and Outlier Duty Cycles as Factors Accelerating UHMWPE Wear in THA: A Finite Element Exploration', *J Orthop Res*, 25 (2007), 30-43.

132 Mai KT, Verioti C, D'Lima D, Colwell CW, Jr., Ezzet, Jr. KA, 'Surface Roughness of Femoral Head Prostheses after Dislocation', *Am J Orthop (Belle Mead NJ)*, 39 (2010), 495-500.

133 Malem D, Nagy MT, Ghosh S, Shah B, 'Catastrophic Failure of Ceramic-on-Ceramic Total Hip Arthroplasty Presenting as Squeaking Hip', *BMJ Case Rep*, 2013 (2013).

134 Maxian TA, Brown TD, Pedersen DR, Callaghan JJ, 'Adaptive Finite Element Modeling of Long-Term Polyethylene Wear in Total Hip Arthroplasty', *J Orthop Res*, 14 (1996), 668-75.

135 Maxian TA, Brown TD, Pedersen DR, Callaghan JJ, 'The Frank Stinchfield Award. 3-Dimensional Sliding/Contact Computational Simulation of Total Hip Wear', *Clin Orthop Relat Res* (1996), 41-50.

136 Maxian TA, Brown TD, Pedersen DR, Callaghan JJ, 'A Sliding-Distance-Coupled Finite Element Formulation for Polyethylene Wear in Total Hip Arthroplasty', *J Biomech*, 29 (1996), 687-92.

137 Maxian TA, Brown TD, Pedersen DR, McKellop HA, Lu B, Callaghan JJ, 'Finite Element Analysis of Acetabular Wear. Validation, and Backing and Fixation Effects', *Clin Orthop Relat Res* (1997), 111-7.

138 McKellop HA, 'The Lexicon of Polyethylene Wear in Artificial Joints', *Biomaterials*, 28 (2007), 5049-57.

139 McKellop HA, Campbell P, Park SH, Schmalzried TP, Grigoris P, Amstutz HC, Sarmiento A, 'The Origin of Submicron Polyethylene Wear Debris in Total Hip Arthroplasty', *Clin Orthop Relat Res* (1995), 3-20.

140 McKellop HA, Sarmiento A, Schwinn CP, Ebramzadeh E, 'In Vivo Wear of Titanium-Alloy Hip Prostheses', *J Bone Joint Surg Am*, 72 (1990), 512-7.

141 McKellop HA, Park SH, Chiesa R, Doorn P, Lu B, Normand P, Grigoris P, and Amstutz H, 'In Vivo Wear of Three Types of Metal on Metal Hip Prostheses During Two Decades of Use', *Clin Orthop Relat Res* (1996), S128-40.

142 McNie CM, Barton DC, Stone MH, Fisher J, 'Prediction of Plastic Strains in Ultra-High Molecular Weight Polyethylene Due to Microscopic Asperity Interactions During Sliding Wear', *Proc Inst Mech Eng H*, 212 (1998), 49-56.

143 McNie CM, Barton DC, Fisher J, Stone MH, 'Modeling of Damage to Articulating Surfaces by Third Body Particles in Total Joint Replacements', *J Mater Sci Mater Med*, 11 (2000), 569-78.

144 McNie CM, Barton DC, Ingham E, Tipper JP, Fisher J, Stone MH, 'The Prediction of Polyethylene Wear Rate and Debris Morphology Produced by Microscopic Asperities on Femoral Heads', *J Mater Sci Mater Med*, 11 (2000), 163-74.

145 Mendenhall S, 'Hip and Knee Implant Review', *Orthopa Netw News*, 17 (2006).

146 Minakawa H, Stone MH, Wroblewski BM, Lancaster JG, Ingham E, Fisher J, 'Quantification of Third-Body Damage and Its Effect on UHMWPE Wear with Different Types of Femoral Head', *J Bone Joint Surg Br*, 80 (1998), 894-9.

147 Mirghany M, Jin ZM, 'Prediction of Scratch Resistance of Cobalt Chromium Alloy Bearing Surface, Articulating against Ultra-High Molecular Weight Polyethylene, Due to Third-Body Wear Particles', *Proc Inst Mech Eng H*, 218 (2004), 41-50.

148 Muller FA, Hagymasi M, Greil P, Zeiler G, Schuh A, 'Transfer of Metallic Debris after Dislocation of Ceramic Femoral Heads in Hip Prostheses', *Arch Orthop Trauma Surg*, 126 (2006), 174-80.

149 Najjar D, Bigerelle M, Migaud H, Iost A, 'Identification of Scratch Mechanisms on a Retrieved Metallic Femoral Head', *Wear*, 258 (2005), 240-50.

150 O'Brien ST, Bohm ER, Petrak MJ, Wyss UP, Brandt JM, 'An Energy Dissipation and Cross Shear Time Dependent Computational Wear Model for the Analysis of Polyethylene Wear in Total Knee Replacements', *J Biomech* (2014).

151 Ollivere B, Wimhurst JA, Clark IC, Donell ST, 'Current Concepts in Osteolysis', *J Bone Joint Surg Br*, 94 (2012), 10-5.

152 Ong KL, Mowat FS, Chan N, Lau E, Halpern MT, Kurtz SM, 'Economic Burden of Revision Hip and Knee Arthroplasty in Medicare Enrollees', *Clin Orthop Relat Res*, 446 (2006), 22-8.

153 Pal S, Haider H, Laz PJ, Knight LA, Rullkoetter PJ, 'Probabilistic Computational Modeling of Total Knee Replacement Wear', *Wear*, 264 (2008), 701-07.

154 Patil S, Bergula A, Chen PC, Colwell, Jr. CW, D'Lima DD, 'Polyethylene Wear and Acetabular Component Orientation', *J Bone Joint Surg Am*, 85-A Suppl 4 (2003), 56-63.

155 Patten EW, Atwood SA, Van Citters DW, Jewett BA, Pruitt LA, Ries DA, 'Delamination of a Highly Cross-Linked Polyethylene Liner Associated with Titanium Deposits on the Cobalt-Chromium Modular Femoral Head Following Dislocation', *J Bone Joint Surg Br*, 92 (2010), 1306-11.

156 Paul MC, Glennon LP, Baer TE, Brown TD, 'Field Variable Associations with Scratch Orientation Dependence of UHMWPE Wear: A Finite Element Analysis', *J Biomech Eng*, 130 (2008), 061019.

157 Pedersen DR, Brown TD, Hillis SL, Callaghan JJ, 'Prediction of Long-Term Polyethylene Wear in Total Hip Arthroplasty, Based on Early Wear Measurements Made Using Digital Image Analysis', *J Orthop Res*, 16 (1998), 557-63.

158 Pedersen DR, Callaghan JJ, Johnston TL, Fetzer GB, Johnston RC, 'Comparison of Femoral Head Penetration Rates between Cementless Acetabular Components with 22-Mm and 28-Mm Heads', *J Arthroplasty*, 16 (2001), 111-5.

159 Penmetsa JP, Laz PJ, Petrella AJ, Rullkoetter PJ, 'Influence of Polyethylene Creep Behavior on Wear in Total Hip Arthroplasty', *J Orthop Res*, 24 (2006), 422-7.

160 Pietrabissa R, Raimondi M, Di Martino E, 'Wear of Polyethylene Cups in Total Hip Arthroplasty: A Parametric Mathematical Model', *Med Eng Phys*, 20 (1998), 199-210.

161 Popoola O, Borgstede L, Heller M, Shen M, Seebeck J, Johnson T, '*In Vitro* Polyethylene Wear in a Spine Total Disc Replacement (TDR) Implant', in *53rd Annual Meeting of the Orthopaedic Research Society* (San Diego, CA: 2007).

162 Que L, Topoleski LD, 'Third-Body Wear of Cobalt-Chromium-Molybdenum Implant Alloys Initiated by Bone and Poly(Methyl Methacrylate) Particles', *J Biomed Mater Res*, 50 (2000), 322-30.

163 Queiroz RD, Oliveira AL, Trigo FC, Lopes JA, 'A Finite Element Method Approach to Compare the Wear of Acetabular Cups in Polyethylene According to Their Lateral Tilt in Relation to the Coronal Plane', *Wear,* 298–299 (2013), 8-13.

164 Raimondi MT, Santambrogio C, Pietrabissa R, Raffelini F, Molfetta L, 'Improved Mathematical Model of the Wear of the Cup Articular Surface in Hip Joint Prostheses and Comparison with Retrieved Components', *Proc Inst Mech Eng H,* 215 (2001), 377-91.

165 Raimondi MT, Vena P, Pietrabissa R, 'Quantitative Evaluation of the Prosthetic Head Damage Induced by Microscopic Third-Body Particles in Total Hip Replacement', *J Biomed Mater Res,* 58 (2001), 436-48.

166 Rawlinson JJ, Punga KP, Gunsallus KL, Bartel DL, Wright TM, 'Wear Simulation of the Prodisc-L Disc Replacement Using Adaptive Finite Element Analysis', *J Neurosurg Spine*, 7 (2007), 165-73.

167 Ribeiro NS, Folgado J, Fernandes PR, Monteiro J, 'Wear Analysis in Anatomical and Reversed Shoulder Prostheses', *Comput Methods Biomech Biomed Engin,* 14 (2011), 883-92.

168 Richards L, Brown C, Stone MH, Fisher J, Ingham E, JL Tipper, 'Identification of Nanometre-Sized Ultra-High Molecular Weight Polyethylene Wear Particles in Samples Retrieved in Vivo', *J Bone Joint Surg Br*, 90 (2008), 1106-13.

169 Sagbas B, Numan Durakbasa M, 'Measurement of Wear in Orthopedic Prosthesis', *Proc Int Congress Adv Appl Phys Mater Sci*, 121 (2011).

170 Saikko V, Calonius O, Keranen J, 'Effect of Counterface Roughness on the Wear of Conventional and Crosslinked Ultrahigh Molecular Weight Polyethylene Studied with a Multi-Directional Motion Pin-on-Disk Device', *J Biomed Mater Res*, 57 (2001), 506-12.

171 Scott DL, Campbell PA, McClung CD, Schmalzried TP, 'Factors Contributing to Rapid Wear and Osteolysis in Hips with Modular Acetabular Bearings Made of Hylamer', *J Arthroplasty*, 15 (2000), 35-46.

172 Sfantos GK, Aliabadi MH, 'A Boundary Element Formulation for Three-Dimensional Sliding Wear Simulation', *Wear,* 262 (2007), 672-83.

173 Sfantos GK, Aliabadi MH, 'Total Hip Arthroplasty Wear Simulation Using the Boundary Element Method', *J Biomech,* 40 (2007), 378-89.

174 Shaver SM, Brown TD, Hillis SL, Callaghan JJ, 'Digital Edge-Detection Measurement of Polyethylene Wear after Total Hip Arthroplasty', *J Bone Joint Surg Am*, 79 (1997), 690-700.

175 Sieber HP, Rieker CB, Kottig P, 'Analysis of 118 Second-Generation Metal-on-Metal Retrieved Hip Implants', *J Bone Joint Surg Br*, 81 (1999), 46-50.

176 Snir N, Kaye IN, Klifto CS, Hamula MJ, Wolfson TS, Schwarzkopf R, Jaffe FF, '10-Year Follow-up Wear Analysis of First-Generation Highly Crosslinked Polyethylene in Primary Total Hip Arthroplasty', *J Arthroplasty* (2013).

177 Soong M, Rubash HE, Macaulay W, 'Dislocation after Total Hip Arthroplasty', *J Am Acad Orthop Surg*, 12 (2004), 314-21.

178 Srinivasan A, Jung E, Russell Levine B, 'Modularity of the Femoral Component in Total Hip Arthroplasty', *J Am Acad Orthop Surg*, 20 (2012), 214-22.

179 Strickland MA, Taylor M, '*In-Silico* Wear Prediction for Knee Replacements--Methodology and Corroboration', *J Biomech*, 42 (2009), 1469-74.

180 Swan A, Ansari F, Chang R, Kung S, Norris TR, SB Gunther, Ries MD, Pruitt LA, 'Microscale Analysis of Linear Abrasion and Scratching Damage on Cobalt Chrome Humeral Head Retrievals Using 3D Profilometry', in *Transactions of the 59th Annual Meeting of the Orthopaedic Research Society.* (New Orleans, LA: 2014).

181 Sychterz CJ, Engh, Jr. CA, Swope SW, McNulty DE, Engh CA, 'Analysis of Prosthetic Femoral Heads Retrieved at Autopsy', *Clin Orthop Relat Res* (1999), 223-34.

182 Sychterz CJ, Moon KH, Hashimoto Y, Terefenko KM, Engh, Jr. CA, Bauer TM, 'Wear of Polyethylene Cups in Total Hip Arthroplasty. A Study of Specimens Retrieved Post Mortem', *J Bone Joint Surg Am*, 78 (1996), 1193-200.

183 Teoh SH, Chan WH, Thampuran R, 'An Elasto-Plastic Finite Element Model for Polyethylene Wear in Total Hip Arthroplasty', *J Biomech*, 35 (2002), 323-30.

184 Tikekar NM, Heiner AD, Kruger KM, Baer TE, Lannutti JJ, Brown TD, 'Bearing-Foreign Material Deposition on Damaged Co-Cr Femoral Heads.', in *58th Annual Meeting of the Orthopaedic Research Society* (San Francisco, CA: 2012), Poster # 1078.

185 Tipper JL, Firkins PJ, Besong AA, Barbour PS, Nevelos J, Stone MH, Ingham E, Fisher J, 'Characterisation of Wear Debris from UHMWPE on Zirconia Ceramic, Metal-on-Metal and Alumina Ceramic-on-Ceramic Hip Prostheses Generated in a Physiological Anatomical Hip Joint Simulator', *Wear*, 250 (2001), 120-28.

186 Tipper JL, Ingham E, Hailey JL, Besong AA, Fisher J, Wroblewski BM, Stone MH, 'Quantitative Analysis of Polyethylene Wear Debris, Wear Rate and Head Damage in Retrieved Charnley Hip Prostheses', *J Mater Sci Mater Med*, 11 (2000), 117-24.

187 Uddin MS, Zhang LC, 'Predicting the Wear of Hard-on-Hard Hip Joint Prostheses', *Wear*, 301 (2013), 192-200.

188 Urban RM, Jacobs JJ, Gilbert JL, Galante JO, 'Migration of Corrosion Products from Modular Hip Prostheses. Particle Microanalysis and Histopathological Findings', *J Bone Joint Surg Am*, 76 (1994), 1345-59.

189 Veeco Instruments, 'Characterizing Surface Quality: What Average Roughness Is Not Enough.', (2003).

190 Vendittoli P, Amzica T, Roy AG, Lusignan D, Girard J, Lavigne M, 'Metal Ion Release with Large-Diameter Metal-on-Metal Hip Arthroplasty', *J Arthroplasty*, 26 (2011), 282-88.

191 Walker PS, Gold BL, 'The Tribology (Friction, Lubrication and Wear) of All-Metal Artificial Hip Joints. 1971', *Clin Orthop Relat Res* (1996), S4-10.

192 Walker PS Salvati E, Hotzler RK, 'The Wear on Removed McKee-Farrar Total Hip Prostheses', *J Bone Joint Surg Am,* 56 (1974), 92-100.

193 Walter WL, O'Toole, Walter WK, Ellis A, Zicat BA, 'Squeaking in Ceramic-on-Ceramic Hips: The Importance of Acetabular Component Orientation', *J Arthroplasty,* 22 (2007), 496-503.

194 Wang A, Essner A, 'Three-Body Wear of UHMWPE Acetabular Cups by PMMA Particles against CoCr, Alumina and Zirconia Heads in a Hip Joint Simulator', *Wear,* 250 (2001), 212-16.

195 Wang A, Polineni VK, Stark C, Dumbleton JH, 'Effect of Femoral Head Surface Roughness on the Wear of Ultrahigh Molecular Weight Polyethylene Acetabular Cups', *J Arthroplasty,* 13 (1998), 615-20.

196 Wilkinson JM, Hamer AJ, Stockley I, Eastell R, 'Polyethylene Wear Rate and Osteolysis: Critical Threshold Versus Continuous Dose-Response Relationship', *J Orthop Res,* 23 (2005), 520-5.

197 Willing R, Kim IY, 'A Holistic Numerical Model to Predict Strain Hardening and Damage of Uhmwpe under Multiple Total Knee Replacement Kinematics and Experimental Validation', *J Biomech,* 42 (2009), 2520-7.

198 Wu JS, Hung JP, Shu CS, Chen JH, 'The Computer Simulation of Wear Behavior Appearing in Total Hip Prosthesis', *Comput Methods Programs Biomed,* 70 (2003), 81-91.

199 Wyant JC, Koliopoulos CL, Bhushan B, Basila D, 'Development of a Three-Dimensional Noncontact Digital Optical Profiler', *J. Tribol.,* 108 (1986), 1-8.

200 Zhang T, Harrison NM, McDonnell PF, McHugh PE, Leen SB, 'A Finite Element Methodology for Wear–Fatigue Analysis for Modular Hip Implants', *Tribol Int,* 65 (2013), 113-27.

201 Zhao D, Sakoda H, Sawyer WG, Banks SA, Fregly BJ, 'Predicting Knee Replacement Damage in a Simulator Machine Using a Computational Model with a Consistent Wear Factor', *J Biomech Eng,* 130 (2008), 011004.